Dynamic Risk Transmission and Dependence Modeling: Copula Studies of China's Real Estate, Carbon Markets, and the AI-Energy Nexus

WANG, YAN

Dynamic Risk Transmission and Dependence Modeling: Copula Studies of China's Real Estate, Carbon Markets, and the AI-Energy Nexus

Total number of volumes: 1
This is volume 1 of 1

Yan Wang

A thesis submitted for the degree of
Doctor of Philosophy

Department of Economics

Durham University

2025

Abstract

This thesis dissects dynamic risk transmission within and across three critical interconnected markets—real estate and carbon trading in China and the global AI-energy nexus—employing advanced econometric and network methodologies. These markets represent critical sectors undergoing significant structural transitions, where understanding risk propagation mechanisms has become essential for financial stability and policy formulation. Despite extensive research on individual market risks, the complex, state-dependent, and potentially non-linear patterns of risk transmission across these sectors remain inadequately explored.

The first study examines China's real estate market (2006-2023) through a state-dependent vine copula network approach. The analysis reveals a persistent center-periphery structure where top-tier cities function as central risk nodes. During high-risk periods, risk contagion intensifies significantly, with network connectivity increasing by approximately 15%. Macroeconomic factors—particularly GDP growth and inflation—substantially influence risk state transitions, with deteriorating fundamentals increasing the probability of entering high-risk regimes and reshaping network topologies.

The second study investigates the impact of China's 2021 national carbon market unification through a multi-layer network framework incorporating both copula-based dependencies and Diebold-Yilmaz spillovers. Following unification, market information efficiency improved substantially (transfer rate increased from 0.432 to 0.516), and the national market emerged as a central coordinator. Regional market roles underwent significant transformations, with Tianjin notably shifting from a primary risk receiver (net spillover -21.5%) to a significant transmitter (net spillover $+26.1\%$), demonstrating how institutional reforms can fundamentally reshape risk transmission patterns.

The third study examines how the artificial intelligence expansion influences global energy market risk under extreme conditions. Using time-varying copulas and spillover indices, the research finds that AI exhibits relatively weak dependence on fossil fuels and carbon prices but significantly stronger connections with clean energy sectors, particularly photovoltaic. These technological sector linkages intensified markedly following the ChatGPT release (tail dependence increasing from 0.32 to 0.52), highlighting how technological breakthroughs can reshape market interdependencies beyond traditional energy-industrial relationships.

Contents

Abstract i

Declaration vi

Statement of Copyright vii

Acknowledgments viii

Data Access Statement ix

1 Introduction 1

2 Dynamic Risk Contagion in China's Real Estate Market: A State-Dependent Network Analysis with Macroeconomic Influences 7

2.1 Introduction 8

2.2 Literature Review 11

2.2.1 Housing Market Risk Contagion: Concepts and Measurement . . . 11

2.2.2 Network Analysis in Real Estate Research 11

2.2.3 China's Tiered Urban Housing Markets and Risk Transmission . . . 12

2.2.4 Macroeconomic Factors and Housing Market Risks 12

2.2.5 Methodological Innovations and Future Directions 13

2.3 Methodology 15

2.3.1 Marginal Distributions: AR-GARCH Modeling of City-Level Returns 15

2.3.2 High-Dimensional Dependence Structure: Vine Copulas 16

2.3.3 Network Representation of Copula Dependencies 17

2.3.4 State-Dependent Analysis: Markov Regime-Switching Model 18

2.3.5 Macroeconomic Determinants of Regime Transitions 18

2.3.6 Hierarchical Urban Structures and Cross-Tier Analysis 19

2.3.7 Robustness and Model Validation 19

2.3.8 Integrated Methodological Framework 20

2.4 Empirical Analysis 21

2.4.1 Data Description and Preliminary Analysis 21

2.4.2 Structural Characteristics of the Risk Contagion Network in China's Real Estate Market . . . 23
2.4.3 Dynamic Characteristics of Risk Contagion Networks under High-Risk and Low-Risk States . . . 27
2.4.4 State-Dependent Impact of Macroeconomic Factors on Housing Market Risk . . . 34
2.5 Robustness Checks . . . 40
2.6 Conclusion . . . 44

3 Risk Transmission Mechanisms and International Integration in China's Carbon Market: A Multi-layer Network Analysis 46
3.1 Introduction . . . 47
3.2 Literature Review . . . 50
3.2.1 Evolution of Carbon Markets and Emerging Challenges . . . 50
3.2.2 Financial Risk Theory Applied to Carbon Markets . . . 51
3.2.3 Market Integration Theory in the Context of Carbon Markets . . . 52
3.2.4 Advancements in Network Analysis for Carbon Markets . . . 53
3.2.5 Identified Research Gaps and Study Contributions . . . 54
3.3 Methodology . . . 56
3.3.1 Data and Preliminary Analysis . . . 57
3.3.2 GARCH Modeling of Volatility Dynamics . . . 58
3.3.3 Copula Analysis for Non-linear Dependencies . . . 59
3.3.4 Diebold-Yilmaz Method for Linear Risk Spillovers . . . 59
3.3.5 Construction of the Multi-layer Risk Network . . . 60
3.3.6 Analysis and Robustness Checks . . . 62
3.4 Empirical Analysis . . . 63
3.4.1 Data Description and Preliminary Analysis . . . 63
3.4.2 Volatility Modeling . . . 65
3.4.3 Market Dependence Structure Analysis . . . 67
3.4.4 Risk Spillover Effect Analysis . . . 69
3.4.5 Network Characteristics Analysis . . . 73
3.4.6 Economic and Policy Implications . . . 83
3.5 Conclusions . . . 87

4 Does the AI Boom Reshape Energy Market Risk? Evidence from Financial Linkages 89
4.1 Introduction . . . 90
4.2 Literature Review and Theoretical Framework . . . 93
4.2.1 Literature Review . . . 93
4.2.2 Conceptual Framework and Hypotheses . . . 94

4.3 Data and Methodology . . . 99
4.3.1 Overview and Methodological Framework . . . 99
4.3.2 Data Structure and Preliminary Transformations . . . 99
4.3.3 Univariate Volatility Modeling: GARCH Framework . . . 100
4.3.4 Multivariate Dependence Modeling via Copulas . . . 101
4.3.5 Dynamic t-Copula Specification . . . 103
4.3.6 Systemic Risk Assessment: Diebold-Yilmaz Framework . . . 104
4.3.7 Event Study Design and Structural Break Analysis . . . 105
4.3.8 Robustness Checks and Model Validation . . . 106
4.3.9 Summary and Methodological Contributions . . . 107
4.4 Empirical Results . . . 108
4.4.1 Data and Methodology Implementation . . . 108
4.4.2 Empirical Evidence for the Four Hypotheses . . . 112
4.4.3 Robustness and Sensitivity Analysis . . . 122
4.4.4 Synthesis: Hypothesis Validation and Theoretical Implications . . . 124
4.5 Conclusions and Implications . . . 127
4.5.1 Main Findings . . . 127
4.5.2 Theoretical Contributions and Policy Implications . . . 128
4.5.3 Investment Implications . . . 128
4.5.4 Limitations and Future Research Directions . . . 129

5 Synthesis and Conclusions **131**
5.1 Summary of Key Findings . . . 132
5.2 Cross-Cutting Themes and Implications . . . 133
5.3 Policy Recommendations . . . 134
5.4 Limitations and Future Research Directions . . . 136
5.5 Concluding Remarks . . . 137

References **139**

A Supplementary Materials for Chapter 2 **148**
A.1 Appendix . . . 148
A.1.1 Copula Models Specification . . . 148

B Supplementary Materials for Chapter 3 **153**
B.1 Appendix . . . 153
B.1.1 Detailed Methodological Explanations . . . 153
B.1.2 Regulatory Background . . . 156

C Supplementary Materials for Chapter 4 **158**
C.1 Appendix 158
C.1.1 Complete Dynamic Copula Estimation Results 158

Declaration

I hereby declare that no material contained in this thesis has previously been submitted for a degree in this or any other university.

I confirm that this thesis is solely my own work and that any material from other sources has been properly and fully acknowledged.

Yan Wang

Date: July 2025

Statement of Copyright

Acknowledgments

This dissertation represents the culmination of a challenging and rewarding academic journey, made possible by the generous support and guidance of many individuals and institutions.

First and foremost, I would like to express my profound gratitude to my supervisor, Dr. Xing Wang, for his exceptional guidance, unwavering support, and insightful feedback throughout my doctoral studies. His expertise in financial econometrics and network theory has been instrumental in shaping this research, and his patience and encouragement have been invaluable during the most challenging phases of this project.

I am deeply grateful to the Department of Economics at Durham University for providing an intellectually stimulating environment and excellent research facilities. The constructive criticism and valuable suggestions from faculty members during departmental seminars have significantly enhanced the quality of this work.

My sincere thanks go to fellow doctoral candidates and colleagues at Durham University, whose camaraderie, intellectual discussions, and moral support have enriched both my research and personal life during these years. The academic community at various conferences and workshops where I presented parts of this work has also provided valuable feedback that improved this dissertation.

I am deeply indebted to my family for their unconditional love, understanding, and encouragement throughout this journey. Their unwavering belief in me has been a constant source of motivation.

Finally, I dedicate this work to my parents, who instilled in me the values of perseverance, curiosity, and academic excellence from an early age. Their sacrifices and support have made all my academic pursuits possible.

Any errors or omissions remain entirely my own responsibility.

Yan Wang
Durham, July 2025

Data Access Statement

The empirical analyses presented in this thesis are based on multiple datasets from publicly available and proprietary sources:

Chapter 2 - Real Estate Market Data: Monthly housing price indices for 70 major Chinese cities (January 2006 to November 2023) were obtained from the National Bureau of Statistics of China (NBSC). Macroeconomic indicators, including M2 money supply, loan interest rates, GDP growth, unemployment rates, and inflation data, were sourced from the People's Bank of China. These datasets are publicly accessible through official government databases.

Chapter 3 - Carbon Market Data: Daily carbon emission allowance prices from eight regional pilot markets (Beijing, Chongqing, Fujian, Guangdong, Hubei, Shanghai, Shenzhen, and Tianjin), the national unified market, and the European Union Emissions Trading System (EU ETS) covering July 2018 to July 2024 were collected from China Emissions Exchange and the European Energy Exchange (EEX). Access to these datasets may require institutional subscriptions.

Chapter 4 - AI and Energy Market Data: Daily financial data, including the GlobalX Robotics & AI ETF, clean energy indices (SPGTCLEN.SPI, GRNSOLAR, GRNBIO, GRNWIND), WTI crude oil prices, and EU Emission Allowances spanning January 2020 to June 2024 were obtained from Bloomberg Terminal, Wind Financial Terminal, EIA/Investing, and ICE. These data sources require commercial licenses.

For specific data requests or clarifications regarding data access, please contact the author at: wangyan941123@gmail.com.

Chapter 1

Introduction

This thesis examines dynamic risk transmission(defined here as the propagation of financial shocks and volatility across interconnected markets) mechanisms across three pivotal and interconnected markets within China's rapidly evolving economy: the established real estate sector, the policy-driven carbon trading market, and the emerging AI-energy nexus. These markets, while distinct in nature, are intertwined through complex economic and financial linkages. Real estate development decisions directly influence carbon emissions through construction materials selection and subsequent energy consumption patterns. Carbon market pricing mechanisms increasingly affect both property valuations and the economic viability of energy-intensive AI operations. AI systems' electricity demand continues to shape energy investment and carbon reduction trajectories. The shared policy frameworks and their collective impact on China's growth trajectory and sustainability goals make studying them in concert a unique lens into the systemic vulnerabilities and opportunities arising during China's complex economic transition, which balances traditional growth engines, environmental mandates, and technological frontiers.

The real estate sector has long been a cornerstone of China's economic development, contributing significantly to GDP growth and household wealth. According to official data, the direct value-added of the real estate industry accounted for about 6–7% of GDP in recent years, while including related industries such as construction and building materials raises the share to roughly 13–14% (National Bureau of Statistics of China, 2023). Beyond these official figures, recent academic estimates suggest that when upstream and downstream linkages are incorporated using China's input–output matrix, the real estate sector contributes to over 25% of aggregate demand, underscoring its systemic importance to China's growth model (Rogoff and Yang, 2024). However, its substantial size, leverage, and deep connections with the financial system have persistently raised concerns regarding systemic risk. Understanding precisely how risks propagate within this market, particularly across the hierarchical structure of different city tiers, remains crucial for maintaining financial stability. This study addresses fundamental questions about how risk contagion within China's real estate market varies across different city tiers and distinct market regimes, such as high-risk versus low-risk states. Of particular interest is the specific role that first-tier and key second-tier cities play within the risk transmission network—whether they function as central hubs that amplify risks or as peripheral nodes that absorb shocks. Furthermore, the research investigates how key macroeconomic factors, particularly GDP growth and inflation, influence the probability of risk state transitions and dynamically shape the structure of the contagion network.

Simultaneously, as the world's largest carbon emitter, China has implemented significant measures in establishing carbon markets to address pressing climate change concerns. The transition from regional pilot markets to a unified national carbon trading system in 2021 represents a significant milestone in China's environmental policy landscape. This structural transformation inevitably reshapes risk transmission pathways within the

carbon market itself and alters its integration with international counterparts, not only influencing carbon price formation mechanisms but potentially impacting the operational cost structures of energy-intensive industries, including real estate and AI computing facilities. These complex interdependencies demand rigorous empirical investigation. The second study in this thesis explores how the unification of China's national carbon market has fundamentally altered the pathways and intensity of risk transmission among the pre-existing regional carbon markets. It identifies which specific regions or markets have emerged as key nodes for risk propagation within the newly unified structure, characterizes the nature and strength of risk transmission mechanisms between China's unified national carbon market and the established EU Emissions Trading System, and assesses the extent to which the degree and pattern of integration between China's carbon market and international markets have changed following national unification.

More recently, the artificial intelligence industry has emerged as a key driver of the digital economy, its applications expanding at an exponential rate. Unlike conventional energy-intensive industries that rely on direct fossil fuel combustion, the AI sector's primary energy input is electricity, powering substantial computational demands. This creates a unique and increasingly significant AI-energy nexus, linking AI development directly to power generation methods, grid stability, and consequently to both clean energy sources and the carbon footprint of electricity production. In particular, in regions with concentrated data centres, AI computational demands can constitute significant electrical loads, which can subsequently influence regional energy planning decisions and carbon reduction pathway choices. The surge in AI development, particularly following breakthroughs such as ChatGPT, raises critical questions concerning its financial interconnections and risk relationships with clean energy markets, fossil fuels, and carbon pricing mechanisms, especially under volatile conditions. The third study investigates whether, during periods of extreme market volatility, the AI industry exhibits financial "decoupling" from traditional fossil fuel and carbon prices compared to traditional energy-intensive sectors. It examines how major policy shifts or significant technological shocks influence the tail dependence structure between AI-related assets and clean energy sectors, and explores whether, under specific extreme scenarios such as abrupt cuts in clean energy subsidies or sharp increases in carbon taxes, the direction of volatility spillover between clean energy and AI reverses, potentially leading to positively correlated downturns.

These three markets, operating under different mechanisms and development stages, share common exposures to network effects, policy sensitivities, and evolving risk transmission patterns. By examining them collectively using advanced methodologies, this thesis aims to develop a comprehensive and nuanced understanding of how risks propagate across interconnected market systems in a major, rapidly transforming economy. Beyond these specific inquiries, the overarching objective is to synthesize findings across these diverse but increasingly interdependent markets to identify common patterns and

unique characteristics of risk transmission within China's rapidly evolving economic landscape. Through this comprehensive analysis, the research aims to provide a more holistic understanding of systemic vulnerabilities and the efficacy of network-based analysis in capturing cross-market risk transmission chains, thereby offering an empirical foundation for macro-prudential supervision.

This thesis employs a range of sophisticated econometric and network analysis techniques specifically chosen to unravel the complex risk transmission mechanisms operating within and between the target markets. This diverse toolkit is necessary because the intricate dynamics—characterized by non-linear dependencies, tail risks, regime shifts, and complex network effects—cannot be adequately captured by traditional linear models. Across the three studies, several advanced methodological approaches are consistently applied to ensure comparability and rigour. GARCH models are utilized to capture the time-varying volatility dynamics inherent in financial and economic time series and to filter returns, providing standardized residuals suitable for subsequent dependence modelling. Copula functions are employed extensively to model complex, potentially non-linear and asymmetric dependence structures, with a particular focus on capturing tail dependencies, which are critical for risk analysis. Network analysis is applied systematically to visualize, quantify, and interpret the structure of risk transmission pathways, identifying central nodes, community structures, and overall network density and efficiency. Regime-specific and event-driven analysis is incorporated where appropriate to distinguish between different market conditions or key structural shifts, acknowledging that risk dynamics are often context-specific. These methods can capture the impact of non-continuous market state changes on the topological structure of risk propagation.

Each study then adapts and combines these core approaches to address its specific research questions effectively. The first study on real estate integrates Markov regime-switching with state-dependent vine copula network analysis to examine how risk contagion structures change across different market states and identify the influence of macroeconomic drivers. This approach is particularly suited to capturing non-linear dynamics and threshold effects in real estate markets, building on financial contagion theory and spatial econometrics. The second study on carbon markets develops a multi-layer network framework, combining copula-based dependence measures with Diebold-Yilmaz spillover indices to provide a comprehensive view of risk transmission changes following market unification. This integrated framework overcomes limitations of traditional linear correlation analysis and single-layer network models, enabling the simultaneous capture of linear and non-linear dependencies between markets. The third study on AI-energy linkages utilises time-varying Copula models, specifically dynamic t-Copulas, to capture evolving tail dependencies and complements this with the Diebold-Yilmaz approach to analyse directional volatility spillovers under extreme conditions and around major technological events. This dual approach reveals how financial markets price the uncertain connections

between emerging technologies and energy transitions. This synergistic methodological strategy allows for both deep dives into the unique features of each market and potential cross-study comparisons regarding the nature of risk transmission in interconnected systems.

The remainder of this thesis is organized as follows. Chapter 2 presents the first study, focusing on dynamic risk contagion in China's real estate market. It examines how risks propagate across different city tiers under varying market conditions and macroeconomic influences, utilizing a state-dependent network framework. Chapter 3 contains the second study, which analyses the risk transmission mechanisms in China's carbon market. It specifically investigates the impact of the national market unification on risk dynamics within China and on its integration with international markets, employing a multi-layer network approach. Chapter 4 comprises the third study, investigating whether the recent AI boom has reshaped energy market risk patterns. It places particular emphasis on extreme market conditions and tail dependencies between AI, clean energy, fossil fuels, and carbon markets, using time-varying Copulas and spillover analysis. Chapter 5 synthesizes the key findings from the three empirical studies. It discusses their collective implications for understanding risk transmission in interconnected markets within a transitioning economy like China, offers policy recommendations based on the empirical evidence, and suggests avenues for future research.

This thesis makes several significant contributions to the academic literature on risk transmission, network analysis, and financial econometrics, as well as offering practical insights for policymakers and market participants. It provides a granular and comparative analysis of risk contagion across three uniquely important and interconnected sectors within China's economy, offering novel insights into their distinct dynamics and shared vulnerabilities. This integrated cross-sector research framework provides an unprecedented perspective for understanding risk spillover mechanisms between different market systems, transcending traditional single-market risk assessment approaches. The research demonstrates the synergistic power of integrating advanced econometric and network techniques—including state-dependent models, various copula families, multi-layer networks, and spillover indices—to capture the complex, non-linear, and time-varying nature of risk transmission mechanisms more effectively than traditional methods. It furnishes empirical evidence on how significant structural changes, such as market unification in the carbon market or major technological disruptions like the AI boom, can fundamentally reshape risk transmission patterns and market interconnectedness. Finally, it offers policy-relevant, empirically grounded insights for designing more targeted and adaptive strategies for managing systemic risk across interconnected market systems. This includes identifying key nodes for intervention, understanding state-dependent risks, and anticipating the cross-market effects of policy decisions, with implications for financial stability, carbon market design, and sustainable energy policy. The findings of this research have practical

application value for regulatory authorities designing macro-prudential policies and for investors developing cross-market risk hedging strategies. By examining these three diverse yet increasingly linked markets through a unified methodological lens focusing on dynamic risk transmission, this thesis contributes to a deeper and more nuanced understanding of risk dynamics in complex economic systems, offering lessons that may extend beyond the specific markets or the Chinese context studied herein.

Chapter 2

Dynamic Risk Contagion in China's Real Estate Market: A State-Dependent Network Analysis with Macroeconomic Influences

2.1 Introduction

The Chinese housing market has undergone a remarkable transformation since the 1998 housing reform, transitioning from a state-allocated system to a market-oriented system. This shift has led to substantial improvements in living conditions and rapid housing price appreciation, particularly in economically dynamic regions (Fang et al., 2016a; Glaeser et al., 2017). However, this rapid growth has also raised concerns regarding housing affordability, potential price bubbles, and systemic risks. As China's financial and real estate sectors become increasingly interconnected, understanding the mechanisms through which housing market risks propagate across cities is of paramount importance. Such understanding is not only crucial for evaluating the stability of the broader economy and financial system, but also for developing effective, targeted policy interventions.

Existing research has provided valuable insights into housing price dependencies and regional spillovers in China and other markets. Prior studies often rely on static frameworks to measure comovement and contagion, using methods such as spatial econometrics or simple pairwise correlations (Wu et al., 2014; Gong et al., 2016; Mao and Shen, 2019). While these approaches have enriched our understanding, they generally assume stable relationships over time and do not explicitly capture how risk contagion patterns may change in different market regimes. As the housing market can shift between tranquil (low-risk) periods and turbulent (high-risk) periods, ignoring regime-dependent dynamics could lead to an incomplete picture of how risks propagate. Furthermore, existing work often focuses on pairwise linkages or linear dependencies, potentially overlooking nonlinear, tail-dependent, and hierarchical relationships that may become prominent during market stress. Another critical gap in the literature concerns the role of macroeconomic conditions. While there is evidence that economic factors such as GDP growth, inflation, or credit conditions influence housing prices, few studies have integrated these variables directly into a framework that not only models multivariate housing market linkages but also allows state transitions and network structures to be endogenously affected by macroeconomic dynamics (Brueckner et al., 2017; Duan et al., 2023; Hu and Fan, 2022).

In addition, China's multi-tiered urban system, characterised by distinct city classes (e.g., first-tier, second-tier, and third-tier cities), presents unique complexity in risk contagion. Higher-tier cities typically have more mature markets, stronger economic fundamentals, and deeper financial linkages, possibly making them central hubs for risk transmission. Lower-tier cities, in contrast, may be peripheral and respond differently to economic shocks or policy interventions (Fang et al., 2016a; Wu et al., 2014; Zhang and Fan, 2019). Accounting for this hierarchical urban structure is essential for disentangling how housing market risks spread through the network, how central and peripheral cities differ in their risk propagation roles, and how this structure changes between high-risk and low-risk states.

This study aims to address these research gaps by providing a dynamic, state-dependent characterization of housing market risk contagion across 70 major Chinese cities from 2006 to 2023. We propose a novel methodological framework that integrates a Markov regime-switching model with a vine copula-based network analysis. First, we employ a Markov regime-switching model to identify and distinguish between high-risk and low-risk states. This approach explicitly recognizes that risk transmission mechanisms may differ between tranquil and turbulent periods. Second, we utilize vine copulas, a flexible tool that enables the modelling of complex, high-dimensional dependence structures with nonlinearity and tail dependence, to construct city-level risk contagion networks for each regime. Vine copulas enable us to decompose multivariate dependencies into a cascade of bivariate copulas, capturing intricate relationships that may not be well-described by simpler multivariate models (Aas et al., 2009; Bedford and Cooke, 2002). Third, we incorporate macroeconomic indicators, such as GDP growth and inflation, into the regime-switching probabilities to analyse how changes in the economic environment influence the likelihood of transitioning between high-risk and low-risk states, and how these conditions reshape the network structure of housing market contagion.

By integrating these components, this study contributes to the literature on multiple fronts. The combination of Markov regime-switching and vine copula techniques allows us to capture the state-dependent, time-varying, and non-linear features of housing risk transmission. Our analysis also sheds light on the hierarchical role of city tiers: we hypothesize that first-tier and key second-tier cities function as central nodes in the risk contagion network, especially under high-risk conditions. The multi-tier structure likely induces a center-periphery pattern, where changes in a few influential markets can reverberate through the network. Furthermore, by modelling macroeconomic factors within transition probabilities, we can directly assess how economic downturns, inflationary pressures, or other macro-shocks influence the tightness and connectivity of the risk network. This approach offers a deeper understanding of the interplay between macro-level conditions and the micro-level structure of city-level risk linkages.

In line with these objectives, we propose three main hypotheses. First, we hypothesize that the housing market risk contagion network exhibits a pronounced center-periphery configuration, with first-tier and strategically important second-tier cities acting as pivotal hubs for risk transmission. Second, we expect that during high-risk states the intensity of risk contagion increases, resulting in a tighter, more interconnected network. In contrast, in low-risk states the network becomes looser, reflecting weaker contagion forces. Third, we hypothesize that macroeconomic factors such as GDP growth and inflation significantly influence state transitions and network structures, with tighter networks emerging during periods of economic slowdown or inflationary pressure. By testing these hypotheses, we enhance the understanding of how macroeconomic conditions shape state-dependent housing market risk dynamics.

This study's findings have important theoretical and practical implications. Theoretically, it shows that risk contagion in housing markets is neither static nor uniformly distributed, but depends critically on prevailing market states and economic conditions. It also highlights the complexity introduced by hierarchical urban systems, where city-level heterogeneity matters for the overall structure and evolution of risk networks. Practically, these results can inform policymakers and regulators who seek to maintain housing market stability. Understanding which cities are central transmitters of risk and how this structure changes under different market conditions can guide targeted macroprudential policies. For example, during periods of economic stress, interventions could focus on core cities identified as key hubs of transmission. By anticipating how macroeconomic shifts alter the state of the market and the configuration of the contagion network, policymakers can design more timely and effective strategies for preventing the spread of systemic risk.

The remainder of this paper is structured as follows. Section 2.2 provides a detailed review of related literature, tracing how our research framework addresses identified gaps. Section 2.3 outlines the methodological design, including the Markov regime-switching model and the vine copula network construction. Section 2.4 introduces the dataset, presents descriptive statistics, and reports the empirical findings. Section 6 conducts robustness checks to confirm the consistency and reliability of our results. Finally, Section 7 concludes with theoretical implications, policy recommendations, and suggestions for future research.

2.2 Literature Review

The study of risk contagion in real estate markets has gained significant attention in recent years, particularly in the context of China's rapidly evolving housing market. This section provides a comprehensive review of the existing literature, focusing on the development of risk measurement methodologies, the application of network analysis in real estate studies, and the unique characteristics of China's tiered urban housing markets.

2.2.1 Housing Market Risk Contagion: Concepts and Measurement

The concept of risk contagion in housing markets refers to the propagation of financial distress or price volatility from one market to another (Miao et al., 2011; Brady, 2011; Cotter et al., 2015). Early studies on housing market risks primarily focused on individual markets, employing traditional time series analysis and volatility models (Yang et al., 2021; Cotter et al., 2015). However, these approaches often failed to capture the complex interdependencies between different housing markets.

The development of copula theory has significantly advanced the modeling of dependencies in financial and real estate markets. Copulas provide a flexible framework for modeling the joint distribution of random variables, independent of their marginal distributions (Sklar, 1959; Nelson, 1991). Zimmer (2012) pioneered the application of copulas in housing market analysis, demonstrating their effectiveness in capturing nonlinear and asymmetric dependencies between housing returns.

Building upon this, (Zimmer, 2015; Heinen et al., 2022) extended the use of copulas to analyze comovements in housing prices across multiple U.S. markets. Their findings highlighted the importance of tail dependence in housing market risk, particularly during periods of market stress. This work laid the foundation for more sophisticated analyses of risk contagion in housing markets.

The introduction of vine copulas by (Aas et al., 2009) and (Bedford and Cooke, 2002) further enhanced the toolkit for modeling high-dimensional dependencies. Vine copulas decompose a multivariate copula into a cascade of bivariate copulas, allowing for greater flexibility in capturing complex dependence structures. This methodology has been increasingly adopted in housing market studies, enabling researchers to model the intricate web of relationships between multiple housing markets simultaneously.

2.2.2 Network Analysis in Real Estate Research

The application of network analysis to real estate markets represents a significant methodological advancement in understanding risk contagion. Network theory provides a powerful

framework for visualizing and quantifying the complex relationships between different housing markets.

Gong et al. (2016) were among the first to apply network analysis to study spatial interrelations in Chinese housing markets. Their research revealed the presence of strong spatial dependencies and hierarchical structures in the Chinese real estate sector. Building on this, Zhang et al. (2014) employed network techniques to investigate regional spillover effects and rising connectedness in China's urban housing prices. Their findings underscored the importance of considering network effects in housing policy design and risk management.

The integration of network analysis with econometric models has opened new avenues for research. Mao and Shen (2019) combined spatial econometrics with network analysis to study housing price bubbles in Chinese cities, demonstrating how network structures can influence the formation and propagation of price bubbles. This approach has proven particularly useful in capturing the dynamic and nonlinear nature of risk contagion in housing markets.

2.2.3 China's Tiered Urban Housing Markets and Risk Transmission

The unique characteristics of China's urban system, with its distinct tier classification of cities, add an additional layer of complexity to the study of housing market risk contagion. Fang et al. (2016a) provided a comprehensive analysis of China's housing boom, highlighting the significant heterogeneity across different tiers of cities. They found that the price-to-income ratios in first-tier cities far exceeded those in lower-tier cities, suggesting different risk profiles and potential contagion patterns.

Wu et al. (2014) further explored the implications of China's tiered urban system on housing price dynamics. Their research revealed that price movements in higher-tier cities often lead to those in lower-tier cities, indicating a potential top-down transmission of market trends and risks. This hierarchical structure of risk transmission has important implications for both investors and policymakers.

The role of economic and policy factors in shaping risk contagion patterns across city tiers has been a focus of recent research. Glaeser et al. (2017) examined the influence of credit conditions and local government policies on housing price growth across Chinese cities. They found that the sensitivity of housing prices to credit conditions varied significantly across city tiers, suggesting differentiated risk transmission mechanisms.

2.2.4 Macroeconomic Factors and Housing Market Risks

The selection of macroeconomic variables is grounded in both theoretical models and empirical findings from leading studies on China's housing market. First, real economic activity is a fundamental driver of housing price dynamics, as GDP growth and income

have been shown to explain substantial variation in housing prices across Chinese cities (Fang et al., 2016b; Wang and Zhang, 2014). Second, monetary conditions play a central role: empirical evidence indicates that interest rate shocks, captured by the one-year benchmark lending rate or the Loan Prime Rate (LPR), exert significant and time-varying effects on housing prices (Lu et al., 2023). Finally, inflation (CPI) influences the housing market both by altering the real return to housing investment and by shaping monetary policy responses, consistent with evidence that house prices and inflation are strongly linked in the Chinese context (Kuang and Liu, 2015).

The interaction between macroeconomic factors and housing market risks has been extensively studied, with particular attention paid to the Chinese context. Brueckner et al. (2017); Miles and Zhu (2023) investigated the impact of monetary policy on housing prices in China, finding significant but heterogeneous effects across different regions and city tiers. Their research highlighted the importance of considering macroeconomic influences in models of housing market risk.

Lu et al. (2023) explored the spillover effects of China's monetary policy on the real estate market, employing a time-varying parameter vector autoregression model. Their findings revealed complex and time-varying relationships between monetary policy actions and housing market dynamics, underscoring the need for dynamic modeling approaches in studying risk contagion.

The global financial crisis of 2008 sparked renewed interest in the role of economic shocks in propagating housing market risks. Glaeser et al. (2017); Garriga and Hedlund (2020) examined how the transmission of housing market shocks evolved during and after the crisis, finding evidence of increased interconnectedness and vulnerability to contagion in the post-crisis period.

2.2.5 Methodological Innovations and Future Directions

Recent years have seen a trend towards integrating multiple methodological approaches to capture the complex dynamics of housing market risk contagion. The combination of copula-based dependency modeling, network analysis, and regime-switching models represents a promising direction for future research.

Hu and Fan (2022) employed a combination of spatial analysis and copula modeling to study risk contagion across regional housing markets in China. Their approach allowed for the simultaneous consideration of spatial dependencies and non-linear associations between markets. Similarly, (Duan et al., 2023) developed a network-based contagion model that incorporates both direct and indirect transmission channels, providing a more comprehensive view of risk propagation in interconnected housing markets.

Despite these advancements, several gaps remain in the literature. First, there is a need for more dynamic models that can capture the time-varying nature of risk contagion

patterns, especially in the context of rapidly evolving markets like China's. Second, the incorporation of microeconomic factors, such as household behaviours and expectations, into macro-level risk contagion models remains underdeveloped. Ultimately, the impact of policy interventions on risk contagion networks, particularly in multi-tiered urban systems, warrants further investigation.

In conclusion, this review has highlighted the significant progress made in understanding and modelling housing market risk contagion, particularly in the context of China's unique urban system. The integration of advanced statistical techniques, network analysis, and economic theory has provided valuable insights into the complex dynamics of risk transmission. However, there remains ample scope for further research, especially in developing more comprehensive, dynamic, and policy-relevant models of housing market risk contagion. This study aims to address some of these gaps by proposing a novel methodological framework that combines state-dependent vine copula models with network analysis, offering a more nuanced understanding of the dynamic risk contagion mechanisms in China's tiered housing markets.

2.3 Methodology

This section introduces a comprehensive and rigorously grounded methodological framework to investigate dynamic risk contagion mechanisms in China's housing market. Our approach integrates four key components: (i) marginal modelling of city-level housing returns using AR-GARCH specifications; (ii) the application of vine copulas to capture high-dimensional, non-linear, and potentially asymmetric dependencies; (iii) a Markov regime-switching model that distinguishes between high-risk and low-risk states, enabling state-dependent network characterization; and (iv) the incorporation of macroeconomic variables into the transition probabilities to link economic fundamentals with shifts in market conditions and consequent changes in the risk contagion network. Each method is chosen and combined based on both theoretical considerations and existing empirical literature, ensuring that our framework is well-suited to the complexities and unique features of China's real estate market.

A growing literature emphasizes the importance of non-linear dependence structures, regime shifts, and macroeconomic influences in understanding housing price co-movements and systemic risks (Fang et al., 2016a; Wu et al., 2014; Gong et al., 2016; Mao and Shen, 2019; Hu and Fan, 2022). Copula-based models, especially vine copulas, have been employed successfully to capture intricate tail dependencies and asymmetries in various financial markets (Aas et al., 2009; Bedford and Cooke, 2002; Heinen et al., 2022), while Markov regime-switching techniques have a long tradition in detecting nonlinear dynamics and structural breaks (Fink et al., 2017). Integrating macroeconomic variables into regime transitions follows recent advances in linking housing risk dynamics to economic fundamentals (Brueckner et al., 2017; Glaeser et al., 2017; Duan et al., 2023). By drawing on these methods, our framework provides a nuanced and flexible toolset to explore how city-level interactions, regime changes, and macroeconomic conditions collectively shape systemic risk in China's housing market.

2.3.1 Marginal Distributions: AR-GARCH Modeling of City-Level Returns

Our analysis begins by focusing on the marginal dynamics of the housing price series for N major Chinese cities. Let $P_{i,t}$ denote the housing price index of city i at time t. We define the log-return as:

$$r_{i,t} = 100 \times (\ln P_{i,t} - \ln P_{i,t-1}). \tag{2.1}$$

Housing returns often exhibit autocorrelation, volatility clustering, and heavy tails (Cotter et al., 2015). To capture these features, we adopt an AR(p)-GARCH(q, p) model

with skewed Student-t innovations:

$$r_{i,t} = \mu_i + \sum_{k=1}^{p} \phi_{i,k} r_{i,t-k} + \varepsilon_{i,t}, \tag{2.2}$$

$$\varepsilon_{i,t} = \sigma_{i,t} z_{i,t}, \tag{2.3}$$

$$\sigma_{i,t}^2 = \omega_i + \sum_{k=1}^{q} \alpha_{i,k} \varepsilon_{i,t-k}^2 + \sum_{l=1}^{p} \beta_{i,l} \sigma_{i,t-l}^2, \tag{2.4}$$

where $z_{i,t} \sim$ Skew-Student-$t(\nu_i, \lambda_i)$, capturing asymmetric heavy-tailed behavior. The parameters $(\omega_i, \alpha_{i,k}, \beta_{i,l})$ are estimated via maximum likelihood. Once fitted, we extract standardized residuals:

$$\hat{z}_{i,t} = \frac{\varepsilon_{i,t}}{\hat{\sigma}_{i,t}}, \tag{2.5}$$

and transform them into $u_{i,t} = F_{\hat{z}_i}(\hat{z}_{i,t})$ using the empirical distribution function $F_{\hat{z}_i}$. These $u_{i,t}$ variables, now approximately $U(0,1)$ distributed, serve as the input to our copula modeling (Nelson, 1991).

The choice of a skewed Student-t distribution for the innovations $(z_{i,t})$ is motivated by the empirical properties of the city-level return series, which consistently exhibit excess kurtosis (fat tails) and non-zero skewness . This realistic distributional assumption is essential for the subsequent copula analysis, as it ensures that the dependence structure is estimated from residuals that accurately reflect the underlying data-generating process, thereby preventing misspecification of the marginals from distorting the measurement of dependence.

2.3.2 High-Dimensional Dependence Structure: Vine Copulas

Traditional correlation measures may fail to capture nonlinear and tail-dependent relationships among multiple housing markets, especially during stress episodes. Copula theory provides a flexible tool to model joint distributions independently of marginal distributions (Sklar, 1959). By Sklar's theorem, for N random variables $U_1, \ldots, U_N$ with continuous marginals $F_1, \ldots, F_N$:

$$F(u_1, \ldots, u_N) = C(F_1(u_1), \ldots, F_N(u_N)), \tag{2.6}$$

where C is the N-dimensional copula. The copula captures the dependence structure, separate from the marginals.

For high-dimensional settings, vine copulas (Bedford and Cooke, 2002; Aas et al., 2009) decompose the joint density into a product of bivariate copulas (pair-copulas). A C-vine

decomposition, for instance, factors as:

$$c(u_1, \ldots, u_N) = \prod_{j=1}^{N-1} \prod_{i=1}^{N-j} c_{i,i+j|1,\ldots,i-1}(F(u_i|u_1, \ldots, u_{i-1}), F(u_{i+j}|u_1, \ldots, u_{i-1})), \tag{2.7}$$

where $c_{i,i+j|1,\ldots,i-1}$ are conditional bivariate copula densities. We select suitable copula families (e.g., Gaussian, t, Clayton, Gumbel, Frank) for each pair-copula using information criteria (AIC, BIC), allowing for rich and flexible dependence structures including asymmetry and tail dependence.

Parameters are estimated by pseudo-maximum likelihood, treating the transformed $u_{i,t}$ as observations. This process yields an estimated vine copula structure and pairwise dependence parameters. From these, we compute pairwise Kendall's τ to gauge the strength and direction of dependence:

$$\tau_{ij} = 4 \int_0^1 \int_0^1 C_{ij}(u, v) dC_{ij}(u, v) - 1. \tag{2.8}$$

2.3.3 Network Representation of Copula Dependencies

We construct a weighted network representation of risk contagion by mapping cities to nodes and defining the edge weight between cities i and j as the Kendall's τ dependence measure τ_{ij}. This graph-theoretic approach bridges copula-derived dependence structures with established systemic risk analysis frameworks (**?**Mao and Shen, 2019). Formally, the adjacency matrix $\mathbf{A}$ is defined as:

$$A_{ij} = \tau_{ij} \quad \text{for} \quad i \neq j, \qquad \text{and} \qquad A_{ii} = 0. \tag{2.9}$$

To characterize the network topology, we compute six canonical metrics informed by spatial econometrics and financial network literature (Gong et al., 2016; Zhang et al., 2014). Degree centrality $C_D(i) = \sum_j A_{ij}$ identifies highly connected risk transmitters. Betweenness centrality $C_B(i) = \sum_{j,k} \sigma_{jk}(i)/\sigma_{jk}$, where $\sigma_{jk}(i)$ denotes the number of shortest paths between j and k traversing i, quantifies brokerage influence. Eigenvector centrality $C_E(i)$, derived from the dominant eigenvector solution to $\mathbf{AC_E} = \lambda \mathbf{C_E}$, captures recursive influence propagation. Network density Density $= 2M/[N(N-1)]$ with M edges and N nodes measures connection intensity. Average path length $L = [N(N-1)]^{-1} \sum_{i \neq j} d_{ij}$, where d_{ij} is the shortest-path distance, assesses systemic efficiency. Finally, modularity optimization detects community structures.

Collectively, these metrics elucidate risk distribution patterns, identify contagion hubs, and evaluate network complexity through three analytical dimensions: nodal centrality, global connectivity, and community organization.

2.3.4 State-Dependent Analysis: Markov Regime-Switching Model

Empirical evidence suggests that housing markets exhibit distinct regimes, alternating between tranquil periods and episodes of heightened turbulence (Fang et al., 2016a; Glaeser et al., 2017). To capture such nonlinear dynamics, we employ a Markov regime-switching model (Hamilton, 1989).

We assume two latent states $S_t \in \{1, 2\}$, representing high-risk and low-risk regimes. State transitions follow:

$$P(S_t = j | S_{t-1} = i) = p_{ij}, \quad i, j \in \{1, 2\}. \tag{2.10}$$

The model is estimated via maximum likelihood or EM algorithms, yielding filtered and smoothed probabilities of being in each regime at each time. We can then condition our vine copula on the state:

$$f(r_t | S_t = k) = c^{(k)}(F_1(r_{1,t}), \ldots, F_N(r_{N,t})) \prod_{i=1}^{N} f_i(r_{i,t}), \tag{2.11}$$

where $c^{(k)}$ is the state-specific copula density. Re-estimating the vine copula and constructing networks separately for each regime reveals how dependence patterns and network topologies differ between high-risk and low-risk states. This approach aligns with the literature that finds stronger correlations and contagion effects during market stress (Cotter et al., 2015; Heinen et al., 2022).

2.3.5 Macroeconomic Determinants of Regime Transitions

The selection of macroeconomic variables is grounded in both theoretical models and empirical findings from the literature on China's housing market. Following (Glaeser et al., 2017), who found that GDP growth is a primary driver of housing price variance in Chinese cities, we include it to capture the influence of real economic activity. To account for monetary conditions, we include the one-year loan rate, as (Hu and Fan, 2022) demonstrated its significant and time-varying impact on housing market dynamics. Finally, inflation (CPI) is included as it affects both the real return on housing investment and the likelihood of counteracting monetary policy, consistent with the framework used by Brueckner et al. (2017).

To incorporate economic drivers into our state transitions, we parameterize $p_{ij,t}$ as a function of macro variables X_t:

$$p_{ij,t} = \frac{\exp(\alpha_{ij} + \beta_{ij}' X_t)}{1 + \exp(\alpha_{ij} + \beta_{ij}' X_t)}, \quad i, j \in \{1, 2\},\ i \neq j. \tag{2.12}$$

Here, X_t may include GDP growth, inflation, credit spreads, or other relevant indicators.

By linking transition probabilities to economic conditions, our model endogenizes regime shifts. Deteriorating fundamentals raise the probability of entering a high-risk regime, thereby tightening dependencies and centralizing the network.

2.3.6 Hierarchical Urban Structures and Cross-Tier Analysis

China's multi-tiered urban system suggests that first-tier cities may serve as "hubs" for risk transmission, while lower-tier cities are more peripheral (Fang et al., 2016a; Wu et al., 2014). To examine this hierarchy, we classify cities into tiers and investigate intra-tier and cross-tier dependencies. Vine copulas can be structured hierarchically:

$$c(u_1, \ldots, u_N) = c_{\text{inter-tier}}(\ldots) \times \prod_{k=1}^{K} c_{\text{intra-tier } k}(\ldots), \tag{2.13}$$

Where K is the number of tiers, comparing tier-level dependence under different regimes and macroeconomic conditions reveals whether top-tier cities exert a disproportionate influence on the network, especially during stress periods.

2.3.7 Robustness and Model Validation

To ensure the reliability and credibility of our findings, we conduct comprehensive robustness checks and formal goodness-of-fit tests across four critical dimensions of model specification.

Model specification robustness is evaluated through sensitivity analyses of core modeling choices. We consider alternative copula families (Gaussian, Student's t, Clayton, Gumbel, and Frank) and vine decompositions (C-vine, D-vine, and R-vine structures), with model selection guided by information criteria (AIC/BIC) and statistical fit tests (Genest et al., 2009b). Further, we examine the stability of results to variations in lag structures for AR-GARCH processes and alternative macroeconomic variable specifications, including substitutions of GDP growth with credit-based indicators.

Predictive validity is assessed via out-of-sample testing: We partition the dataset to evaluate the forecast accuracy of state transition probabilities and network topology metrics, thereby ensuring identified contagion patterns are not artifacts of sample overfitting.

Formal specification testing follows the methodological frameworks of Genest et al. (2009a) and Joe (2005) to verify dependence structure adequacy. This includes hypothesis tests of the form:

$$H_0 : \mathcal{C}_{\text{emp}} = \mathcal{C}_{\hat{\theta}} \tag{2.14}$$

where $\mathcal{C}_{\text{emp}}$ denotes the empirical copula and $\mathcal{C}_{\hat{\theta}}$ the parametrically estimated copula. Significant deviations from H_0 indicate misspecification requiring structural adjustments.

Comparative model performance is benchmarked against simplified alternatives,

including static correlation networks and single-regime copula specifications. The superior fit and predictive accuracy of our regime-switching vine copula framework, quantified through likelihood ratio tests and forecasting error metrics, justify its added complexity.

2.3.8 Integrated Methodological Framework

Our analytical framework integrates six complementary methodological components to comprehensively model housing market risk contagion. First, AR-GARCH specifications capture city-level return dynamics while generating uniform marginal distributions required for copula analysis. Second, vine copula constructions flexibly estimate high-dimensional dependence structures, accommodating potential nonlinearities and tail dependencies across urban housing markets. Third, Markov regime-switching mechanisms identify and characterize distinct market states—particularly discriminating between high-risk and low-risk regimes—thereby capturing temporal variations in systemic vulnerability.

Fourth, transition probabilities parametrized by macroeconomic fundamentals provide structural interpretations of regime shifts, elucidating how economic shocks propagate through the housing system. Fifth, a hierarchical modelling perspective incorporates China's tiered urban structure, empirically testing whether top-tier cities function as contagion hubs. Sixth, comprehensive robustness checks and formal goodness-of-fit procedures ensure the statistical validity and stability of our inferences.

This integrated approach offers three principal analytical advantages. First, it jointly models city-level interactions, regime transitions, and macroeconomic linkages within a unified framework, enabling simultaneous examination of multiple dimensions of housing market dynamics. Second, it accommodates complex dependence patterns through vine copulas while maintaining interpretability via regime-specific network representations, thereby balancing methodological sophistication with empirical transparency. Third, it establishes causal pathways from economic fundamentals to contagion dynamics through parametrized transition probabilities, providing explicit mechanisms linking underlying economic conditions to observable market phenomena. Grounded in rigorous econometric theory and validated through extensive sensitivity analyses, this framework provides a robust foundation for both policy formulation and scholarly advancement in urban housing market research.

2.4 Empirical Analysis

2.4.1 Data Description and Preliminary Analysis

This study utilizes monthly housing price index data for 70 major Chinese cities from January 2006 to November 2023, sourced from the National Bureau of Statistics of China (NBSC).To account for the hierarchical nature of China's urban system, the 70 sample cities are categorized into three tiers. This classification is based on the framework outlined in the *China City Statistical Yearbook*. Tier 1 comprises Beijing, Shanghai, Guangzhou, and Shenzhen. Tier 2 includes 31 major provincial capitals and developed coastal cities. The remaining 35 cities are classified as Tier 3. Additionally, we incorporate macroeconomic data obtained from the People's Bank of China, including variables such as M2 money supply, loan interest rates, GDP growth, unemployment rates, and inflation indicators. This comprehensive dataset allows for a nuanced examination of housing market dynamics and their relationship with broader economic trends.

Our analysis encompasses 215 monthly observations for each city, providing a robust time series for investigating housing price dynamics. The housing price data is transformed into monthly returns, calculated as $R_t = 100 \times (lnP_t - lnP_{t-1})$, where P_t denotes the housing price index at time t. This transformation ensures stationarity and facilitates meaningful comparisons across cities and time periods.

Descriptive statistics reveal considerable variation in housing price returns across the sampled cities. For instance, Sanya exhibits the highest volatility with a standard deviation of 1.7583, while Shanghai shows the lowest at 0.5236. Interestingly, most cities have a median return of 0, indicating a balanced distribution of positive and negative returns over the study period. Taiyuan stands out with the highest average monthly return (0.0162%), while Luzhou records the lowest (-0.0166%). This disparity underscores the heterogeneity in housing market performance across different Chinese cities.

Table 2.1: Distributional Properties of Monthly Housing Price Returns for Selected Chinese Cities, 2006-2023

City	**Mean**	**Std. Dev.**	**Min**	**Max**	**Q_1**	**Median**	**Q_3**
Beijing	-0.0056	0.6225	-4.1855	2.3577	-0.2987	0.0000	0.2004
Shanghai	0.0033	0.5236	-2.6511	3.6790	-0.1958	0.0000	0.1998
Guangzhou	-0.0116	0.7943	-3.5411	3.4486	-0.3010	0.0000	0.2023
Shenzhen	-0.0093	0.8900	-4.7237	4.7011	-0.2992	0.0000	0.3011
Sanya	-0.0065	1.7583	-16.4543	15.4830	-0.2987	0.0000	0.3011

Notes: This table reports the summary statistics of monthly housing price returns (in percentages) for selected cities in China from January 2006 to November 2023. The returns are calculated as $R_t = 100 \times (\ln P_t - \ln P_{t-1})$, where P_t is the housing price index at time t. Q_1 and Q_3 represent the first and third quartiles, respectively. Standard deviation (Std. Dev.) measures the volatility of returns over the sample period.

Time series analysis of the housing price indices reveals distinct patterns and trends across different cities. First-tier cities like Beijing and Shanghai generally exhibit steeper growth trajectories compared to lower-tier cities. Notably, there are periods of accelerated growth, particularly evident in the years following 2015, as well as episodes of price corrections or stagnation.

To ensure the validity of our subsequent analyses, we conducted Augmented Dickey-Fuller (ADF) tests to examine the stationarity of the housing price return series for each city. The results indicate that all city return series are stationary (p-value < 0.05), allowing for the direct application of various time series modeling techniques without the need for differencing or other transformations.

The macroeconomic variables included in our study show considerable variation over the observed period. For instance, GDP growth rates range from -6.90% to 18.70%, reflecting periods of rapid economic expansion as well as contractions, likely including the impact of global events such as the 2008 financial crisis and the COVID-19 pandemic. Similarly, M2 growth rates fluctuate between 8.00% and 29.74%, indicating significant changes in monetary policy over the study period.

Table 2.2: Descriptive Statistics of Macroeconomic Indicators in China, 2006-2023

Variable	**Min**	**Q_1**	**Median**	**Mean**	**Q_3**	**Max**
M2 Growth (%)	8.00	10.10	12.90	13.77	16.66	29.74
GDP Growth (%)	-6.90	6.82	7.57	8.01	10.31	18.70
CPI (%)	-1.80	1.44	2.10	2.41	3.00	8.70
Fixed Asset Investment Growth (%)	-24.50	6.55	16.50	15.66	25.35	35.00

Notes: This table presents the summary statistics of key macroeconomic variables that potentially influence housing market dynamics in China from January 2006 to November 2023. M2 Growth represents the growth rate of the broad money supply. GDP Growth indicates the real GDP growth rate. CPI measures the Consumer Price Index inflation rate. Fixed Asset Investment Growth captures the year-over-year change in fixed asset investments.

To account for the hierarchical nature of China's urban system, we categorize the 70 cities into three tiers based on their economic development and administrative importance. This classification reveals distinct patterns in housing price dynamics across city tiers. Tier 1 cities (Beijing, Shanghai, Guangzhou, and Shenzhen) show the highest average price index (100.499), followed by Tier 2 cities (100.381), and Tier 3 cities (100.280). This tiered structure underscores the hierarchical nature of China's urban housing markets and suggests potential differences in risk transmission patterns across tiers.

Our preliminary analysis reveals significant heterogeneity in housing market performance across Chinese cities, with varying degrees of volatility and growth patterns. The observed stationarity of housing price returns facilitates further time series analysis without the need for complex transformations. Moreover, the substantial fluctuations in macroeconomic variables suggest complex influences on housing market dynamics. The tiered

structure of Chinese cities is reflected in their housing price indices, with higher-tier cities generally showing higher and potentially more volatile price levels.

These initial findings set the stage for our subsequent in-depth analysis of risk contagion mechanisms in China's housing market. The observed heterogeneity and complex relationships among cities and macroeconomic factors underscore the importance of a nuanced, multi-faceted approach to understanding housing market risks in China. Our study aims to provide a comprehensive examination of these dynamics, contributing to a deeper understanding of the mechanisms driving housing market risks and their potential implications for economic policy and urban development in China.

2.4.2 Structural Characteristics of the Risk Contagion Network in China's Real Estate Market

This section presents a comprehensive analysis of the structural characteristics of the risk contagion network in China's real estate market. We employ a vine copula model to construct the network and utilize various network metrics to elucidate its topological features, identify key cities, and examine the patterns of risk transmission. This approach allows us to uncover the complex interdependencies in the Chinese real estate market and provides valuable insights for risk management and policy formulation.

Overall Network Topology

The risk contagion network, derived from the first generating tree of the vine copula model, comprises 70 nodes representing major Chinese cities and 69 edges representing significant risk linkages. This network exhibits several distinctive topological features that provide insights into the structure of risk transmission in China's real estate market.

Figure 2.1 presents a visualization of the risk contagion network, where nodes represent cities and edges represent significant risk transmission channels. The size of the nodes is proportional to their degree centrality, while the color intensity of the edges reflects the strength of the risk transmission relationship as measured by Kendall's τ.

The network demonstrates a relatively sparse structure with a density of 0.0286, indicating that only about 2.86% of all possible connections are realized. This sparsity suggests that risk transmission in China's real estate market is selective rather than ubiquitous, with risks primarily propagating through specific channels rather than indiscriminately across all city pairs. This finding has important implications for risk management, as it suggests that targeted interventions focusing on key transmission channels may be more effective than broad-based measures.

The network exhibits a short average path length of 2.70, coupled with a diameter of 5.67. These metrics indicate that despite its sparsity, the network is relatively compact, facilitating rapid risk transmission across the system. On average, a risk shock originating

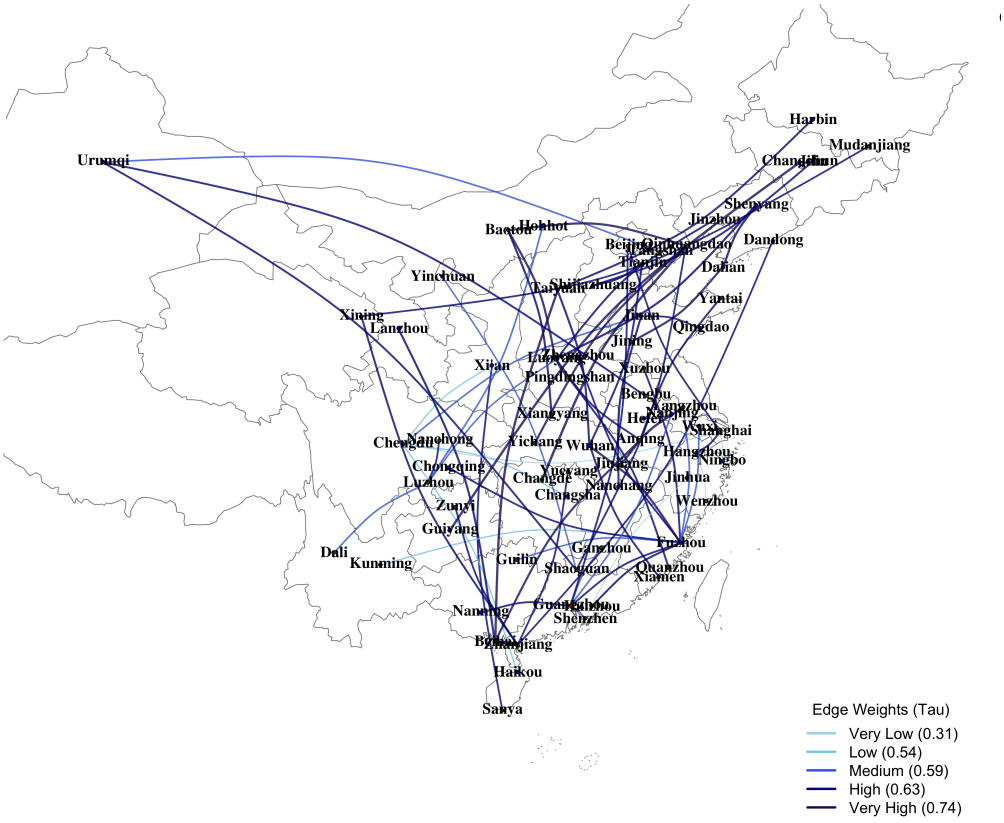

Figure 2.1: High-Risk State Network Structure of Housing Price Risk Contagion in Chinese Cities (2006-2023). Node size represents degree centrality, edge thickness indicates strength of dependence (Kendall's τ), and node color designates community membership. Key central nodes include Fuzhou (53), Luoyang (43), and Guangzhou (30), which display heightened betweenness centrality and serve as critical risk transmission hubs during market stress periods.

in one city can reach any other city in fewer than three steps, underscoring the potential for swift contagion effects in the Chinese real estate market. This observation highlights the need for prompt and coordinated responses to localized market disturbances, as their effects can quickly propagate throughout the system.

A particularly interesting feature of the network is its high modularity score of 0.746, with the community detection algorithm identifying nine distinct communities. This community structure suggests that the risk contagion network is characterized by clusters of cities with stronger within-group connections and weaker between-group linkages. Such a structure may reflect regional or economic similarities among cities within each community, potentially due to shared economic fundamentals, policy environments, or geographical proximity. This finding has significant implications for both risk assessment and policy design, suggesting that risk mitigation strategies may need to be tailored to specific city clusters rather than applied uniformly across the national market.

The network's structure, characterized by its tree-like nature, provides a clear representation of the most critical risk transmission pathways in the Chinese real estate market. While this approach necessarily simplifies some aspects of the market's complex dynamics, it offers a powerful tool for identifying the primary channels through which risks are likely to propagate. This information is invaluable for policymakers and market participants seeking to monitor and manage systemic risks in the real estate sector.

Identification of Key Cities and Their Roles in Risk Transmission

To identify the pivotal cities in the risk contagion network, we employ various centrality measures. Table 2.3 presents the top five cities for each centrality metric.

The centrality analysis reveals several key insights with significant implications for understanding risk transmission in China's real estate market:

1) Wuhan, Nanning, Xuzhou, and Yantai consistently rank among the top cities across all centrality measures, indicating their crucial roles in the risk contagion network. These cities serve as major hubs for risk transmission, potentially due to their economic importance or strategic positions in regional networks. The prominence of these cities, which are not typically classified as first-tier, suggests that the dynamics of risk transmission in the Chinese real estate market are more complex than a simple hierarchy based on city tiers.

2) Nanning exhibits the highest betweenness and closeness centrality, suggesting its critical role as an intermediary in risk transmission pathways and its ability to quickly influence or be influenced by other cities in the network. This finding underscores the importance of considering not only the size or economic output of a city, but also its position in the network of market relationships when evaluating its systemic significance.

3) The high betweenness centrality of cities like Yantai and Xuzhou indicates their crucial role in bridging different parts of the network. These cities may act as conduits for

Table 2.3: Top Five Cities by Centrality Measures in China's Real Estate Risk Contagion Network (2006–2023)

Centrality Measure	**City Rankings**				
	1st	**2nd**	**3rd**	**4th**	**5th**
Degree Centrality					
Cities	Wuhan	Nanning	Xuzhou	Yantai	Xining
Values	6	6	6	6	5
Betweenness Centrality					
Cities	Nanning	Yantai	Xuzhou	Wuhan	Fuzhou
Values	1,693	1,301	1,032	942	728
Closeness Centrality					
Cities	Nanning	Yantai	Wuhan	Xuzhou	Ningbo
Values	0.00917	0.00846	0.00798	0.00788	0.00728

Note: This table presents the top five cities ranked by three centrality measures in China's real estate risk contagion network. Degree centrality indicates the number of direct connections. Betweenness centrality measures a city's role as an intermediary in risk transmission paths. Closeness centrality reflects the speed of risk propagation from a city to all others in the network. Higher values indicate greater systemic importance in the risk contagion network.

risk transmission between different regional clusters, suggesting that they could be key points for monitoring and intervening in the spread of market risks.

The vine copula results provide additional insights into the strongest pairwise dependencies in the network, as shown in Table 2.4.

Table 2.4: Strongest Risk Transmission Channels: Key Pairwise Dependencies from the Vine Copula Model

City Pair	**Copula**	**Kendall's τ**	**Dependence Structure**
Shanghai–Hangzhou	Gaussian	0.55	Symmetric dependence
Nanning–Xuzhou	Frank	0.56	Weak tail dependence
Nanjing–Shanghai	Gumbel	0.54	Upper tail dependence
Wuhan–Zhengzhou	Gumbel	0.53	Upper tail dependence
Yantai–Nanning	Frank	0.51	Weak tail dependence

Note: Kendall's $\tau \in [0,1]$ measures the ordinal association between city pairs, with values closer to 1 indicating stronger dependence. *Copula families*: Gumbel—captures asymmetric upper tail dependence, relevant for modeling co-movements during market booms; Gaussian—models symmetric dependence without tail emphasis; Frank—captures symmetric dependence with weak tail behavior, suitable for moderate co-movements.

These strong pairwise connections often link economically significant cities or cities within the same region, highlighting the importance of both economic ties and geographical proximity in shaping the risk contagion structure. The variety of copula families used to model these dependencies (Gaussian, Gumbel, Frank) suggests complex and diverse

relationships between city pairs, potentially reflecting different underlying economic linkages or market dynamics.

A particularly noteworthy finding is the emergence of non-first-tier cities like *Fuzhou* and *Luoyang* as central nodes in the risk network. Their prominence is not explained by economic scale alone but by their structural roles within the risk network. Fuzhou's high betweenness centrality (1,375 in the high-risk state) suggests it acts as a critical intermediary. This may stem from its unique position as the core city of the Haixi Economic Zone, where real estate market dynamics are influenced by a distinct mix of national policies and cross-strait investment flows, creating a unique risk transmission pathway. Luoyang's centrality, while more surprising, may reflect its role as a major industrial base whose real estate market is highly sensitive to national industrial policies and commodity price cycles, thus propagating these specific shocks throughout the network.

The identification of these key cities and strong pairwise dependencies provides valuable information for both policymakers and market participants. For policymakers, it suggests that monitoring and intervention strategies should focus not only on the largest or most economically prominent cities but also on those that play crucial roles in the risk transmission network. For market participants, understanding these network dynamics can inform investment strategies and risk management practices, allowing for more nuanced approaches to diversification and risk assessment.

In conclusion, our analysis reveals a complex and nuanced structure of risk contagion in China's real estate market. The network is characterized by sparse yet efficient connections, a strong community structure, and a risk transmission dynamic that does not strictly adhere to conventional notions of city importance. These findings provide valuable insights for risk assessment, policy formulation, and further research into the dynamics of China's real estate market. By identifying key transmission nodes and pathways, this network analysis offers a powerful tool for understanding and managing systemic risks in this crucial sector of the Chinese economy.

2.4.3 Dynamic Characteristics of Risk Contagion Networks under High-Risk and Low-Risk States

This section examines the structural and dynamic characteristics of risk contagion networks in China's real estate market under different risk regimes. We employ a Markov regime-switching model in conjunction with our vine copula approach to identify distinct market states and analyze the corresponding network structures.

Identification of Market Regimes and Dynamic Characteristics of Risk State Transitions

We begin by estimating a two-state Markov switching model to identify high-risk and low-risk regimes in China's real estate market. Table 2.5 presents the results of this analysis.

Table 2.5: Two-State Markov Regime-Switching Model Results for China's Housing Market

Parameter	**State 1 (High-Risk Regime)**	**State 2 (Low-Risk Regime)**
Model Parameters		
Intercept (α_i)	0.2740	0.6144
Standard deviation (σ_i)	0.1060	0.1073
Transition Probability Matrix		
P_{11}	0.9260	—
P_{21}	0.0740	—
P_{12}	—	0.0304
P_{22}	—	0.9696
Regime Characteristics		
Expected duration (months)	13.51	32.89
Unconditional probability	0.2913	0.7087

Note: Estimation results from a two-state Markov regime-switching model applied to China's housing market returns (2006–2023). State 1 represents a high-risk regime with lower expected returns; State 2 represents a low-risk regime with higher expected returns. P_{ij} denotes the probability of transitioning from state j to state i. Expected duration = $(1-P_{ii})^{-1}$. Unconditional probabilities represent the long-run proportion of time spent in each regime.

The expected duration for each regime, which reflects the persistence of market conditions, is computed as $E[D_i] = 1/(1 - P_{ii})$, where P_{ii} is the probability of remaining in regime i. This measure indicates how long, on average, the system tends to stay in a given state before switching. Based on the estimates, the high-risk regime has an expected duration of approximately 13.5 months, suggesting relatively frequent shifts away from unstable market conditions. In contrast, the low-risk regime is considerably more persistent, with an expected duration of nearly 33 months, implying that stable periods dominate the long-run dynamics of China's housing market.

The model identifies two distinct regimes: a high-risk state (State 1) characterized by lower returns and higher volatility, and a low-risk state (State 2) with higher returns and slightly lower volatility. The analysis of risk state transitions reveals several important dynamic features:

1. *Persistence of States*: Both states exhibit high persistence, with $P(High|High) = 0.9260$ and $P(Low|Low) = 0.9696$, indicating that both high-risk and low-risk regimes tend to persist once established.

2. *Asymmetric Transition Patterns*: The probability of transitioning from low-risk to high-risk ($P(High|Low) = 0.0304$) is lower than the probability of transitioning from high-risk to low-risk ($P(Low|High) = 0.0740$), suggesting a slight tendency for the market to revert to a low-risk state.

3. *Expected Duration of States*: Based on the transition probabilities, the expected duration of the high-risk state is approximately 13.5 months, while the low-risk state has an expected duration of about 32.9 months, indicating longer periods of stability interrupted by shorter periods of market stress.

Figure 2.2 illustrates the smoothed probabilities of high-risk and low-risk states over the sample period, highlighting the temporal dynamics of risk regimes in China's real estate market.

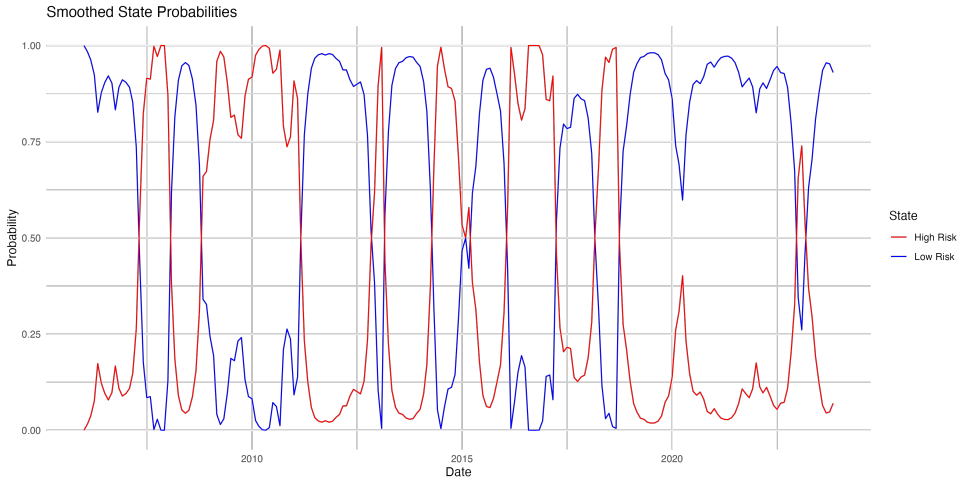

Figure 2.2: Regime Identification in China's Housing Market (2006–2023): Smoothed Probabilities of High-Risk and Low-Risk States

Note: This figure displays the smoothed probabilities of the two-state Markov regime-switching model estimated for China's real estate market. The blue shaded areas represent the probability of being in the high-risk state (State 1), characterized by lower returns and potentially stronger risk contagion between cities.

Network Characteristics in High-Risk State

In the high-risk state, the risk contagion network exhibits several distinctive features:

1. *Network Connectivity*: While maintaining the same number of edges (69) as the overall network, the high-risk state displays significantly different connectivity patterns.

2. *Stronger Pairwise Dependencies*: The high-risk state is characterized by generally stronger pairwise dependencies. For instance, the connection between Xi'an and Sanya exhibits a Kendall's τ of 0.58, compared to 0.36 in the low-risk state.

3. *Emergence of New Central Nodes*: Cities such as Fuzhou (53), Luoyang (43), and Guangzhou (30) gain prominence in the high-risk network, suggesting a shift in risk transmission pathways during market stress.

4. *Increased Average Path Length*: The average path length increases to 6.67, indicating that risk transmission becomes more complex and indirect during high-risk periods.

Table 2.6 presents the top 5 cities by centrality measures in the high-risk state.

Table 2.6: Central Nodes in Risk Contagion Network During High-Risk State

Centrality Measure	**Top Five Cities (Ranked)**				
	1st	**2nd**	**3rd**	**4th**	**5th**
Degree Centrality *(number of direct connections)*					
Cities	Fuzhou*	Luoyang†	Guangzhou	Chengdu	Zhanjiang
Values	10	6	6	5	5
Betweenness Centrality *(intermediary role in risk paths)*					
Cities	Fuzhou*	Wuhan†	Beihai	Taiyuan†	Luoyang†
Values	1,375	1,373	1,337	1,215	1,115
Closeness Centrality *(speed of risk propagation)*					
Cities	Wuhan†	Taiyuan†	Fuzhou*	Beihai	Anqing
Values	0.003,30	0.003,26	0.003,19	0.003,17	0.002,95

Note: Network structure during high-risk states (State 1 from the Markov regime-switching model). * indicates that Fuzhou appears in all three centrality rankings, demonstrating its systemic importance during market stress. † denotes cities appearing in multiple centrality measures. The concentration of high centrality values suggests a more hierarchical network structure during crisis periods.

Network Characteristics in Low-Risk State

The low-risk state network demonstrates markedly different characteristics:

1. *Shift in Central Nodes*: Cities such as Nanning (12), Xi'an (58), and Harbin (18) become more central in the low-risk state.

2. *Weaker Pairwise Dependencies*: The low-risk state generally shows weaker dependencies between cities. For instance, the strongest connection (Shanghai-Nanjing) has a Kendall's τ of 0.54, lower than many of the strongest connections in the high-risk state.

3. *Decreased Average Path Length*: The average path length decreases to 6.40, suggesting more direct risk transmission pathways in stable market conditions.

Table 2.7 presents the top 5 cities by centrality measures in the low-risk state.

Table 2.7: Central Nodes in Risk Contagion Network During Low-Risk State

Centrality Measure	**Top Five Cities (Ranked)**				
	1st	**2nd**	**3rd**	**4th**	**5th**
Degree Centrality *(number of direct connections)*					
Cities	Xi'an	Xuzhou*	Harbin	Yantai*	Zhengzhou
Values	6	5	5	5	4
Betweenness Centrality *(intermediary role in risk paths)*					
Cities	Nanning	Fuzhou	Huizhou	Xuzhou*	Yantai*
Values	1,511	1,424	1,245	1,014	925
Closeness Centrality *(speed of risk propagation)*					
Cities	Nanning	Huizhou	Fuzhou	Xuzhou*	Yantai*
Values	0.003,68	0.003,62	0.003,50	0.003,29	0.003,25

Note: Network structure during low-risk states (State 2 from the Markov regime-switching model). * indicates cities that appear in all three centrality rankings, suggesting their robust importance across different network perspectives. Low-risk periods are characterized by more dispersed network connectivity compared to high-risk states.

Comparative Analysis of Network Structures

The comparison between high-risk and low-risk states reveals significant structural shifts, which are visually represented in Figures 2.3 and 2.4.

As evident from these network visualizations, there are notable differences in the risk transmission structures between the two states:

1. *Network Connectivity*: While both networks maintain the same number of edges (69), the high-risk state (Figure 2.3) shows denser connections among certain city clusters, particularly around central nodes like Fuzhou (53) and Wuhan (39). In contrast, the low-risk state (Figure 2.4) exhibits a more distributed connectivity pattern.

2. *Centrality Shifts*: Different cities emerge as central nodes in each state. In the high-risk state, Fuzhou (53), Luoyang (43), and Guangzhou (30) play crucial roles, as evidenced by their central positions and numerous connections. The low-risk state sees Xi'an (58), Xuzhou (31), and Nanning (12) taking more central positions.

3. *Cluster Formation*: The high-risk network shows more pronounced clustering, with tighter groups of interconnected cities. This is particularly noticeable around nodes like Fuzhou (53) and Wuhan (39). The low-risk network, while still showing some clustering, has a more dispersed structure.

4. *Edge Strength*: The thickness of edges in the high-risk network generally appears greater, indicating stronger pairwise dependencies. This aligns with our earlier observation of more frequent use of t-copulas and Gumbel copulas in the high-risk state, suggesting stronger tail dependencies and asymmetric risk transmission.

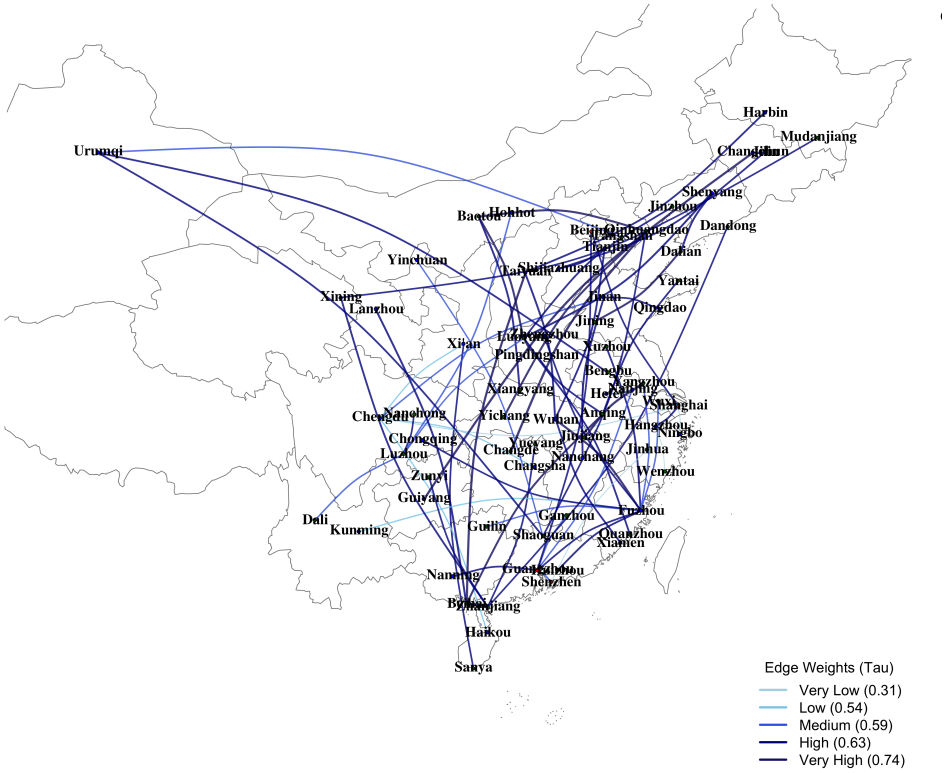

Figure 2.3: Risk Contagion Network Structure During High-Risk State (2006–2023)

Note: This figure visualizes the risk contagion network during high-risk periods in China's housing market. Node size represents degree centrality, edge thickness indicates strength of risk transmission (Kendall's τ), and node color represents city tier (red = first-tier, blue = second-tier, green = third-tier). The network exhibits a higher density (0.0355) and more pronounced clustering around key nodes like Fuzhou (53), Wuhan (39), and Guangzhou (30), reflecting intensified risk transmission channels during market stress.

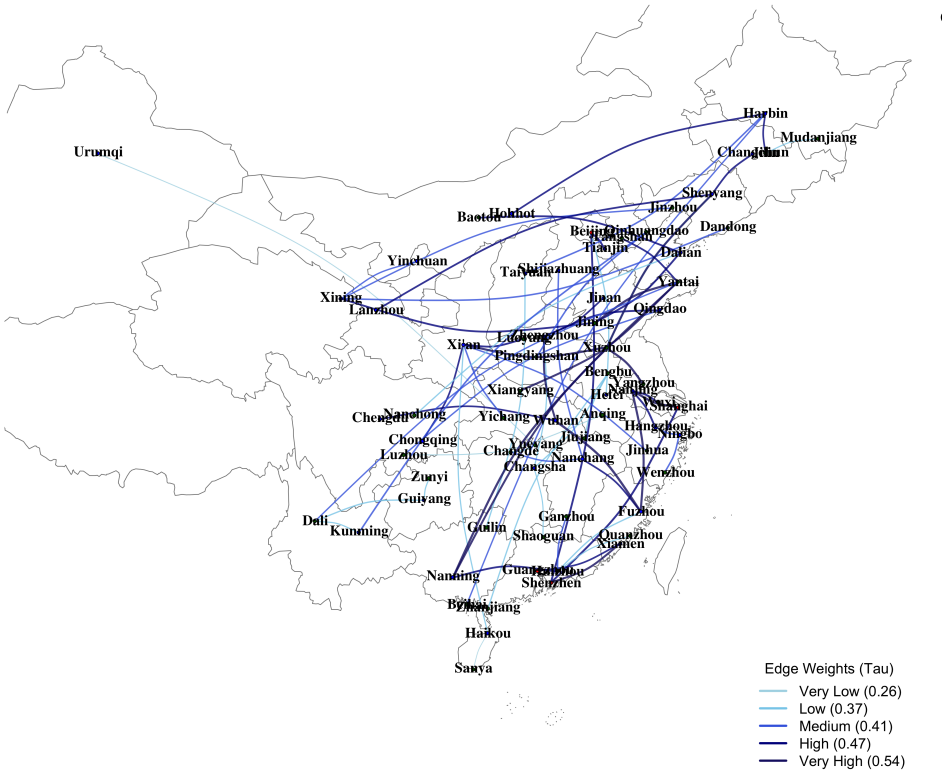

Figure 2.4: Risk Contagion Network Structure During Low-Risk State (2006–2023)

Note: This figure depicts the risk contagion network during low-risk periods. Compared to the high-risk state, this network exhibits lower density (0.0307) and a more distributed structure with different cities (Xi'an (58), Nanning (12), Xuzhou (31)) emerging as central nodes. The weaker connections and more dispersed arrangement suggest more localized and contained risk transmission during stable market conditions. This structural shift highlights the state-dependent nature of housing market risk contagion in China.

5. *Periphery Structure*: The high-risk network has fewer isolated or peripheral nodes, suggesting that more cities become integral to the risk transmission process during turbulent periods. In contrast, the low-risk network shows more cities in peripheral positions, indicating a more localized risk transmission pattern during stable periods.

These structural differences underscore the need for adaptive risk management strategies that can respond to the evolving network topology as market conditions change. The shift in central nodes and the varying intensity of connections between states suggest that policymakers and market participants should be prepared to adjust their focus and strategies as the market transitions between high-risk and low-risk regimes.

Furthermore, the more pronounced clustering in the high-risk state implies that targeted interventions in key cities or city clusters could potentially have a significant impact on mitigating systemic risk during turbulent periods. Conversely, the more distributed structure in the low-risk state suggests that broader, market-wide policies may be more appropriate during stable periods.

In conclusion, our analysis reveals that the risk contagion network in China's real estate market undergoes substantial structural changes as it transitions between high-risk and low-risk states. These changes are characterized by shifts in central nodes, varying connection strengths, and differing cluster formations. Understanding these dynamic network characteristics is crucial for developing effective, state-dependent strategies for risk management and policy formulation in China's complex and evolving real estate market.

2.4.4 State-Dependent Impact of Macroeconomic Factors on Housing Market Risk

This section examines how macroeconomic factors influence risk state transitions in China's real estate market and their implications for the risk contagion network structure. We employ a Markov switching model with time-varying transition probabilities and conduct complex network analysis to elucidate the dynamic relationship between economic conditions and housing market risks.

Regime Identification and Transition Dynamics

Our Markov switching model identifies two distinct regimes in China's housing market: a high-risk state (Regime 1) and a low-risk state (Regime 2). Figure 2.5 illustrates the smoothed probabilities of these states over the sample period.

The estimated transition probabilities (P(Regime 1 | Regime 1) = 0.8537, P(Regime 2 | Regime 2) = 0.8720) indicate high persistence in both regimes, with slightly higher persistence in the low-risk state. This suggests that both high-risk and low-risk conditions in the Chinese housing market tend to persist once established.

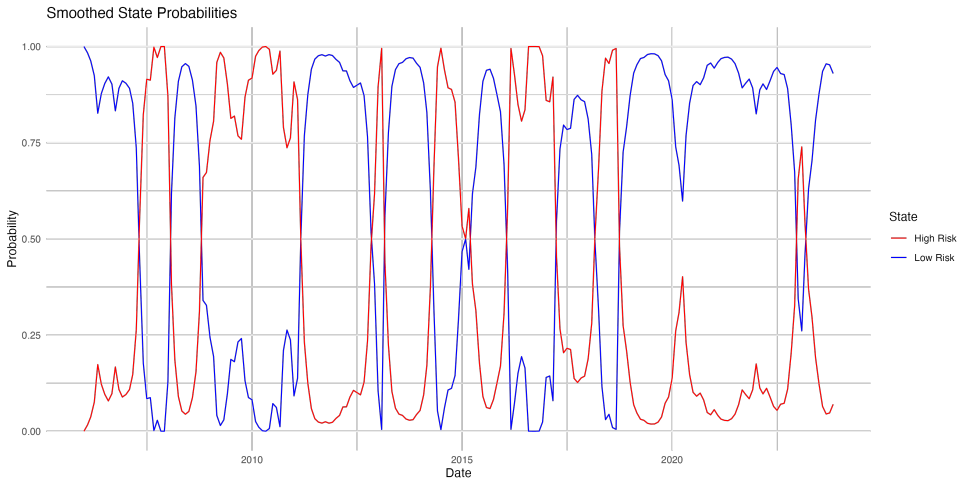

Figure 2.5: Time-Varying Smoothed Probabilities of Risk Regimes in China's Housing Market (2006-2023). This figure displays the estimated probabilities from the two-state Markov regime-switching model. The high-risk state (State 1) is characterized by lower returns and higher volatility, while the low-risk state (State 2) exhibits higher returns and slightly lower volatility.

Asymmetric Effects of Macroeconomic Factors Across Regimes

Table 2.8 presents the estimation results of our Markov switching model, revealing significant heterogeneity in the impact of macroeconomic factors across the two regimes.

In the high-risk regime, monetary policy (one-year loan rate) exhibits a strong negative effect (-0.2377, $p < 0.001$) on housing prices, suggesting that tighter monetary conditions exert downward pressure during market stress. Unemployment demonstrates a substantial negative effect (-0.5863, $p < 0.01$), underscoring the critical role of labor market stability. Conversely, fixed asset investment (0.0183, $p < 0.01$) and Manufacturing PMI (0.0381, $p < 0.01$) show positive effects, indicating their role in supporting housing prices even during turbulent periods.

In the low-risk regime, fewer macroeconomic factors show significant impacts. Notably, the one-year loan rate exhibits a positive effect (0.0571, $p < 0.05$), contrary to its impact in the high-risk regime. This suggests that during stable periods, higher interest rates may reflect overall economic strength. Industrial value added (0.0048, $p < 0.05$) and Manufacturing PMI (0.0120, $p < 0.001$) maintain positive effects, highlighting the consistent influence of industrial performance on housing prices.

Evolving Network Structure Under Different Risk Regimes

Complex network analysis reveals distinct patterns in the risk contagion network structure under high-risk and low-risk states. Figures 2.6 and 2.7 illustrate these structural differences. Table 2.9 summarizes key network metrics for both states.

In the high-risk state, the network exhibits higher connectivity (average degree: 2.45)

Table 2.8: State-Dependent Effects of Macroeconomic Factors on Housing Market Dynamics

	High-Risk Regime		Low-Risk Regime	
Variable	**Coef.**	**SE**	**Coef.**	**SE**
Intercept	2.0432*	1.0963	0.3819	0.3665
Monetary Policy				
M2 Growth (%)	−0.0074	0.0078	0.0020	0.0042
Loan Rate, 1y (%)	−0.2377***	0.0466	0.0571*	0.0254
Bond Yield, 10y (%)	0.0150	0.0194	0.0022	0.0095
Real Economy				
GDP Growth (%)	−0.0185*	0.0090	0.0003	0.0042
Unemployment (%)	−0.5863**	0.2182	−0.1914*	0.0861
Industrial VA (%)	−0.0083	0.0049	0.0048*	0.0023
Manufacturing PMI	0.0381**	0.0139	0.0120***	0.0034
Investment				
Fixed Asset Inv. (%)	0.0183**	0.0066	−0.0016	0.0027
Real Estate Inv. (%)	0.0068	0.0044	−0.0024	0.0020
Prices				
CPI (%)	0.0193	0.0162	−0.0149	0.0091
PPI (%)	−0.0153***	0.0045	−0.0089*	0.0044
Observations: 216	Log-likelihood: −142.76		AIC: 337.52	

Note: * $p < 0.05$, ** $p < 0.01$, *** $p < 0.001$. High-risk periods are characterized by strong negative responses to monetary tightening and economic slowdown, while low-risk periods show fundamentally different transmission mechanisms with positive loan rate effects suggesting normal market functioning.

Table 2.9: Structural Changes in Risk Contagion Networks Across Market Regimes

Network Measure	**High-Risk State**	**Low-Risk State**	**Change (%)**
Connectivity Measures			
Average degree	2.45	2.12	+15.6
Network density	0.0355	0.0307	+15.6
Average path length	6.67	6.40	+4.2
Community Structure			
Number of communities	7	9	−22.2
Modularity	0.6823	0.7124	−4.2

Note: Network topology measures calculated from the estimated risk contagion networks in each market regime. The high-risk state shows increased connectivity (+15.6% in both degree and density) but fewer, less distinct communities. The lower modularity during high-risk periods indicates stronger cross-regional spillovers, consistent with systemic risk amplification during market stress.

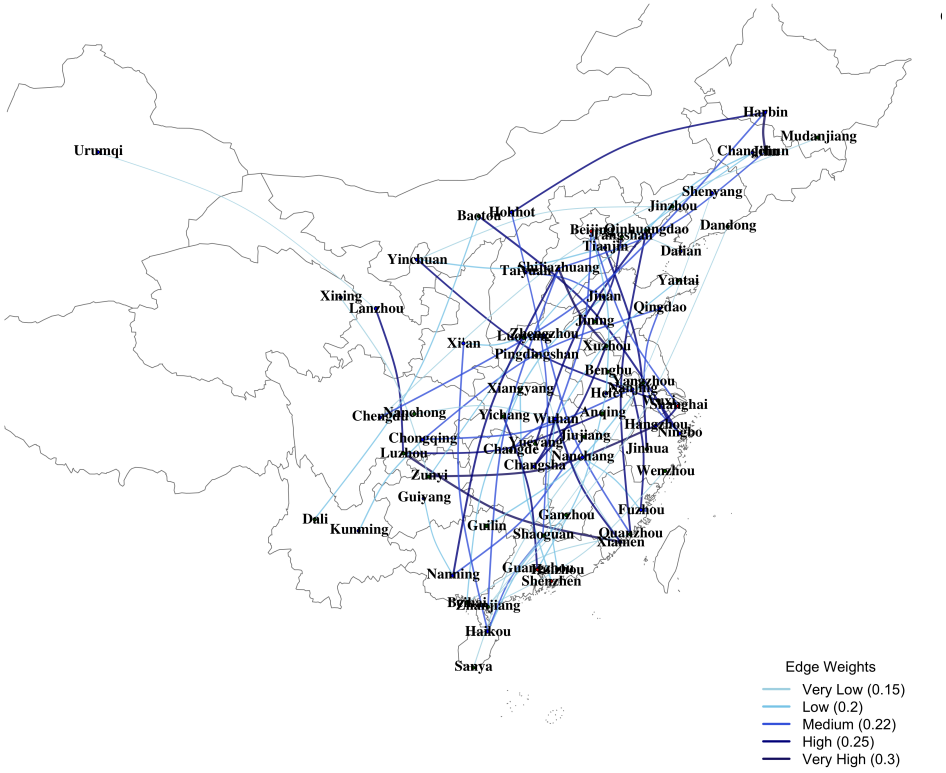

Figure 2.6: Macroeconomic-Driven Risk Contagion Network in Chinese Housing Market (High-Risk State)

Note: This figure visualizes the risk contagion network structure during high-risk periods when accounting for macroeconomic factors. Nodes represent cities with size proportional to betweenness centrality, and edges indicate significant risk transmission channels with thickness reflecting dependence strength. The network exhibits increased density (0.0355) and stronger interconnections, with cities like Fuzhou (53), Wuhan (39), and Beijing (8) emerging as key transmission hubs. This pattern suggests that during economic downturns, risk contagion intensifies and becomes more concentrated through specific metropolitan centers.

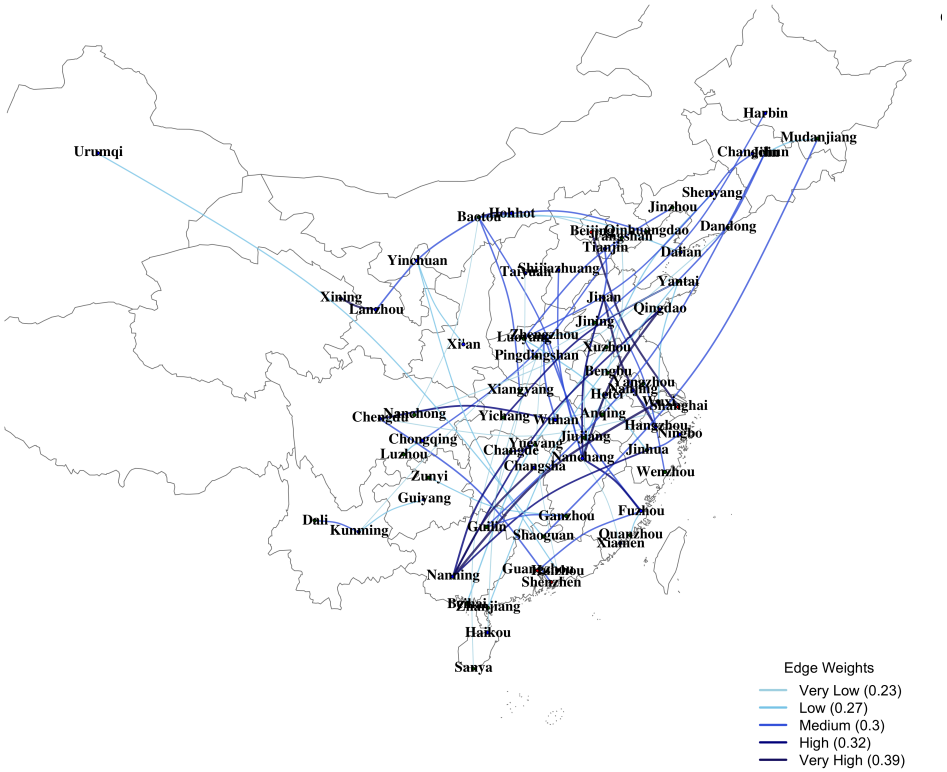

Figure 2.7: Macroeconomic-Driven Risk Contagion Network in Chinese Housing Market (Low-Risk State)

Note: This figure presents the risk contagion network during low-risk periods with macroeconomic influences incorporated. Compared to the high-risk network, this structure shows lower density (0.0307), more dispersed connections, and different central nodes (Nanchang (13), Nanning (12), Qingdao (69)). The more fragmented community structure (modularity 0.7124) reflects regional segmentation of housing markets during stable economic conditions, when local factors tend to dominate over system-wide influences, resulting in more contained risk transmission channels.

and a longer average path length (6.67), suggesting more complex risk transmission pathways. Cities like Fuzhou (53), Wuhan (39), and Beijing (8) emerge as central nodes, as evidenced by their high betweenness centrality scores (1446, 1400, and 1375, respectively).

Conversely, the low-risk state network demonstrates a more distributed structure with lower connectivity (average degree: 2.12) and shorter average path length (6.40). Cities such as Nanchang (13), Nanning (12), and Qingdao (69) gain prominence, with betweenness centrality scores of 1697, 1369, and 1160, respectively.

The shift in central nodes between regimes indicates that risk transmission channels change with macroeconomic conditions. The higher modularity in the low-risk state (0.7124 vs 0.6823) suggests more distinct community structures during stable periods, potentially reflecting regional economic clusters.

These findings highlight the complex interplay between macroeconomic factors, risk states, and the structure of risk contagion in China's housing market. They provide evidence for the necessity of state-dependent policy approaches that consider both prevailing economic conditions and the changing dynamics of risk transmission across cities. Future research could further explore the mechanisms through which macroeconomic factors influence network structure and the potential for targeted interventions in key cities to mitigate systemic risk during periods of market stress.

2.5 Robustness Checks

To validate the reliability and stability of our main results, we conduct a comprehensive analysis by city tiers, considering the hierarchical nature of the Chinese urban system. This robustness check examines whether risk contagion patterns differ significantly across different tiers of cities and how these patterns evolve under various market conditions.

Following the official classification criteria of the National Bureau of Statistics of China, we categorize the 70 sample cities into three tiers based on their economic development level, population size, and other socioeconomic factors: 4 first-tier cities, 31 second-tier cities, and 35 third-tier cities. This classification allows us to investigate the heterogeneity in housing price dynamics and risk contagion patterns across the urban hierarchy.

We begin by examining the heterogeneity in housing price growth rates across city tiers. Figure 2.8 presents the box plots and time series of monthly housing price growth rates for each city tier.

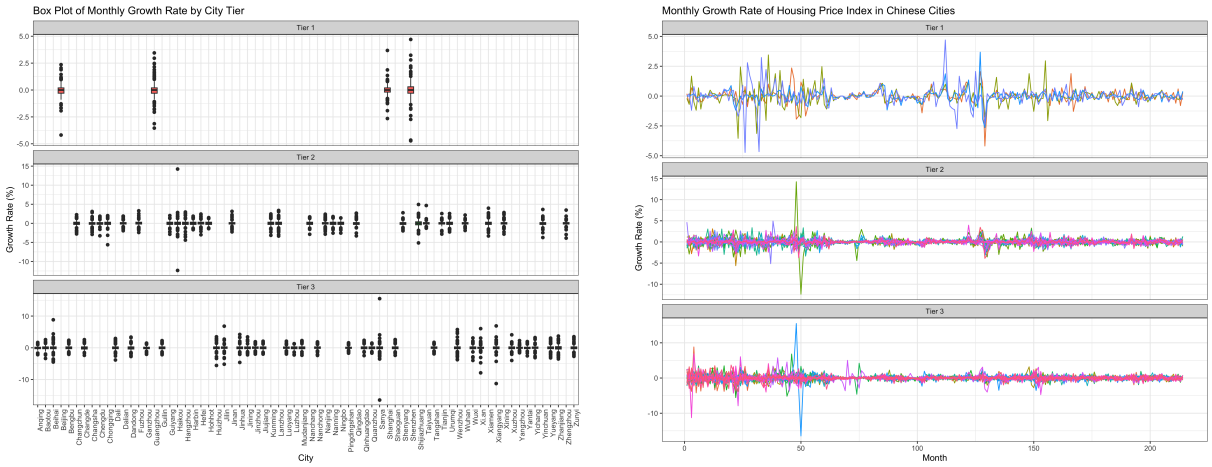

(a) Distribution of Monthly Growth Rates by City Tier

(b) Temporal Evolution of Monthly Growth Rates by City Tier (2006–2023)

Figure 2.8: Heterogeneity in Housing Price Dynamics Across China's Tiered Urban System

Note: This figure illustrates the heterogeneous patterns in housing price dynamics across China's tiered urban system. Panel (a) shows that first-tier cities exhibit higher median growth rates and larger interquartile ranges, indicating both higher returns and greater volatility. Second-tier and third-tier cities demonstrate more moderate growth rates with narrower distributions. Panel (b) reveals that first-tier cities experience more pronounced fluctuations over time, suggesting greater sensitivity to macroeconomic shocks and policy changes, while lower-tier cities show relatively smoother growth trajectories. This hierarchical pattern in market volatility corresponds to the differentiated risk transmission roles observed in the network analysis.

The analysis reveals distinct patterns across city tiers. First-tier cities exhibit higher median growth rates and larger interquartile ranges, indicating both higher returns and greater volatility. Second-tier and third-tier cities generally experience lower median growth rates with narrower interquartile ranges, suggesting more stable but modest price appreciation. The time series plot further illustrates that first-tier cities demonstrate more pronounced fluctuations over time, potentially reflecting greater sensitivity to market

shocks and policy changes. In contrast, lower-tier cities show relatively smoother growth patterns, indicating higher resilience to external disturbances.

To examine the risk contagion patterns across city tiers, we employ hierarchical copula models. Table 2.10 presents the Equidependence Gaussian Copula estimates for each city tier.

Table 2.10: Intra-tier Dependence Structure: Gaussian Copula Parameter Estimates

	City Tier		
Parameter	First-tier	Second-tier	Third-tier
ρ	0.4463	0.2847	0.2080
	(0.0330)	(0.0130)	(0.0130)

Notes: This table reports the Gaussian copula correlation parameter (ρ) estimates for each city tier. Standard errors are reported in parentheses. The significantly higher correlation parameter for first-tier cities indicates stronger market integration and potential for rapid risk transmission compared to lower-tier cities.

The results indicate the strongest intra-tier correlation in first-tier cities ($\rho = 0.4463$), suggesting high market integration and potential for rapid risk transmission. Second-tier ($\rho = 0.2847$) and third-tier ($\rho = 0.2080$) cities exhibit weaker intra-tier correlations, indicating more fragmented housing market structures.

To capture the cross-tier risk contagion dynamics, we employ vine copula models for full-sample, high-risk, and low-risk periods. Tables 2.11, 2.12, and 2.13 present the estimation results for these periods, respectively.

Table 2.11: Cross-Tier Risk Contagion: Vine Copula Estimation Results for Full Sample Period

Tree	Edge	Copula Family	Parameter (θ)	Kendall's τ
1	(Tier 1, Tier 2)	Clayton	0.11	0.05
1	(Tier 2, Tier 3)	Rotated Clayton	0.09	-0.04
2	(Tier 1, Tier 3|Tier 2)	Gaussian	-0.05	-0.03

Notes: This table presents the estimated parameters of the vine copula model for the entire sample period (2006-2023). Tier 1 includes 4 first-tier cities, Tier 2 includes 31 second-tier cities, and Tier 3 includes 35 third-tier cities. Positive values of Kendall's τ indicate positive dependence between tiers, while negative values indicate negative dependence.

The vine copula analysis reveals several key findings. In the full sample, we observe weak but significant upper tail co-movements between first and second-tier cities ($\tau = 0.05$), while the negative tail dependence between second and third-tier cities ($\tau = -0.04$) suggests potential risk diversification benefits. During high-risk periods, the tail dependence between adjacent tiers intensifies dramatically, with τ reaching 0.62 for the first-second tier pair and 0.85 for the second-third tier pair. This indicates rapid risk propagation through the

Table 2.12: Cross-Tier Risk Contagion: Vine Copula Estimation Results for High-Risk State

Edge	Copula Family	Parameter (θ)	Kendall's τ
(Tier 1, Tier 2)	Gaussian	0.83	0.62
(Tier 2, Tier 3)	Gaussian	0.97	0.85
(Tier 1, Tier 3|Tier 2)	Rotated Gumbel	-1.54	-0.35

Notes: This table presents the estimated parameters of the vine copula model during high-risk periods identified by the Markov regime-switching model. The substantial increase in Kendall's τ values compared to the full sample estimates indicates stronger risk contagion across city tiers during market stress.

Table 2.13: Cross-Tier Risk Contagion: Vine Copula Estimation Results for Low-Risk State

Edge	Copula Family	Parameter (θ)	Kendall's τ
(Tier 1, Tier 2)	Survival Gumbel	2.68	0.63
(Tier 2, Tier 3)	Gaussian	0.98	0.86
(Tier 1, Tier 3|Tier 2)	Rotated Gumbel	-1.71	-0.42

Notes: This table presents the estimated parameters of the vine copula model during low-risk periods identified by the Markov regime-switching model. While Kendall's τ values remain high, the change in copula families (particularly for the Tier 1-Tier 2 relationship) suggests different dependence structures compared to high-risk periods.

urban hierarchy under stressed market conditions. The asymmetric pattern underscores the nonlinear and state-dependent nature of housing price risk contagion across city tiers.

To visualize these complex risk contagion patterns, we construct a cross-tier risk contagion network based on the vine copula results. Figure 2.9 presents the network structure derived from the full-sample estimation.

The network analysis reveals the stability of the hierarchical structure of risk contagion (Tier1 – Tier2 – Tier3) across different risk states. The connections between tiers illustrate the potential pathways for risk transmission, with the strength of connections varying according to market conditions. This visualization provides an intuitive understanding of the complex interdependencies in China's tiered urban housing markets.

These findings confirm and extend our main results, highlighting the crucial role of the hierarchical structure of the Chinese urban system in housing market risk contagion. The analysis demonstrates significant heterogeneity in risk contagion patterns across city tiers, with first-tier cities showing stronger market integration and potential for rapid risk transmission. While the intensity of risk linkages varies between high- and low-risk periods, the fundamental cross-tier risk transmission mechanism remains relatively stable.

This robustness check underscores the importance of adopting a system-wide perspective in monitoring and assessing housing market risks, considering the interdependence and potential spillovers among city tiers. Policy measures aimed at mitigating risk contagion

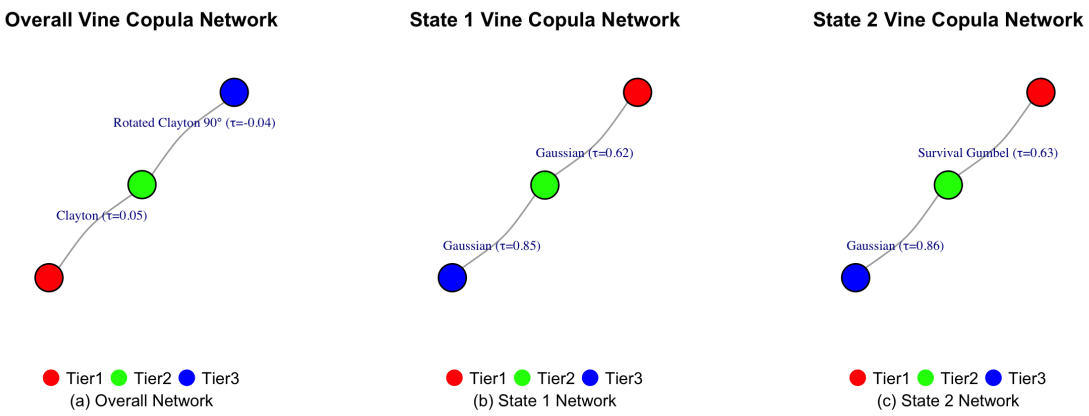

Figure 2.9: Hierarchical Risk Contagion Network in China's Real Estate Market

Notes: This network visualization represents the risk transmission structure across China's tiered urban housing markets. Nodes represent city tiers (Tier 1: first-tier cities; Tier 2: second-tier cities; Tier 3: third-tier cities), while edges indicate significant risk linkages estimated from the vine copula model. Edge thickness corresponds to the strength of dependence (Kendall's τ), with thicker edges indicating stronger risk transmission channels. The hierarchical structure (Tier 1–Tier 2–Tier 3) remains stable across different market regimes, though the intensity of connections varies according to market conditions. This visualization illustrates the complex interdependencies in China's urban housing system and potential pathways for risk propagation.

should consider both the stable interdependence properties of the urban hierarchy and the time-varying intensity of risk linkages. Our analysis not only validates the robustness of our main findings but also provides deeper insights into the complex dynamics of housing market risk contagion in China's hierarchical urban system.

2.6 Conclusion

This study offers a comprehensive and dynamic characterization of risk contagion in China's housing market by integrating advanced copula-based dependency modeling, Markov regime-switching frameworks, and complex network analysis. Drawing on monthly data for 70 major Chinese cities from 2006 to 2023, our approach provides granular insights into how housing market risk is transmitted, how these patterns shift across different market regimes, and how macroeconomic conditions shape these dynamics.

Our empirical findings are quantitatively robust and multifaceted. First, we document that the housing market risk transmission network, while sparse (with an average network density of about 2.9%), still enables rapid contagion due to a short average path length of roughly 2.70. This metric indicates that even when fewer than 3% of all possible city pairs are directly connected, a shock originating in one city can propagate to others in fewer than three steps. Moreover, we find strong evidence of state dependence: during high-risk regimes, the network's average degree centrality rises from approximately 2.12 to 2.45, and the average path length increases from 6.40 to 6.67. Cities such as Fuzhou, Luoyang, and Guangzhou emerge as central hubs in turbulent periods, supplanting the influence of other nodes that dominate in low-risk states. Tail dependencies also intensify in these high-risk conditions: for instance, Kendall's τ between certain city pairs increases by more than 0.20 when shifting from tranquil to stressed regimes, underscoring the nonlinear and asymmetric nature of contagion.

Second, our Markov regime-switching analysis reveals that transitions into high-risk states, while initially low in probability (around 3% from a low-risk regime), become more likely under deteriorating macroeconomic fundamentals. The integration of macroeconomic variables into transition probabilities shows that a one-percentage-point decline in GDP growth or a tightening of monetary policy (e.g., higher one-year loan rates) significantly elevates the probability of entering a high-risk state. These macroeconomic shifts not only raise the systemic vulnerability but also reshape the network: average Kendall's τ between key city pairs increases by up to 0.10- 0.20 during periods of economic slowdown, and previously peripheral nodes gain prominence as intermediaries of contagion.

Third, the hierarchical structure of China's urban system has substantial implications for risk transmission. Contrary to conventional assumptions, centrality metrics consistently identify not only top-tier cities but also select second- and third-tier cities (e.g., Nanning, Xuzhou, Yantai) as pivotal transmission hubs. For instance, the betweenness centrality of Nanning reaches as high as 1697 in the low-risk state and remains elevated in turbulent periods, indicating its stable role as a conduit of shocks. Such findings highlight the need for broader risk surveillance that moves beyond a narrow focus on first-tier cities, recognizing that systemic vulnerabilities can arise in unexpected locales under certain regime conditions.

These quantitative insights yield meaningful policy implications. Regulators and market participants must adopt a state-contingent perspective when implementing macroprudential measures. For example, during macroeconomic downturns or in anticipation of weaker industrial activity, targeted oversight in cities identified as high centrality nodes could mitigate systemic spillovers. Because tail dependencies and clustering intensify under stress, policies that enhance market resilience—such as improved liquidity channels or targeted credit controls—could be deployed preemptively in cities that exhibit sharp increases in network connectivity or centrality measures when entering a high-risk state.

While our study advances the understanding of regime-dependent, macro-driven risk transmission, it also invites further research. Future work might utilize micro-level transaction data to disentangle household behaviors or explore cross-national comparisons to determine how institutional differences moderate network resilience. Additionally, evaluating the effectiveness of specific policy interventions in reducing network density or weakening tail dependencies during high-risk episodes would provide actionable guidance for regulators.

In sum, by integrating detailed quantitative evidence with sophisticated empirical methods, this study offers a richer, data-driven perspective on how risk propagates through China's urban housing markets, how macroeconomic conditions influence these contagion patterns, and which cities serve as critical nodes in different states. Our findings underscore that housing market risk is inherently dynamic and hierarchical, necessitating nuanced, evidence-based strategies for monitoring and managing systemic vulnerabilities.

Chapter 3

Risk Transmission Mechanisms and International Integration in China's Carbon Market: A Multi-layer Network Analysis

3.1 Introduction

Carbon markets have emerged as a crucial policy instrument for addressing climate change through market-based mechanisms to control and reduce greenhouse gas emissions. Operating on the "polluter pays" principle, these markets internalize the negative externalities of emissions while providing flexibility in achieving the reduction target (Mansanet-Bataller and Pardo, 2008). As of January 2024, 28 carbon trading systems are operational worldwide, with more than 20 additional systems under development. These markets now encompass approximately 17% of global greenhouse gas emissions and 55% of global GDP, demonstrating their growing importance in global climate action (ICAP, 2022).

China, as the world's largest carbon emitter, plays a pivotal role in global climate change mitigation efforts(Liu et al., 2015; Dargusch, 2017).China has demonstrated significant progress in this arena, beginning with the establishment of seven regional pilot markets—*Beijing*, *Shanghai*, *Tianjin*, *Chongqing*, *Guangdong*, *Shenzhen*, and *Hubei*—which were launched between 2013 and 2014. A subsequent pilot in *Fujian* was introduced in late 2016, bringing the total to eight regional markets prior to the initiation of the national ETS. The country achieved a major milestone with the launch of its national carbon market on July 16, 2021, initially incorporating 2,162 power generation enterprises and covering over 4.5 billion tons of emissions in its first year(Jia et al., 2024). By December 2023, the national market had facilitated cumulative transactions of 442 million tons of carbon emission allowances, with a total transaction value of 24.919 billion yuan, establishing China as a significant player in global carbon trading and marking a new phase in market-based climate action (Xin-gang et al., 2023).

Despite the importance of this transition, current research falls short in several key areas. While extensive literature exists on established markets like the European Union ETS (EU ETS) (Ellerman et al., 2010; Mansanet-Bataller et al., 2007), the unique characteristics of China's evolving carbon market remain inadequately explored. Recent studies examining the initial impact of China's unified carbon market (Wu et al., 2023)have provided preliminary evidence of market integration effects(Wu et al., 2023). However, these studies primarily focus on price convergence, leaving the complex dynamics of risk transmission and network effects unexplored. The potential for both linear and non-linear dependencies and complex network effects in risk transmission has been largely overlooked in the context of emerging carbon markets. Moreover, the application of network theory to understand systemic risk in carbon markets remains limited, despite its proven utility in analyzing financial market interconnections (Acemoglu et al., 2015; Hautsch et al., 2015).

To address these critical gaps, this paper investigates the evolution of risk transmission mechanisms within China's carbon market and between China and international markets, particularly after the unification of China's national carbon market in 2021. Based on market integration theory and previous empirical evidence, we propose three main

hypotheses: First, market unification should significantly affect risk spillover intensity among regional markets due to enhanced interconnectedness. Second, the national market is expected to play a significant role in the risk transmission network, given its position as a unified trading platform. Third, international market integration should evolve while maintaining distinct domestic market characteristics due to regulatory differences.

Our investigation focuses on four interconnected research questions that test these hypotheses: (1) How has the national market unification altered risk transmission pathways and intensities among regional markets? (2) Which regions have emerged as key nodes in risk transmission within the unified structure? (3) What is the nature of risk transmission mechanisms between China's national market and the EU ETS? (4) To what extent has the integration between China's carbon market and international markets changed post-unification?

Our empirical analysis reveals significant changes in risk transmission pathways following the unification of China's carbon market. We find that after national market unification, the average risk spillover intensity between regional markets decreased by 5.60% (from 3.517 to 3.320), indicating evolving market dynamics. The national market emerged as a risk absorber with a net spillover of -3.013%, while maintaining moderate centrality (eigenvector centrality 0.412). In the international context, the EU ETS shifted from being a net risk receiver (-4.773%) to a net transmitter (15.828%), with strengthened linkages particularly with Beijing (0.077) and Guangdong (0.067) markets.

This study contributes to the literature in several ways. Theoretically, we extend the application of multi-layer network analysis to emerging carbon markets, building on the work of (Wu et al., 2022) to provide a novel framework for understanding complex risk dynamics in these evolving systems. Methodologically, we integrate multiple econometric techniques into a unified analytical framework, addressing the challenges of market heterogeneity and evolving trading relationships identified in recent studies (Yang et al., 2024). Empirically, we provide the first comprehensive evidence on the changing nature of risk transmission in China's transitioning carbon market, contributing to the broader literature on market structure and systemic risk in emerging financial systems.

The evidence suggests that market unification has led to significant structural changes. Shanghai maintained its position as a major risk transmitter (net spillover 21.582%), while Tianjin transformed from a net receiver (-21.502%) to a major transmitter (26.115%). Information transfer efficiency improved from 0.432 to 0.516, indicating enhanced market responsiveness. These findings have important implications for market regulation and risk management strategies.

The remainder of this paper is structured as follows. Section 2 reviews the relevant literature on carbon markets and risk transmission, highlighting the current gaps in understanding China's unified market. Section 3 details our data sources and presents our multi-layer network methodological framework. Section 4 presents our empirical results,

analyzing changes in risk transmission patterns before and after market unification. Section 5 discusses the implications of our findings for policymakers, market participants, and international market integration. Section 6 concludes with policy recommendations and suggestions for future research.

3.2 Literature Review

To comprehensively situate this study, this literature review synthesizes insights from four critical and interconnected domains. We begin by charting the evolution of carbon markets, both globally and within China, to establish the institutional context and identify the unique challenges posed by the recent national unification. Building on this context, we then introduce foundational concepts from financial risk theory, which provide the essential tools for measuring and interpreting risk propagation. Subsequently, we examine market integration theory, which offers a lens through which to understand how the unification process is expected to alter these risk dynamics. Finally, we review recent advancements in network analysis, the primary methodological framework used in this study to visualize and quantify the complex, evolving web of relationships within and beyond China's carbon market. This structured review progressively builds the theoretical and methodological foundation, culminating in the identification of the specific research gaps this chapter aims to address.

3.2.1 Evolution of Carbon Markets and Emerging Challenges

The development of carbon markets has been a pivotal strategy in global efforts to mitigate climate change. Early theoretical work laid the foundation for market-based environmental policies. Stavins (1995)analyzed the application of market mechanisms in environmental policy, highlighting the efficiency gains from tradable permits over traditional regulatory approaches. Tietenberg (2010) further explored the design and implementation of emissions trading systems, emphasizing allocation methods, compliance mechanisms, and market oversight.

The European Union Emissions Trading System (EU ETS), established in 2005, serves as a benchmark for cap-and-trade systems worldwide. Kruger and Pizer (2004)examined the early phases of carbon emissions trading in Europe, identifying critical factors influencing market performance, such as allocation methods and regulatory frameworks. Schmalensee and Stavins (2017) provided an in-depth assessment of the EU ETS, evaluating its environmental effectiveness and economic efficiency, and underscored the need for continuous policy adjustments to enhance market performance.

Building on these insights, empirical research has focused on price formation mechanisms, market efficiency, and factors influencing carbon price volatility. Chevallier (2009) analyzed the relationship between macroeconomic conditions and carbon price volatility in the EU ETS, suggesting that carbon markets are influenced by a complex interplay of environmental policies and broader economic factors.

In emerging markets, carbon price formation exhibits distinct characteristics. Cong and Lo (2017) demonstrated that these markets show heightened sensitivity to policy

interventions and reduced responsiveness to market fundamentals. Chang et al. (2018); Zhu et al. (2020) identified regulatory uncertainty, market liquidity constraints, and industrial transitions as key determinants of carbon price volatility in developing markets. These findings underscore the unique challenges faced by emerging carbon markets in establishing efficient price discovery mechanisms.

China's carbon market development has been characterized by gradual experimentation and regional pilots since 2011 (Zhang and Hao, 2017). Chang et al. (2018) analyzed trading patterns across these pilot markets, revealing significant heterogeneity in market liquidity and price discovery efficiency.Zhang et al. (2019) emphasized the importance of standardized rules and monitoring systems by examining how regulatory differences influence market performance.

More recent studies have focused on the initial performance of China's national carbon market. Xiao et al. (2022); Sun et al. (2022) investigated the impact of market unification on trading volumes and price stability, finding that while unification has improved infrastructure, challenges such as uneven regional participation persist. Zhao et al. (2022) analyzed the role of government policies in shaping market expectations, highlighting the influence of regulatory signals on market behavior. These studies indicate that while progress has been made, issues like regional disparities and regulatory influence remain critical areas for further study.

Having established the unique institutional context of China's evolving carbon market, understanding the transmission of shocks within this system requires a robust theoretical toolkit. Therefore, we now turn to financial risk theory to define the core concepts of risk propagation central to our analysis.

3.2.2 Financial Risk Theory Applied to Carbon Markets

Understanding risk transmission mechanisms is essential for analyzing emerging markets, and financial risk theory offers valuable frameworks in this regard. Tobias and Brunnermeier (2016) developed methodologies for measuring market risk through CoVaR, emphasizing the importance of distinguishing between systemic and individual risks.Antonakakis et al. (2020) advanced the application of time-varying parameter vector autoregression models, providing insights into evolving market structures and dynamic connectedness.

Systemic risk measurement and transmission channels in interconnected markets have been focal points in recent studies. Diebold and Yılmaz (2014) proposed a framework for analyzing connectedness in networked financial systems, highlighting how market structure influences shock transmission. Elliott et al. (2014)extended this analysis to financial networks, demonstrating how contagion mechanisms operate in interconnected systems.

Applying financial risk theory to carbon markets reveals unique challenges. Balcılar et al. (2016) examined risk spillovers across energy and carbon markets, highlighting the

significant impact of market interactions and volatility transmission. Zhang and Sun (2016) documented how energy price volatility affects carbon markets, indicating interconnections with other commodity markets.

In China's carbon market, risk transmission exhibits distinctive patterns. Zhu et al. (2020) showed stronger interconnectedness between regional pilot markets, with significant risk spillover effects. This emphasizes the critical role of market integration in risk management. Recent studies by Zhao et al. (2022) employed advanced volatility models to capture the dynamic interactions between stock, commodity, and carbon markets in China, suggesting that extreme event shocks significantly influence market behavior. Wen et al. (2020) further documented the asymmetric relationship between carbon emission trading and stock markets in China, indicating that traditional models may not fully capture the market's unique risk profile. Therefore, integrating advanced risk assessment techniques tailored to China's specific context is crucial for accurate analysis and effective risk management.

With these risk measurement frameworks in mind, the central event of this study—the national market unification—can be understood through the lens of market integration theory. The next subsection explores how this theory predicts structural changes in risk and information flow following such a consolidation.

3.2.3 Market Integration Theory in the Context of Carbon Markets

Market integration theory provides insights into how interconnected markets influence risk transmission.Diebold and Yılmaz (2014) established that increased integration enhances information flow and capital allocation efficiency but may amplify systemic risk exposure. This framework is pertinent for carbon markets, where integration efforts must balance efficiency gains with stability concerns.

Research on carbon trading systems has expanded our understanding of integration dynamics. Jia et al. (2024) analyzed drivers of market integration in international carbon markets, identifying regulatory harmonization and infrastructure development as key facilitators. Their findings suggest that technical compatibility and institutional alignment are crucial for successful integration.

Challenges in linking international carbon markets have been extensively studied. Zhang and Hao (2017) identified quota allocation and efficiency principles as crucial factors affecting market integration. Mehling et al. (2018) examined the evolving challenges, emphasizing political economy factors and institutional capacity in determining outcomes.Xiao et al. (2022) examined the time-varying spillovers among pilot markets, emphasizing market maturity and institutional development in determining outcomes.

In China's context, market integration faces unique hurdles due to regional heterogene-

ity.Chang et al. (2018) documented how variations in market liquidity and price dynamics across provinces affect integration potential. Shen (2015) documented how variations in abatement costs and market readiness across provinces affect integration potential. Wang et al. (2019) observed gradual convergence in trading patterns post-unification but noted persistent barriers, including regional policy differences and varying market maturity levels.

Recent research by Chen et al. (2022) explored the volatility connectedness between carbon markets. They identified significant interactions between markets but also highlighted challenges related to market efficiency and risk transmission. These findings emphasize that understanding market connectedness and addressing regional disparities are essential steps toward achieving effective integration and risk mitigation in China's carbon market.

The theories of market integration highlight the need for a methodology that can capture this complex web of interdependencies. Network analysis provides precisely such a framework, setting the stage for the multi-layer network approach employed in this study.

3.2.4 Advancements in Network Analysis for Carbon Markets

Network analysis has evolved as a powerful tool for understanding complex market interactions. Early studies by Mantegna (1999); Haldane and May (2011) utilized single-layer network models to analyze asset correlations and credit exposures, effectively identifying systemically important entities and potential contagion paths.

Recognizing the complexity of modern financial systems, recent advancements have introduced multi-layer network analysis. Kivelä et al. (2014) established theoretical foundations for this approach, enabling simultaneous capture of multiple interaction dimensions. Battiston et al. (2016) applied it to financial systems, illustrating how different market relationships interact to create complex risk transmission channels.

Applying multi-layer network theory to financial risk analysis has yielded significant insights.Poledna et al. (2015) showed that traditional analyses might underestimate systemic risk, while Montagna and Kok (2016) demonstrated amplification of financial instability through interacting network layers.Billio et al. (2012) showed the importance of interconnectedness measures in systemic risk assessment, while Diebold and Yilmaz (2015) demonstrated the evolution of volatility connectedness between financial institutions.

In carbon markets, network analysis is emerging as a valuable approach. Chen et al. (2022)Chen et al. (2022) applied quantile connectedness analysis to examine relationships between energy, metal, and carbon markets, highlighting the necessity of considering multiple dependencies. Their findings suggest that price formation and risk transmission operate through interconnected channels, requiring comprehensive analysis.

Recent studies on China's carbon market have begun to employ network analysis. Zhu et al. (2020)examined risk spillover effects among pilot markets, identifying patterns of market interconnectedness. Their work revealed how market structure shapes risk trans-

mission dynamics.Xiao et al. (2022) utilized time-varying spillover analysis to examine the evolution of China's pilot carbon markets, finding that market maturity can significantly alter connectivity patterns. These studies demonstrate that considering market interconnectedness is essential for accurately assessing risk transmission and market behavior in China's unique regulatory environment.

3.2.5 Identified Research Gaps and Study Contributions

Despite extensive research on carbon markets, several critical gaps remain in understanding risk transmission, particularly in the context of China's evolving market structure. One significant gap is the limited integration of foundational theories and practical insights from seminal works into analyses of China's carbon market. Incorporating perspectives from established studies on market-based environmental policies and emissions trading systems can enrich our understanding of China's unique context and provide a more robust theoretical foundation.

Furthermore, the application of advanced risk analysis techniques to China's carbon market has been insufficient. Existing models often fail to capture unique characteristics such as policy uncertainty and market fragmentation. This indicates a need for methodologies tailored to China's specific conditions, as conventional models may not adequately reflect the complexities of its market dynamics and risk profiles.

Another area that warrants attention is the scarcity of empirical analyses on China's market unification process. The significant structural changes resulting from the transition from regional pilots to a unified national system have far-reaching implications for risk transmission. However, systematic studies employing advanced analytical frameworks to examine this transition are limited, leaving a gap in our understanding of how unification affects market behavior and risk mechanisms.

In addition, there is a lack of exploration into multi-layer network structures when analyzing China's carbon market. Most existing studies focus on single-layer networks or isolated market aspects, potentially oversimplifying the complex interdependencies inherent in the market. A comprehensive approach that considers multiple layers of interaction is essential to accurately capture the nuances of risk transmission and market dynamics within China's carbon trading system.

Lastly, the mechanisms of cross-border risk transmission in the context of international integration of China's carbon market remain inadequately understood. This limitation hampers our comprehension of global carbon pricing and the potential for market integration, which are crucial for developing coordinated international climate policies and strategies.

Addressing these gaps is essential for advancing both theoretical and practical understanding of China's carbon market. Our study aims to bridge these gaps by integrating

foundational theories with analytical methods tailored to China's specific conditions. By applying multi-layer network analysis and exploring international linkages, we seek to provide a nuanced understanding of risk dynamics. This approach not only enhances the academic discourse but also offers valuable insights for policymakers and market participants navigating the complexities of China's evolving carbon trading environment.

3.3 Methodology

This study employs a comprehensive methodological framework to analyze risk transmission and inter-dependencies among China's carbon markets, integrating advanced econometric techniques with network analysis. Figure 3.1 presents our analytical framework, which combines GARCH modeling, Copula analysis, and the Diebold-Yilmaz spillover index to construct a multi-layer risk network. This approach facilitates a nuanced understanding of both linear and non-linear risk dependencies within domestic carbon markets and between domestic and international markets.

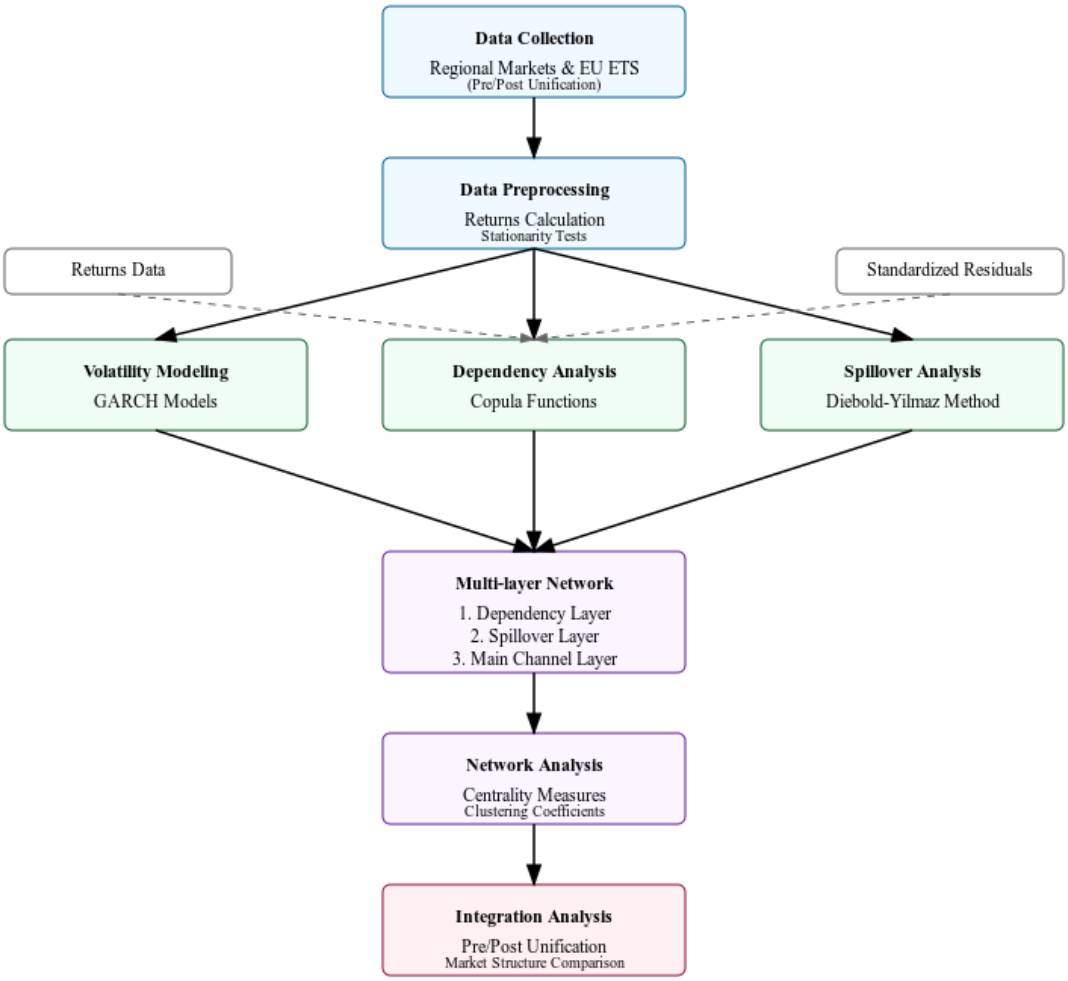

Figure 3.1: Methodological Framework for Multi-layer Network Analysis of Carbon Markets
Note: This framework illustrates our four-stage analytical approach: (1) Data processing of pre/post-unification market data from regional and international carbon markets, (2) Core analysis components including volatility analysis through GARCH modeling, dependency analysis using Copula functions, and spillover analysis based on the Diebold-Yilmaz index, (3) Construction of three network layers capturing different aspects of market relationships: dependency network, risk transfer network, and main channel network, and (4) Integration analysis examining the evolution of market structure and integration patterns. The arrows indicate the flow of analysis and the interconnections between different stages.

The framework consists of four main stages. First, we process the data from both pre- and post-unification periods of China's carbon market, including regional pilot markets and international markets. Second, we employ three core analytical components: GARCH modeling for volatility dynamics, Copula analysis for market dependencies, and the Diebold-Yilmaz approach for spillover effects. Third, we construct a three-layer network structure, where each layer captures different aspects of market relationships. Finally, we integrate these analyses to examine the evolution of market structure and integration patterns.

3.3.1 Data and Preliminary Analysis

Data Description and Rationale

We utilize daily carbon emission allowance (EA) prices from multiple Chinese carbon trading markets, including the eight regional pilot markets (Beijing, Chongqing, Fujian, Guangdong, Hubei, Shanghai, Shenzhen, and Tianjin), the national unified market, and the European Union Emissions Trading System (EU ETS) as an international benchmark. The sample period spans from July 16, 2018, to July 16, 2024, covering three years before and after the unification of China's national carbon market on July 16, 2021. This period selection allows for a thorough comparative analysis of risk transmission dynamics before and after the market unification.

Data are sourced from official exchanges and databases, including the China Emissions Exchange for domestic markets and the European Energy Exchange (EEX) for the EU ETS. Utilizing official data sources ensures accuracy and enhances the transparency and reproducibility of our research.

Data Preprocessing

To ensure a continuous time series, we address missing data points arising from non-overlapping trading holidays using the Last Observation Carried Forward (LOCF) method. This technique replaces a missing value with the most recent available observation ($P_{i,t}$ is replaced by $P_{i,t-1}$). This choice is justified for high-frequency financial price data as prices often exhibit high persistence, making the previous day's price the best predictor in the absence of new information. This simple yet robust method avoids introducing artificial volatility and minimizes potential distortions(Tsay, 2005).

We compute the daily logarithmic returns for each market to stabilize variance and normalize the data:

$$r_{i,t} = 100 \times \ln\left(\frac{P_{i,t}}{P_{i,t-1}}\right), \tag{3.1}$$

where $r_{i,t}$ is the return of market i on day t, and $P_{i,t}$ is the closing price.

The Augmented Dickey-Fuller (ADF) test is applied to each return series to verify stationarity. All series are found to be stationary at the 1% significance level, consistent with the properties of financial return data (Dickey and Fuller, 1979). Descriptive statistics, including mean, standard deviation, skewness, and kurtosis, are computed to understand the distributional properties of the return series.

Pairwise Pearson correlation coefficients among the markets are calculated to assess the degree of linear relationships. High correlations are observed between certain markets, reflecting potential interconnectedness. However, we retain all markets in our analysis to preserve the integrity of the network structure, acknowledging that high correlations will be addressed in the modeling process.

3.3.2 GARCH Modeling of Volatility Dynamics

To capture the volatility clustering and heteroscedasticity inherent in financial time series, we employ univariate GARCH(1,1) models for each market's return series (Bollerslev, 1987). The GARCH(1,1) model is specified as:

$$r_{i,t} = \mu_i + \varepsilon_{i,t}, \tag{3.2}$$

$$\sigma^2_{i,t} = \omega_i + \alpha_i \varepsilon^2_{i,t-1} + \beta_i \sigma^2_{i,t-1}, \tag{3.3}$$

Where $r_{i,t}$ is the return of market i at time t, μ_i is the mean return, $\varepsilon_{i,t}$ is the error term assumed to follow a standardized Student's t-distribution to account for leptokurtosis (Bollerslev, 1987), and $\sigma^2_{i,t}$ is the conditional variance. Parameters ω_i, α_i, and β_i are estimated, with constraints $\omega_i > 0$, $\alpha_i \geq 0$, $\beta_i \geq 0$, and $\alpha_i + \beta_i < 1$ to ensure stationarity and positive variance.

We estimate the GARCH models using Maximum Likelihood Estimation (MLE). Diagnostic checks, including the Ljung-Box Q-test and Engle's ARCH test, are performed on the standardized residuals and squared standardized residuals to ensure that autocorrelation and ARCH effects have been adequately captured.

After fitting the GARCH models, we extract the standardized residuals:

$$z_{i,t} = \frac{\varepsilon_{i,t}}{\sigma_{i,t}}. \tag{3.4}$$

These standardized residuals, representing the shocks to market i at time t adjusted for time-varying volatility, are used in the subsequent Copula analysis to model dependencies independent of individual market volatility dynamics.

3.3.3 Copula Analysis for Non-linear Dependencies

To capture complex, potentially non-linear dependencies between different carbon markets, we employ Copula functions. Copulas allow for modeling the joint distribution of random variables by separating the marginal distributions from the dependence structure (Sklar, 1959).

We select the Student's t-Copula for our analysis due to its ability to model symmetric tail dependence, which is crucial for capturing extreme co-movements during periods of market stress (Demarta and McNeil, 2005). The t-Copula is particularly suitable for financial data where joint extreme events are of interest. Alternative Copula families, including the Gaussian Copula and Archimedean Copulas (Clayton, Gumbel), are also considered to assess the robustness of our results.

Based on Sklar's Theorem, the joint distribution of the standardized residuals can be expressed as:

$$F(z_1, z_2, \ldots, z_n) = C(F_1(z_1), F_2(z_2), \ldots, F_n(z_n)), \tag{3.5}$$

Where $F_i(z_i)$ are the marginal cumulative distribution functions (CDFs) of the standardized residuals, and $C(\cdot)$ is the Copula function capturing the dependence structure.

For the t-Copula, the density function is:

$$c(u_1, \ldots, u_n) = \frac{\Gamma\left(\frac{\nu+n}{2}\right)}{\Gamma\left(\frac{\nu}{2}\right)(\pi\nu)^{n/2}|\mathbf{R}|^{1/2}} \left(1 + \frac{\mathbf{q}'\mathbf{R}^{-1}\mathbf{q}}{\nu}\right)^{-\frac{\nu+n}{2}}, \tag{3.6}$$

where $u_i = F_i(z_{i,t})$ are the uniform transformed variables, $\mathbf{q} = (t_\nu^{-1}(u_1), \ldots, t_\nu^{-1}(u_n))$, ν is the degrees of freedom parameter, $\mathbf{R}$ is the correlation matrix, and $\Gamma(\cdot)$ is the gamma function.

Parameters are estimated using the Inference Functions for Margins (IFM) method (Joe, 1997). Goodness-of-fit tests, such as the Cramér-von Mises and Kolmogorov-Smirnov tests, are conducted to assess the adequacy of the Copula models. The Akaike Information Criterion (AIC) and Bayesian Information Criterion (BIC) are used for model selection among different Copula families(Akaike, 1974; Schwarz, 1978).

3.3.4 Diebold-Yilmaz Method for Linear Risk Spillovers

To quantify linear risk spillovers between markets, we employ the Diebold-Yilmaz spillover index methodology, which is based on forecast error variance decomposition (FEVD) from vector autoregression (VAR) models (Diebold and Yilmaz, 2009, 2012, 2023).Intuitively, the Diebold–Yilmaz (DY) approach answers a simple question: When a particular market experiences an unexpected shock, what percentage of the future price uncertainty in other markets can be explained by this shock? By decomposing the forecast error variance from

a Vector Autoregression (VAR) model, the DY index measures how much of the error in forecasting a market's volatility comes from its own shocks versus shocks from others. This allows us to identify systemic "net transmitters" and "net receivers" of risk, providing a comprehensive map of the risk transmission network.

We specify a VAR(p) model for the vector of returns:

$$\mathbf{r}_t = \sum_{k=1}^{p} \mathbf{A}_k \mathbf{r}_{t-k} + \boldsymbol{\varepsilon}_t, \tag{3.7}$$

Where $\mathbf{r}_t$ is the vector of returns at time t, $\mathbf{A}_k$ are coefficient matrices, and $\boldsymbol{\varepsilon}_t$ is the vector of error terms, assumed to be serially uncorrelated with covariance matrix $\boldsymbol{\Sigma}$.

The optimal lag order p is determined using information criteria, including the Akaike Information Criterion (AIC), Schwarz Bayesian Criterion (SBC), and the Hannan-Quinn Criterion (HQC). Residual diagnostic tests are conducted to ensure that the VAR model adequately captures the dynamics of the data(Akaike, 1974; Schwarz, 1978).

We compute the generalized forecast error variance decomposition (GFEVD), which allows for correlated shocks without requiring orthogonalization via Cholesky decomposition, thus avoiding sensitivity to variable ordering (Koop et al., 1996; Pesaran and Shin, 1998). The GFEVD is given by:

$$\theta_{ij}(H) = \frac{\sigma_{jj}^{-1} \sum_{h=0}^{H-1} \left(e_i' \boldsymbol{\Phi}_h \boldsymbol{\Sigma} e_j\right)^2}{\sum_{h=0}^{H-1} \left(e_i' \boldsymbol{\Phi}_h \boldsymbol{\Sigma} \boldsymbol{\Phi}_h' e_i\right)} \tag{3.8}$$

where $\boldsymbol{\Phi}_h$ are the moving average coefficient matrices, e_i is a selection vector with one in the i-th position and zeros elsewhere, and σ_{jj} is the standard deviation of the error term for market j.

We set the forecast horizon H to 10 days, balancing the trade-off between capturing medium-term dynamics and maintaining estimation accuracy (Diebold and Yilmaz, 2012). Sensitivity analysis is conducted by varying H to ensure the robustness of the results.

Using the GFEVD, we compute the total spillover index, directional spillover indices, and net spillover index, which help identify markets that are net transmitters or receivers of spillovers, providing insights into the directional risk transmission among markets.

3.3.5 Construction of the Multi-layer Risk Network

To comprehensively capture the risk transmission characteristics among China's carbon markets, we construct a multi-layer network consisting of three layers, each representing a different type of dependency. The multi-layer network framework allows us to simultaneously consider multiple types of interactions between markets, capturing the complexity of risk transmission mechanisms (Kivelä et al., 2014).

Layer 1: Non-linear Dependency Layer (Copula Layer)

This layer represents the non-linear dependencies and tail co-movements between markets, as captured by the Copula analysis. The adjacency matrix for this layer is defined as:

$$W_{ij}^{\text{Copula}} = \hat{\rho}_{ij}^{\text{Copula}}, \tag{3.9}$$

where $\hat{\rho}_{ij}^{\text{Copula}}$ is the estimated dependence parameter between markets i and j from the Copula model.

Layer 2: Linear Spillover Layer (Diebold-Yilmaz Layer)

This layer captures the linear risk spillovers between markets, as quantified by the Diebold-Yilmaz spillover indices. The adjacency matrix for this layer is defined as:

$$W_{ij}^{\text{DY}} = \theta_{ij}(H), \tag{3.10}$$

where $\theta_{ij}(H)$ is the GFEVD-based spillover from market j to market i.

Layer 3: Primary Transmission Path Layer

This layer highlights the most significant risk transmission paths, focusing on the strongest connections. The adjacency matrix for this layer is defined as:

$$W_{ij}^{\text{Primary}} = \begin{cases} 1, & \text{if } \theta_{ij}(H) = \max_{k \neq i} \theta_{ik}(H), \\ 0, & \text{otherwise.} \end{cases} \tag{3.11}$$

By analyzing these layers collectively, we gain a comprehensive understanding of the risk structure and can identify markets that are central across multiple dimensions.

Network Metrics and Analysis

For each layer, we compute various centrality measures to assess the importance and influence of each market within the network, including degree centrality, closeness centrality, betweenness centrality, and eigenvector centrality. These metrics provide insights into the roles of individual markets in the network, such as identifying key risk transmitters or receivers.

We apply the Louvain algorithm for community detection, which optimizes modularity to identify clusters of markets with stronger internal connections (Blondel et al., 2008). Community detection helps identify subgroups within the network that may share common characteristics or be subject to similar risks.

3.3.6 Analysis and Robustness Checks

We conduct the analysis for two distinct periods: pre-unification (July 16, 2018, to July 15, 2021) and post-unification (July 16, 2021, to July 16, 2024). This allows us to assess the impact of the national carbon market unification on risk transmission and network structure.

Furthermore, we perform analyses under two scenarios: domestic markets only (including the eight regional pilot markets and the national unified market) and all markets (including domestic markets and the EU ETS). By comparing these scenarios, we evaluate the degree of international integration and its effect on domestic risk dynamics.

To ensure the reliability of our results, we conduct several robustness checks. Alternative Copula specifications, such as the Gaussian Copula and Archimedean Copulas, are used to test the sensitivity of our results to the choice of Copula family(Demarta and McNeil, 2005). We vary the lag order p in the VAR models and test different forecast horizons H to assess the stability of the spillover indices over different time horizons(Diebold and Yılmaz, 2014).

A bootstrap resampling procedure is employed to estimate confidence intervals for the network metrics and spillover indices (Efron and Tibshirani, 1994). This allows us to assess the statistical significance of our findings and account for sampling variability. We also perform a rolling window analysis with a fixed window size (e.g., 250 trading days) to examine the dynamic evolution of the network structure and risk transmission over time.

3.4 Empirical Analysis

In the preceding sections, we have explored the theoretical foundations of carbon markets, the existing literature on China's carbon market development, and the potential implications of market unification on risk transmission mechanisms. To empirically validate our hypotheses, this section employs the methodological framework outlined earlier to analyze the impact of China's carbon market unification on market dependence structures, risk spillover effects, network characteristics, and overall market efficiency and international integration. Specifically, we conduct a comparative analysis of pre- and post-unification periods to uncover the structural changes and their economic implications.

3.4.1 Data Description and Preliminary Analysis

This study investigates the dynamic risk transmission mechanisms in China's carbon markets surrounding the implementation of the national unified carbon market. We utilize daily carbon emission allowance (CEA) prices from ten markets: eight regional pilot markets in China (Beijing, Chongqing, Fujian, Guangdong, Hubei, Shanghai, Shenzhen, and Tianjin), the national CEA market, and the European Union Emissions Trading System (EU ETS). The sample period spans from July 1, 2017, to July 31, 2024, encompassing 1,857 trading days. We divide the sample into pre-unification (July 1, 2017, to July 15, 2021) and post-unification (July 16, 2021, to July 31, 2024) periods.

Tables 3.1 and 3.2 present the descriptive statistics of daily returns for the pre- and post-unification periods, respectively.

Table 3.1: Statistical Properties of Daily Carbon Market Returns Before National Market Unification (July 2018 - July 2021)

Carbon Market	**Mean (%)**	**Std. Dev. (%)**	**Skewness**	**Excess Kurtosis**
Shenzhen (SZ)	−0.152	40.136	0.071	10.906
Shanghai (SH)	0.007	5.099	0.160	9.229
Beijing (BJ)	−0.019	7.189	−0.301	8.712
Guangdong (GD)	0.147	25.263	−0.412	26.456
Tianjin (TJ)	0.118	3.074	1.357	38.631
Hubei (HB)	0.065	4.581	0.107	5.375
Chongqing (CQ)	0.304	6.539	−0.194	3.854
Fujian (FJ)	−0.095	8.516	0.453	29.415
EU ETS (EUA)	0.164	3.071	−0.678	7.426

Notes: This table reports summary statistics for the daily logarithmic returns of eight regional Chinese carbon markets and the European Union Emissions Trading System (EU ETS) before the implementation of China's national unified carbon market. The sample period spans from July 16, 2018, to July 15, 2021, covering 783 trading days.

Table 3.2: Statistical Properties of Daily Carbon Market Returns After National Market Unification (July 2021 - July 2024)

Carbon Market	**Mean (%)**	**Std. Dev. (%)**	**Skewness**	**Excess Kurtosis**
National CEA	0.072	1.865	0.275	9.206
Shenzhen (SZ)	0.245	27.506	1.173	59.255
Shanghai (SH)	0.083	2.308	−0.094	8.415
Beijing (BJ)	0.058	7.865	−0.187	6.000
Guangdong (GD)	0.014	8.435	−0.017	76.623
Tianjin (TJ)	0.022	7.045	−0.036	149.396
Hubei (HB)	0.033	2.543	−0.092	8.311
Chongqing (CQ)	0.033	3.444	−0.127	6.205
Fujian (FJ)	0.163	16.814	−1.335	35.636
EU ETS (EUA)	0.031	2.833	−0.473	8.196

Notes: This table presents summary statistics for the daily logarithmic returns of China's national carbon market (CEA), eight regional Chinese carbon markets, and the European Union Emissions Trading System (EU ETS) after the implementation of China's national unified carbon market. The sample period spans from July 16, 2021, to July 16, 2024, covering 784 trading days.

Before unification, the markets exhibited considerable heterogeneity in their return distributions. Mean daily returns range from −0.152% (Shenzhen) to 0.304% (Chongqing). Six out of nine markets show positive average returns, indicating generally positive market performance in this period. Volatility levels vary significantly, with Shenzhen exhibiting the highest volatility (standard deviation of 40.136%), suggesting high uncertainty and possible market immaturity. In contrast, Tianjin shows the lowest volatility (3.074%), indicating more stable market conditions.

Skewness and kurtosis values reveal asymmetries and fat tails in the return distributions, indicative of potential extreme movements. For instance, Tianjin displays high positive skewness (1.357) and kurtosis (38.631), suggesting a higher probability of extreme positive returns.

Post-unification, notable changes are observed. The national CEA market exhibits the lowest volatility (1.865%), indicating increased market stability, possibly due to centralized regulation and increased liquidity. Mean returns across markets become predominantly positive, suggesting improved market sentiment following unification.

However, some markets display increased volatility and extreme movements. For example, Shenzhen's standard deviation remains high at 27.506%, and its kurtosis increases to 59.255, indicating persistent high volatility and a higher probability of extreme returns. Tianjin's kurtosis dramatically increases to 149.396, highlighting significant changes in return distribution tails.

Changes in skewness indicate shifts in the asymmetry of return distributions. Fujian's skewness shifts from positive (0.453) to strong negative (−1.335), suggesting a higher

likelihood of extreme negative returns in the post-unification period.

These observations suggest that while market unification has generally led to increased stability and positive returns, heterogeneity remains across regional markets. The varying volatility and higher moments indicate that regional factors continue to influence market dynamics.

3.4.2 Volatility Modeling

To capture the volatility dynamics of the carbon markets and facilitate the analysis of risk transmission mechanisms, we estimate univariate GARCH(1,1) models for each market's return series in both pre- and post-unification periods. The estimated parameters are presented in Table 3.3.

Table 3.3: Estimated GARCH(1,1) Parameters

Market	Pre-Unification			Post-Unification		
	ω	α	β	ω	α	β
Shenzhen	0.469	0.095	0.859	48.424	0.982	0.017
Shanghai	0.000	0.899	0.019	0.000	0.773	0.008
Beijing	0.000	0.957	0.009	0.000	0.623	0.018
Guangdong	0.000	0.619	0.379	0.842	0.611	0.388
Tianjin	0.000	0.862	0.012	0.000	0.963	0.001
Hubei	9.871	0.637	0.362	6.848	0.926	0.073
Chongqing	0.000	0.947	0.047	0.079	0.388	0.611
Fujian	0.000	0.788	0.211	0.014	0.265	0.734
CEA	—	—	—	0.000	0.773	0.008
EUA	61.393	0.381	0.618	0.182	0.071	0.907

Note: The GARCH(1,1) model is specified as $r_t = \mu + \varepsilon_t,\ \varepsilon_t = z_t\sigma_t,\ \sigma_t^2 = \omega + \alpha\varepsilon_{t-1}^2 + \beta\sigma_{t-1}^2$, where r_t is the return at time t, μ is the mean return, ε_t is the error term, σ_t^2 is the conditional variance, ω is the constant term, α captures the news impact (ARCH effect), β captures the volatility persistence (GARCH effect), and z_t is an i.i.d. error term.

In the pre-unification period, the estimated α coefficients, representing the sensitivity to new information, are relatively high for markets such as Beijing ($\alpha = 0.957$), Chongqing ($\alpha = 0.947$), and Shanghai ($\alpha = 0.899$), indicating strong reactions to market shocks. The β coefficients, reflecting the persistence of volatility, are low for these markets, suggesting that volatility shocks have a short-lived effect. Shenzhen and Hubei display higher β coefficients ($\beta = 0.859$ and $\beta = 0.362$, respectively), implying that past volatility has a more persistent influence on current volatility in these markets. The sum $\alpha + \beta$ is close to one for most markets, indicating high overall volatility persistence.

In the post-unification period, significant shifts in volatility dynamics are observed. Shenzhen's α increases dramatically from 0.095 to 0.982, while β decreases from 0.859 to 0.017, suggesting that volatility is now almost entirely driven by new information, with minimal persistence from past volatility. This change may reflect enhanced market

efficiency and responsiveness to information post-unification.

Conversely, Chongqing experiences a decrease in α from 0.947 to 0.388 and an increase in β from 0.047 to 0.611, indicating a shift towards greater volatility persistence and reduced immediate sensitivity to new shocks. The national CEA market, introduced in the post-unification period, exhibits a high α of 0.773 and a low β of 0.008, indicating that volatility is predominantly influenced by recent news, consistent with its status as a newly established market where historical volatility patterns are still developing.

For the EU ETS, the α coefficient decreases from 0.381 to 0.071, and β increases from 0.618 to 0.907, reflecting decreased sensitivity to new information and increased volatility persistence, characteristic of a mature and stable market.

These findings suggest that market unification has led to heterogeneous changes in the volatility structure of China's carbon markets. Some markets have become more reactive to new information, while others exhibit increased volatility persistence. The varying responses underscore the complexity of the markets and the influence of regional factors.

Figure 3.2 illustrates the estimated conditional volatilities for selected markets over the sample period. The national CEA market has demonstrated low and stable volatility since its inception, while regional markets like Shenzhen and Guangdong show periods of heightened volatility, especially post-unification, indicating increased market activity and sensitivity to news.

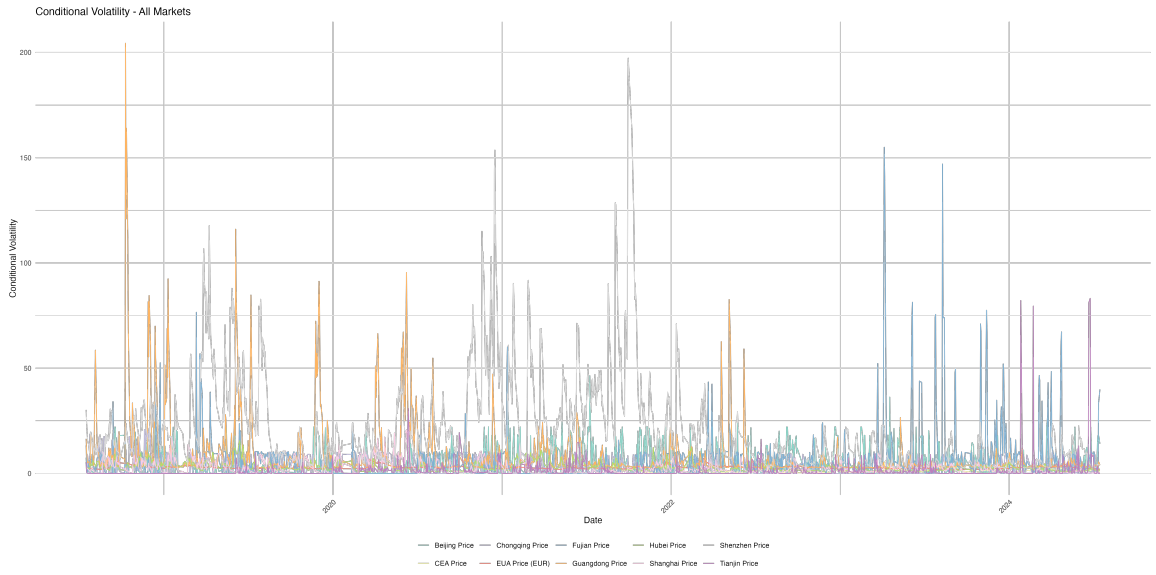

Figure 3.2: Temporal Evolution of Conditional Volatility in Chinese and European Carbon Markets (2018-2024)

Notes: This figure illustrates the estimated conditional volatility from GARCH(1,1) models for selected carbon markets over the full sample period (July 2018 to July 2024). The vertical dashed line indicates the implementation of China's national carbon market on July 16, 2021.

These results have important implications for understanding risk transmission in China's carbon markets. The changes in volatility dynamics highlight the evolving nature of the

markets and the potential impact of unification on market efficiency and integration. The observed heterogeneity suggests that regional characteristics continue to play a significant role, necessitating a nuanced approach in analyzing risk transmission mechanisms.

3.4.3 Market Dependence Structure Analysis

Understanding the changes in market dependence structures is crucial for assessing how market unification affects information transmission and price co-movement among regional carbon markets. This subsection examines the dependence structures before and after the unification, providing insights into the first hypothesis regarding increased market interconnectedness.

Pre-unification Dependence Structure

Using a copula-based dependence analysis, we find that the interconnections among regional carbon markets prior to unification were relatively weak. Table 3.4 presents the matrix of dependence parameters.

Table 3.4: Copula Dependence Parameters Matrix: Pre-unification Period

Market	SZ	SH	BJ	GD	TJ	HB	CQ	FJ
Shenzhen (SZ)	1.000	0.040	−0.043	−0.019	−0.051	0.001	−0.015	0.034
Shanghai (SH)	0.040	1.000	0.069	−0.017	0.030	−0.040	−0.065	−0.008
Beijing (BJ)	−0.043	0.069	1.000	−0.042	0.018	0.027	−0.007	−0.044
Guangdong (GD)	−0.019	−0.017	−0.042	1.000	0.010	0.029	0.024	0.051
Tianjin (TJ)	−0.051	0.030	0.018	0.010	1.000	0.046	−0.006	0.002
Hubei (HB)	0.001	−0.040	0.027	0.029	0.046	1.000	−0.024	0.002
Chongqing (CQ)	−0.015	−0.065	−0.007	0.024	−0.006	−0.024	1.000	−0.017
Fujian (FJ)	0.034	−0.008	−0.044	0.051	0.002	0.002	−0.017	1.000

Notes: This table presents the estimated dependence parameters from Student's t-copula models for pairs of Chinese regional carbon markets before the unification of China's national carbon market (July 2018 to July 2021). The parameters measure the strength and direction of dependency between markets, with values ranging from -1 (perfect negative dependence) to 1 (perfect positive dependence), and 0 indicating independence.

The dependence parameters range from -0.065 to 0.069, with a mean of 0.0004 and a standard deviation of 0.0331, indicating generally weak market integration. Notable dependency pairs include:

Several notable dependency pairs emerge from the analysis. The Shanghai-Beijing pair exhibits the strongest positive dependence (0.069), which may reflect their similar levels of economic development and carbon market policies. Conversely, Shanghai and Chongqing show the strongest negative dependence (-0.065), potentially due to differences in industrial structure and development stages. Guangdong and Fujian have a moderate positive dependence (0.051), possibly stemming from geographical proximity and similar industrial

compositions. Additionally, the negative dependence between Shenzhen and Tianjin (−0.051) suggests divergent market characteristics and policy frameworks.
Overall, the low dependence levels suggest that, prior to unification, regional carbon markets operated largely independently, with limited price co-movement and information transmission. This fragmentation likely reflects differences in regional policy frameworks, market maturity, and industrial structures.

Post-unification Dependence Structure

Following the introduction of the national carbon market (CEA), the market dependence structure exhibited notable changes. Table 3.5 presents the dependence parameters matrix for the post-unification period.

Table 3.5: Copula Dependence Parameters Matrix: Post-unification Period

Market	CEA	SZ	SH	BJ	GD	TJ	HB	CQ	FJ
CEA	1.000	0.025	0.048	0.029	0.011	0.003	0.053	0.003	−0.020
Shenzhen (SZ)	0.025	1.000	0.022	0.016	0.042	0.006	0.021	0.006	0.111
Shanghai (SH)	0.048	0.022	1.000	−0.038	−0.035	−0.036	−0.003	0.039	−0.035
Beijing (BJ)	0.029	0.016	−0.038	1.000	0.003	0.010	−0.022	−0.029	0.014
Guangdong (GD)	0.011	0.042	−0.035	0.003	1.000	0.007	−0.017	−0.075	0.033
Tianjin (TJ)	0.003	0.006	−0.036	0.010	0.007	1.000	−0.043	−0.042	0.009
Hubei (HB)	0.053	0.021	−0.003	−0.022	−0.017	−0.043	1.000	−0.014	−0.025
Chongqing (CQ)	0.003	0.006	0.039	−0.029	−0.075	−0.042	−0.014	1.000	−0.024
Fujian (FJ)	−0.020	0.111	−0.035	0.014	0.033	0.009	−0.025	−0.024	1.000

Notes: This table presents the estimated dependence parameters from Student's t-copula models for pairs of Chinese carbon markets after the implementation of the national unified carbon market (July 2021 to July 2024).

The post-unification period exhibits several significant changes in market dependencies. The CEA shows the strongest positive dependence with Hubei (0.053) and Shanghai (0.048), and most regional markets display positive but modest dependence with the CEA. Notably, only Fujian shows a negative dependence (−0.020) with the CEA. Among regional markets, the dependence between Shenzhen and Fujian increases significantly to 0.111, making it the strongest dependency pair in the post-unification period. The Guangdong-Chongqing pair shows the strongest negative dependence (−0.075). Additionally, the relationship between Shanghai and Beijing reverses from positive (0.069) to negative (−0.038).
The dependence parameters now range from −0.075 to 0.111, with a mean dependence of 0.0014 and a standard deviation of 0.0356. These changes suggest a significant transformation in market integration patterns following unification. The emergence of stronger dependencies, both positive and negative, indicates more complex market interactions and potentially improved information transmission mechanisms.

Discussion

Comparing the pre- and post-unification dependence structures reveals significant changes in market integration patterns, providing evidence relevant to our first hypothesis regarding increased market interconnectedness. Table 3.6 summarizes the statistics of dependence parameters before and after unification.

Table 3.6: Evolution of Market Integration Following Unification: Comparative Analysis of Dependency Parameters (2018-2024)

Statistical Indicator	**Pre-Unification**	**Post-Unification**
Minimum Dependency Value	-0.065	-0.075
Maximum Dependency Value	0.069	0.111
Mean Dependency	0.0004	0.0014
Standard Deviation	0.0331	0.0356
Number of Strong Dependencies ($\lvert\rho\rvert > 0.04$)	5	8
Percentage of Positive Dependencies	33.3%	56.3%

Notes: This table presents a comparative analysis of Student's t-copula dependence parameters before unification (July 2018 to July 2021) and after unification (July 2021 to July 2024) of China's carbon market. The data reveals substantial structural changes in market integration patterns following unification.

Key structural changes include an increase in the range and strength of dependencies. The range of dependence parameters widened from $[-0.065, 0.069]$ to $[-0.075, 0.111]$, and the average dependence strength increased by 250% (from 0.0004 to 0.0014). The number of significant dependencies (absolute value greater than 0.04) increased from 5 to 8, and the proportion of positive dependencies rose from 33.3% to 56.3%.

These findings provide strong support for our first hypothesis (H1) regarding increased market interconnectedness following unification. The quantitative evidence, including the increase in mean dependence and the growth in significant dependencies, indicates stronger overall market integration. Qualitative changes, such as a more balanced distribution of positive and negative dependencies and the emergence of stronger regional market clusters, further support this conclusion. Statistical tests, including the Wilcoxon signed-rank test (p-value < 0.05) and F-test (p-value < 0.10), confirm the significance of these changes.

3.4.4 Risk Spillover Effect Analysis

While the dependence structure analysis provides insights into the co-movement of markets, it is essential to examine whether these changes have affected the way risk is transmitted across markets. Building on the findings from the previous subsection, we now analyze the risk spillover effects before and after market unification to understand the evolution of risk transmission mechanisms.

Pre-unification Spillover Effects

Prior to market unification, the risk spillover patterns revealed significant asymmetries in the transmission of market shocks. Table 3.7 presents the variance decomposition matrix for this period.

Table 3.7: Variance Decomposition Matrix: Pre-unification Period (%)

From/To	SZ	SH	BJ	GD	TJ	HB	CQ	FJ
Shenzhen	96.665	0.233	0.628	0.534	0.195	0.181	0.434	1.122
Shanghai	0.649	97.473	0.285	0.605	0.246	0.226	0.371	0.145
Beijing	0.182	0.351	97.395	0.348	1.050	0.146	0.253	0.275
Guangdong	0.661	2.277	0.297	93.874	1.219	0.174	0.734	0.766
Tianjin	0.174	2.209	0.441	1.680	94.475	0.239	0.117	0.022
Hubei	0.859	0.524	0.605	0.341	0.344	96.031	0.351	0.365
Chongqing	0.446	0.647	0.261	0.968	0.086	0.019	97.134	0.439
Fujian	0.539	0.184	0.705	0.329	0.038	0.231	0.335	97.629

Notes: This table presents the generalized forecast error variance decomposition matrix based on the Diebold-Yilmaz methodology for China's regional carbon markets before national market unification (July 2018 to July 2021). Values are expressed as percentages. Each element (i, j) represents the contribution of market j to the forecast error variance of market i. The diagonal elements (highlighted in bold) represent own-market effects, indicating the percentage of price movements explained by the market's own shocks. The off-diagonal elements reveal cross-market spillover effects.

Table 3.8 provides the directional and net spillover effects. Key findings from the pre-unification period include Shanghai emerging as the primary source of risk transmission, with a net spillover of 48.834%, and Hubei showing the highest net risk absorption at −27.251%. The high diagonal elements in Table 3.7 (ranging from 93.874% to 97.629%) indicate strong own-market effects and limited cross-market spillovers, which are mostly below 1%. These patterns suggest a fragmented market structure with limited risk-sharing mechanisms and hierarchical relationships in risk transmission.

Post-unification Spillover Effects

Following the introduction of the national carbon market, the risk transmission landscape underwent significant changes. Tables 3.9 and 3.10 present the variance decomposition matrix and directional spillover effects for the post-unification period.

Key changes in the post-unification period include the CEA's role as a moderate risk absorber (net spillover: −3.013%) and the emergence of more balanced risk transmission roles among regional markets. Shanghai's dominance as a risk transmitter has moderated, with its net spillover decreasing from 48.834% to 21.582%. Tianjin transformed from a major receiver to a significant transmitter (net spillover increased by 49.617 percentage points). Hubei maintained its position as a primary risk receiver.

These findings suggest that market unification has led to more efficient risk-sharing

Table 3.8: Risk Transmission Roles Before Market Unification: Directional and Net Spillover Effects (2018-2021)

Market	**To Others (%)**	**From Others (%)**	**Net Spillover (%)**
Shanghai (SH)	80.417	31.584	+48.834
Fujian (FJ)	39.172	29.631	+9.541
Beijing (BJ)	40.266	32.564	+7.702
Shenzhen (SZ)	43.878	41.686	+2.192
Chongqing (CQ)	32.660	35.825	−3.164
Guangdong (GD)	64.320	68.388	−4.068
Tianjin (TJ)	37.737	61.239	−23.502
Hubei (HB)	15.295	42.545	−27.251

Notes: This table presents the directional and net spillover effects among China's regional carbon markets before national market unification (July 2018 to July 2021), based on the Diebold-Yilmaz spillover index derived from generalized forecast error variance decomposition. Markets are sorted by net spillover position, with net transmitters in the upper section and net receivers in the lower section. The "To Others" column quantifies each market's influence on other markets, while the "From Others" column measures its susceptibility to external shocks. The "Net Spillover" column (difference between "To Others" and "From Others") identifies whether a market predominantly transmits risk (positive values) or absorbs risk (negative values).

Table 3.9: Risk Transmission Network After Market Unification: Generalized Variance Decomposition Matrix (2021-2024)

From / To	**CEA**	**SZ**	**SH**	**BJ**	**GD**	**TJ**	**HB**	**CQ**	**FJ**
National CEA	95.506	0.075	0.043	0.074	0.128	0.137	0.063	0.012	0.099
Shenzhen (SZ)	1.358	96.154	0.172	0.354	0.043	0.023	0.507	0.831	0.268
Shanghai (SH)	0.529	0.115	97.221	0.445	0.209	0.011	0.125	0.211	0.516
Beijing (BJ)	0.193	0.297	1.032	95.565	0.250	1.079	0.353	0.610	0.425
Guangdong (GD)	0.501	0.319	0.547	0.089	97.829	0.122	0.159	0.031	0.120
Tianjin (TJ)	0.184	0.035	0.049	0.509	0.047	97.982	0.624	0.182	0.035
Hubei (HB)	0.446	1.348	0.748	0.268	0.368	1.298	93.443	0.461	0.756
Chongqing (CQ)	0.442	0.203	1.010	0.648	0.551	0.476	0.438	95.632	0.348
Fujian (FJ)	0.155	0.220	0.236	0.278	0.370	0.175	0.318	0.257	97.636

Notes: This table presents the generalized forecast error variance decomposition matrix following the Diebold-Yilmaz methodology for China's carbon markets after national market unification (July 2021 to July 2024). Values are expressed as percentages. Each element (i, j) represents the contribution of market j to the forecast error variance of market i. Diagonal elements indicate the percentage of price movements explained by each market's own shocks.

Table 3.10: Transformation of Market Roles After Unification: Directional and Net Spillover Effects (2021-2024)

Market	**To Others (%)**	**From Others (%)**	**Net Spillover (%)**
Tianjin (TJ)	46.296	20.181	+26.115
Shanghai (SH)	49.372	27.790	+21.582
Fujian (FJ)	38.353	23.638	+14.715
Guangdong (GD)	24.949	21.709	+3.240
National CEA	42.071	45.084	−3.013
Shenzhen (SZ)	33.027	38.456	−5.429
Beijing (BJ)	34.043	44.345	−10.302
Chongqing (CQ)	32.158	43.678	−11.520
Hubei (HB)	38.139	65.569	−27.430

Notes: This table presents the directional and net spillover effects among China's carbon markets after national market unification (July 2021 to July 2024), based on the Diebold-Yilmaz spillover index. Markets are sorted by net spillover position, with net risk transmitters in the upper section and net risk receivers in the lower section.

mechanisms, better-organized risk transmission channels, enhanced market stability, and a more balanced distribution of market influence.

Analysis of Market Roles

The comparison of pre- and post-unification periods reveals substantial transformations in market roles and risk transmission mechanisms, providing evidence relevant to our second and third hypotheses. Table 3.11 summarizes the evolution of market roles.

Table 3.11: Evolution of Market Roles: Pre- vs. Post-unification

Market	Net Spillover (%)		Change	Role Evolution
	Pre	Post		
CEA	–	−3.013	–	New Risk Coordinator
Shanghai	48.834	21.582	−27.252	Moderated Transmitter
Tianjin	−23.502	26.115	+49.617	Receiver to Transmitter
Hubei	−27.251	−27.430	−0.179	Consistent Receiver
Fujian	9.541	14.715	+5.174	Enhanced Transmitter
Guangdong	−4.068	3.240	+7.308	Receiver to Transmitter
Beijing	7.702	−10.302	−18.004	Transmitter to Receiver
Shenzhen	2.192	−5.429	−7.621	Transmitter to Receiver

The CEA has emerged as a central coordinator with balanced spillovers, supporting our second hypothesis regarding the central role of the national market. The transformation of regional market roles, such as Tianjin's shift from a risk receiver to a transmitter and Shanghai's moderated transmission role, provides evidence for our third hypothesis on regional market integration.

3.4.5 Network Characteristics Analysis

The preceding analysis highlights the changes in dependence structures and risk spillover effects. To gain a more comprehensive understanding of how market unification has restructured the overall market architecture, we now examine the evolution of network characteristics using the multi-layer network framework.

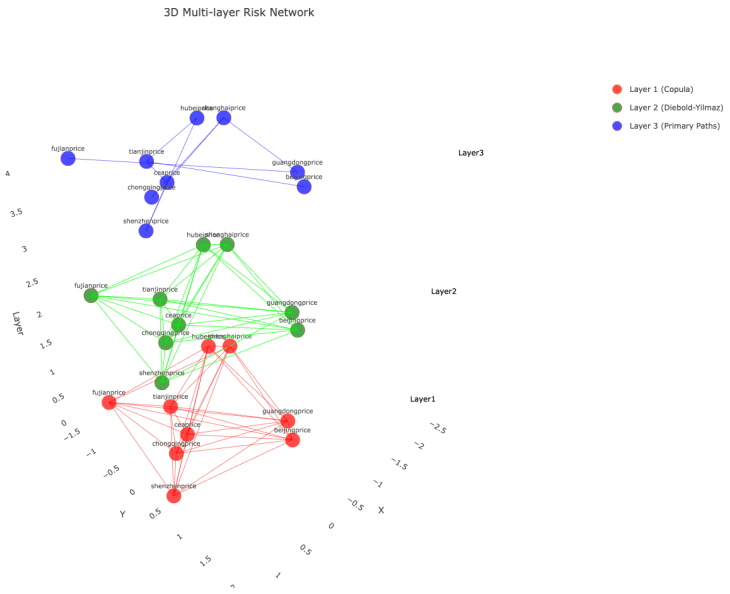

Figure 3.3: Multi-layer Network Structure of China's Carbon Market

Note: This figure illustrates the multi-layer network framework used to analyze the complex risk transmission mechanisms in China's carbon market. The visualization comprises three distinct but interconnected analytical layers that capture different aspects of market relationships: (1) The upper layer (Market Dependency Network) represents bilateral market relationships derived from Student's t-copula analysis, revealing non-linear dependencies and tail co-movements between markets; (2) The middle layer (Risk Transfer Network) illustrates directed risk transmission pathways based on Diebold-Yilmaz spillover indices, with edge weights indicating the magnitude of volatility spillovers; (3) The bottom layer (Primary Transmission Channels) highlights the most significant pathways for information and risk flow, identifying the primary channels through which shocks propagate.

Figure 3.3 presents the multilayer network structure of China's carbon market. The visualisation comprises three distinct but interconnected layers, each capturing different aspects of market relationships and risk transmission patterns. The top layer represents market dependencies derived from Copula analysis, showing the strength and nature of bilateral market relationships. The middle layer illustrates the risk transfer network based on the Diebold-Yilmaz spillover index, with directed edges indicating the flow and magnitude of risk transmission. The bottom layer highlights the primary transmission channels, identifying the most significant pathways for information and risk flow. The dotted vertical lines connecting the corresponding nodes across layers demonstrate the integrated nature of these market relationships and facilitate the analysis of cross-layer interactions.

Market Integration and Network Evolution

This paper examines how the integration of China's carbon market affects market architecture and risk transmission through network analysis. We construct a multilayer network framework to decompose and analyse market relationships. Our empirical findings demonstrate that market integration significantly reshapes network topology and alters risk transmission patterns.

Network Architecture Evolution We characterize market architecture through three distinct but interconnected network layers: the dependency structure layer capturing bilateral market relationships, the risk transfer layer measuring risk transmission patterns, and the main channel layer identifying critical transmission pathways. For each layer, we compute standard network metrics including density, weighted degree, path length, and clustering coefficients.

Table 3.12: Network Architecture Evolution

Layer	Network Density	Average Weighted Degree	Average Path Length	Clustering Coefficient	Maximum Weight
Panel A: Pre-integration Network Metrics					
Dependency	1.000	0.195	1.000	1.000	0.069
Risk Transfer	1.000	0.070	1.000	1.000	0.023
Main Channel	0.143	0.025	2.700	0.000	0.023
Panel B: Post-integration Network Metrics					
Dependency	1.000	0.215	1.000	1.000	0.111
Risk Transfer	1.000	0.066	1.000	1.000	0.014
Main Channel	0.125	0.018	2.857	0.000	0.014
Panel C: Changes in Key Metrics (%)					
Dependency	0.00	+10.3	0.00	0.00	+60.9
Risk Transfer	0.00	-5.7	0.00	0.00	-39.1
Main Channel	-12.6	-28.0	+5.8	0.00	-39.1

Note: This table reports network metrics before and after market integration. Network density measures the ratio of actual to possible connections. Average weighted degree captures the mean strength of connections. Average path length represents the mean number of steps between any two markets. The clustering coefficient measures the degree of market clustering. Maximum weight indicates the strongest individual connection in each layer.

The empirical evidence reveals substantial changes in network architecture following market integration. As shown in Panels A and B of Table 1, the dependency layer exhibits increased connectivity strength, with the average weighted degree rising from 0.195 to 0.215. More striking is the 60.9% increase in maximum dependency weight from 0.069 to 0.111, suggesting significantly strengthened bilateral market relationships. The preservation of unity network density and clustering coefficients indicates maintained complete market connectivity.

The risk transfer layer presents a different pattern. Panel B shows that the average weighted degree decreases from 0.070 to 0.066, while the maximum weight drops by 39.1% from 0.023 to 0.014. This concurrent decline in both metrics, while maintaining complete network connectivity, suggests a more distributed risk transfer structure post-integration.

The main channel layer demonstrates the most dramatic structural changes. Panel C reveals that network density falls from 0.143 to 0.125, accompanied by a 28.0% decrease in average weighted degree. These substantial reductions, combined with a 5.8% increase in average path length (from 2.700 to 2.857), indicate a fundamental restructuring of primary transmission channels.

Market Role Transformation To understand how integration affects individual market behavior, we analyze changes in market roles through risk transfer patterns and external dependencies. Tables 3.13 quantify these transformations through detailed market-level metrics.

Table 3.13: Market Role Evolution

Panel A: Pre-integration Market Characteristics				
Market	Outward Transfer (%)	Inward Reception (%)	Net Transfer (%)	External Dependency
Shanghai	80.417	31.584	+48.834	0.040
Beijing	40.266	32.564	+7.702	-0.043
Guangdong	60.230	76.581	-16.351	-0.019
Tianjin	39.737	61.240	-21.502	-0.051
Hubei	15.295	42.545	-27.251	0.001
Panel B: Post-integration Market Characteristics				
CEA	42.071	45.084	-3.013	0.025
Shanghai	49.372	27.790	+21.582	0.048
Beijing	34.043	44.345	-10.302	0.029
Tianjin	46.296	20.181	+26.115	0.003
Hubei	38.139	65.569	-27.430	0.053

Note: This table presents market-level metrics before and after integration. Outward Transfer and Inward Reception represent the percentage of risk transmitted to and received from other markets, respectively. Net Transfer is the difference between outward and inward flows. External Dependency measures the correlation with external markets based on Copula parameters.

Panel A of Tables 3.13 reveals significant heterogeneity in pre-integration market roles. Shanghai dominates as a risk transmitter with a net transfer position of +48.834%, while Hubei serves as the primary risk receiver with -27.251%. Panel B documents substantial changes post-integration. Shanghai's net transfer position moderates to +21.582%, while Tianjin transforms from a significant risk receiver (-21.502%) to a major risk transmitter (+26.115%). The newly established national market (CEA) emerges with a relatively balanced profile, showing a modest net receiver position of -3.013

External dependencies also exhibit notable changes. Beijing's dependency shifts from -0.043 to +0.029, while Shanghai strengthens its positive dependency from 0.040 to 0.048. CEA's moderate positive external dependency (0.025) suggests measured integration with external markets. These changes in market roles and dependencies indicate a fundamental transformation in market structure, though longer-term data would be necessary to assess the persistence of these changes.

Risk Transmission Mechanism Analysis

In this section, we examine how market integration affects risk transmission patterns within China's carbon market network. We analyze both domestic risk transmission structures and their evolution following the introduction of the national market (CEA).

Domestic Risk Network Evolution Table 3.14 presents the risk transfer matrices before and after market integration, documenting significant changes in risk transmission patterns among domestic markets.

Table 3.14: Domestic Risk Transfer Evolution

Panel A: Pre-integration Risk Transfer Matrix (%)					
From/To	Shanghai	Beijing	Guangdong	Hubei	Shenzhen
Shanghai	97.473	0.285	0.605	0.226	0.233
Beijing	0.351	97.395	0.348	0.146	0.628
Guangdong	2.277	0.297	93.874	0.174	0.534
Hubei	0.524	0.605	0.341	96.596	0.184
Shenzhen	0.233	0.628	0.534	0.184	96.665
Panel B: Post-integration Risk Transfer Matrix (%)					
From/To	CEA	Shanghai	Beijing	Hubei	Shenzhen
CEA	95.506	0.043	0.074	0.063	0.075
Shanghai	0.529	97.221	0.445	0.125	0.172
Beijing	0.193	1.032	95.565	0.353	0.297
Hubei	0.446	0.748	0.268	93.443	1.348
Shenzhen	1.358	0.172	0.354	0.507	96.154

Note: This table reports the percentage of risk transferred between markets. Each element (i,j) represents the percentage of risk transmitted from market i to market j. Diagonal elements show the proportion of risk retained within each market. Values are computed using the Diebold-Yilmaz methodology based on variance decomposition.

Panel A documents substantial heterogeneity in pre-integration risk retention, with self-risk retention rates ranging from 93.874% (Guangdong) to 97.473% (Shanghai). The off-diagonal elements reveal asymmetric risk transmission patterns, with Shanghai exhibiting the strongest outward spillover to Guangdong (2.277%).

Post-integration patterns in Panel B show notable changes. The newly established CEA demonstrates strong risk absorption capacity with 95.506% self-risk retention. Mean-

while, bilateral risk transmission patterns evolve significantly. For instance, Shenzhen's risk spillover to Hubei increases from 0.184% to 1.348%, while Shanghai's influence on Guangdong diminishes.

To further analyze these changes, we examine the net risk transfer positions and their evolution in Tables 3.15.

Table 3.15: Risk Transfer Directional Analysis

Market	TO Others	FROM Others	Net Transfer	Directional Spillover	Pairwise Spillover	Self Effect
Panel A: Pre-integration Directional Effects						
Shanghai	80.417	31.584	48.834	3.385	2.277	97.473
Beijing	40.266	32.564	7.702	1.815	0.628	97.395
Guangdong	60.230	76.581	-16.351	3.282	2.277	93.874
Hubei	15.295	42.545	-27.251	1.654	0.605	96.596
Shenzhen	43.878	41.686	2.192	1.579	0.628	96.665
Panel B: Post-integration Directional Effects						
CEA	42.071	45.084	-3.013	0.255	1.358	95.506
Shanghai	49.372	27.790	21.582	2.492	1.032	97.221
Beijing	34.043	44.345	-10.302	1.141	0.445	95.565
Hubei	38.139	65.569	-27.430	2.810	1.348	93.443
Shenzhen	33.027	38.456	-5.429	2.391	1.358	96.154

Note: This table reports directional risk transfer metrics. TO Others and FROM Others represent total risk transmitted to and received from other markets, respectively. Net Transfer is the difference between TO and FROM measures. Directional Spillover quantifies the strength of unidirectional risk transmission. Pairwise Spillover shows the maximum bilateral risk transmission. Self-Effect represents risk retained within each market.

The directional analysis reveals several key findings. First, market integration leads to more balanced risk transfer patterns, evidenced by the reduction in extreme net transfer positions. Shanghai's dominant position moderates substantially, with its net transfer declining from 48.834% to 21.582%. Second, the introduction of CEA creates a new equilibrium in risk distribution, manifested in its modest net receiver position (-3.013%) and balanced directional spillover effects (0.255%).

Particularly noteworthy is the evolution of pairwise spillover effects. The maximum bilateral spillover decreases from 2.277% (Shanghai-Guangdong) in the pre-integration period to 1.358% (Shenzhen-CEA) post-integration, suggesting more dispersed risk transmission channels. This structural change is accompanied by an overall decrease in directional spillover intensity, as evidenced by the generally lower spillover metrics in Panel B.

International Risk Integration Patterns This section examines how domestic market integration affects risk transmission between China's carbon market and the EU Emissions Trading System (EUA). Table 3.16 presents the evolution of cross-border risk relationships.

Table 3.16: International Risk Network Analysis

Market	Dependency Parameter	Risk TO EUA (%)	Risk FROM EUA (%)	Net Transfer	Maximum Spillover
Panel A: Pre-integration EUA Relationships					
Shanghai	-0.053	0.668	0.780	-0.112	0.780
Beijing	-0.045	0.589	0.063	+0.526	0.589
Guangdong	0.022	0.069	0.994	-0.925	0.994
Hubei	-0.021	0.540	0.292	+0.248	0.540
Shenzhen	-0.036	0.057	0.057	0.000	0.057
Panel B: Post-integration EUA Relationships					
CEA	0.012	0.262	0.037	+0.225	0.262
Shanghai	-0.031	0.617	0.719	-0.102	0.719
Beijing	0.077	0.195	0.739	-0.544	0.739
Guangdong	0.067	0.284	0.528	-0.244	0.528
Hubei	-0.005	0.864	0.665	+0.199	0.864
Shenzhen	0.001	0.289	0.020	+0.269	0.289

Note: This table reports metrics characterizing relationships with the EU carbon market (EUA). The Dependency Parameter is estimated using the Gaussian Copula. Risk TO and FROM EUA represent directional risk transmission percentages. Net Transfer indicates the net risk transmission position relative to EUA. Maximum Spillover shows the larger of the bilateral spillover effects.

The empirical evidence reveals significant changes in international risk integration patterns following domestic market unification. In the pre-integration period, Panel A shows predominantly negative dependency parameters with EUA, ranging from -0.053 (Shanghai) to -0.021 (Hubei), with Guangdong as the notable exception (0.022). Risk transmission patterns were similarly heterogeneous, with net transfer positions varying from -0.925% (Guangdong) to +0.526% (Beijing).

Post-integration data in Panel B documents a fundamental shift in these relationships. Most notably, dependency parameters turn predominantly positive, with Beijing (0.077) and Guangdong (0.067) showing the strongest positive dependencies with EUA. The newly established CEA exhibits a moderate positive dependency (0.012), suggesting measured integration with international markets.

To further analyze these evolving relationships, we examine the detailed risk transmission structure in Tables 3.17.

The cross-border risk transfer matrices reveal several key developments. First, EUA's risk retention rate shows a modest decline from 96.505% to 96.097%, suggesting slightly increased interaction with Chinese markets. Second, the pattern of risk spillovers becomes more balanced post-integration. For instance, the maximum risk spillover from EUA to Chinese markets decreases from 0.994% (to Guangdong) to 0.739% (to Beijing), while spillovers from Chinese markets to EUA show less extreme variation.

The introduction of CEA appears to play a stabilizing role in international risk

Table 3.17: Cross-border Risk Transfer Matrix

Panel A: Pre-integration Cross-border Transfer (%)						
From/To	EUA	Shanghai	Beijing	Guangdong	Hubei	Shenzhen
EUA	96.505	0.780	0.063	0.994	0.292	0.057
Shanghai	0.668	97.473	0.285	0.605	0.196	0.233
Beijing	0.589	0.371	97.395	0.348	0.146	0.628
Guangdong	0.069	2.277	0.297	93.874	0.179	0.534
Hubei	0.540	0.524	0.605	0.341	96.596	0.184
Shenzhen	0.057	0.233	0.628	0.537	0.184	96.665
Panel B: Post-integration Cross-border Transfer (%)						
From/To	EUA	CEA	Shanghai	Beijing	Hubei	Shenzhen
EUA	96.097	0.037	0.719	0.739	0.665	0.020
CEA	0.262	95.506	0.043	0.074	0.063	0.075
Shanghai	0.617	0.529	97.221	0.445	0.125	0.172
Beijing	0.195	0.193	1.032	95.565	0.353	0.297
Hubei	0.864	0.446	0.748	0.268	93.443	1.348
Shenzhen	0.289	1.358	0.172	0.354	0.507	96.154

Note: This table presents the percentage of risk transferred between the EUA and Chinese markets. Each element (i,j) represents the percentage of risk transmitted from market i to market j. Values are computed using the Diebold-Yilmaz methodology based on generalized variance decomposition.

transmission. Its moderate bilateral spillovers with EUA (0.262% outward, 0.037% inward) and balanced risk profile suggest it functions as a measured intermediary in international risk transmission. This is consistent with its modest positive dependency parameter (0.012) and balanced net transfer position (+0.225%).

Network Efficiency Analysis

Layer-specific Performance Evolution We analyze the evolution of network efficiency through a detailed examination of layer-specific performance metrics. Table 3.18 presents the comprehensive analysis of network structure changes across different layers.

The layer-specific analysis reveals distinct evolutionary patterns across network layers. In the dependency layer, while network density remains constant at 1.000, we observe a substantial increase in maximum weight (+60.87%) accompanied by increased standard deviation (+15.79%). These changes suggest greater differentiation in bilateral market relationships while maintaining comprehensive market connectivity.

To further examine the structural changes, we analyze the inter-layer relationship patterns in Tables 3.19.

The inter-layer analysis shows evolving relationships between network layers following market integration. The correlation between Layers 1 and 2 strengthens modestly (Pearson correlation increasing from 0.078 to 0.098), while the strong correlation between Layers 2

Table 3.18: Layer-specific Network Evolution

Period	Network Density	Average Weight	Maximum Weight	Minimum Weight	Standard Deviation
Panel A: Dependency Layer Metrics					
Pre-integration	1.000	0.028	0.069	0.001	0.019
Post-integration	1.000	0.027	0.111	0.001	0.022
Change (%)	0.00	-3.57	+60.87	0.00	+15.79
Panel B: Risk Transfer Layer Metrics					
Pre-integration	1.000	0.005	0.023	0.000	0.005
Post-integration	1.000	0.004	0.014	0.000	0.003
Change (%)	0.00	-20.00	-39.13	0.00	-40.00
Panel C: Main Channel Layer Metrics					
Pre-integration	0.143	0.012	0.023	0.006	0.006
Post-integration	0.125	0.009	0.014	0.004	0.004
Change (%)	-12.59	-25.00	-39.13	-33.33	-33.33

Note: This table reports layer-specific network metrics before and after market integration. Network Density measures the ratio of actual to possible connections. Weights represent connection strengths. Standard Deviation captures the dispersion of connection strengths within each layer.

Table 3.19: Inter-layer Correlation Analysis

Layer Pair	Pearson Correlation	Spearman Correlation	Cosine Similarity	Layer1 Density	Layer2 Density
Panel A: Pre-integration Layer Correlations					
Layer1-Layer2	0.078	0.339	0.572	1.000	1.000
Layer1-Layer3	-0.027	0.016	0.231	1.000	0.143
Layer2-Layer3	0.783	0.532	0.757	1.000	0.143
Panel B: Post-integration Layer Correlations					
Layer1-Layer2	0.098	0.330	0.588	1.000	1.000
Layer1-Layer3	-0.002	0.120	0.229	1.000	0.125
Layer2-Layer3	0.655	0.457	0.652	1.000	0.125

Note: This table presents correlation metrics between network layers. Pearson and Spearman correlations measure linear and rank-based relationships, respectively. Cosine similarity captures the angular similarity of layer structures. Layer densities are reported for reference.

and 3 moderates (decreasing from 0.783 to 0.655).

To examine the efficiency implications of these structural changes, we analyze the layer-specific transmission patterns in Tables 3.20 .

Table 3.20: Layer-specific Transmission Analysis

Layer	Average Path Length	Direct Effect	Indirect Effect	Self Retention	Cross-layer Spillover
Panel A: Pre-integration Transmission Metrics					
Dependency	1.000	0.195	0.028	0.964	0.435
Risk Transfer	1.000	0.070	0.005	0.783	0.331
Main Channel	2.700	0.025	0.012	0.572	0.143
Panel B: Post-integration Transmission Metrics					
Dependency	1.000	0.215	0.027	0.956	0.397
Risk Transfer	1.000	0.066	0.004	0.655	0.356
Main Channel	2.857	0.018	0.009	0.588	0.125

Note: This table reports transmission-related metrics for each network layer. Average Path Length measures the mean steps between markets. Direct and Indirect Effects capture immediate and mediated transmission impacts. Self-retention represents the proportion of effects retained within the layer. Cross-layer Spillover measures transmission effects across layers.

The transmission analysis reveals significant changes in network efficiency characteristics. The dependency layer shows increased direct effects (0.195 to 0.215) while maintaining stable indirect effects. In contrast, the risk transfer layer exhibits reduced transmission intensities across both direct (0.070 to 0.066) and indirect (0.005 to 0.004) effects. The main channel layer shows the most substantial changes, with decreased direct effects (0.025 to 0.018) and modified transmission paths (average path length increasing from 2.700 to 2.857).

Market Structure Effectiveness

We examine the economic implications of market integration through a detailed analysis of structural changes and their effects on market functioning. Table 3.21 presents key structural effectiveness metrics before and after integration.

The empirical evidence reveals substantial changes in market structure following integration. Most notably, while maintaining complete network connectivity (density = 1.000), bilateral market relationships strengthen significantly, as evidenced by the 60.87% increase in maximum dependency. Simultaneously, the risk transfer rate moderates from 0.070 to 0.066, suggesting more balanced risk distribution patterns.

To examine the implications for market stability, we analyze the evolution of risk concentration patterns in Tables 3.22 .

The risk concentration analysis reveals significant structural improvements in market stability. The reduction in maximum spillover effects (from 2.277% to 1.358%) and the

Table 3.21: Market Structure Effectiveness Metrics

Panel A: Network Structure Indicators			
Metric	Pre-integration	Post-integration	Change (%)
Network Density	1.000	1.000	0.00
Maximum Dependency	0.069	0.111	+60.87
Risk Transfer Rate	0.070	0.066	-5.71
Average Path Length	2.700	2.857	+5.81
Panel B: Market Position Analysis			
Maximum Net Transfer	48.834	26.115	-46.52
Average External Dependency	-0.027	0.020	-
Cross-market Dispersion	0.019	0.022	+15.79
Risk Retention (Mean)	96.401	95.578	-0.85

Note: This table reports key metrics characterizing market structure effectiveness. Network metrics are calculated from the multi-layer network analysis. Market position metrics are derived from risk transfer and dependency analyses. All changes are computed relative to pre-integration values.

Table 3.22: Risk Concentration Evolution

Panel A: Pre-integration Risk Distribution					
Market	Risk Retention	Maximum Spillover	Net Risk Position	Self Effect	Spillover Concentration
Shanghai	97.473	2.277	+48.834	0.195	0.069
Beijing	97.395	0.628	+7.702	0.070	0.023
Guangdong	93.874	2.277	-16.351	0.025	0.023
Panel B: Post-integration Risk Distribution					
CEA	95.506	1.358	-3.013	0.215	0.111
Shanghai	97.221	1.032	+21.582	0.066	0.014
Beijing	95.565	0.739	-10.302	0.018	0.014

Note: This table examines the evolution of risk concentration patterns. Risk Retention represents the percentage of risk retained within each market. Maximum Spillover shows the largest risk transmission to any single market. Net Risk Position indicates the balance of risk inflows and outflows. Spillover Concentration measures the degree of risk transmission concentration.

moderation of extreme net risk positions (maximum absolute position decreasing from 48.834% to 21.582%) suggest more balanced risk distribution patterns post-integration.

To quantify the implications for market efficiency, we examine the evolution of network transmission characteristics in Tables 3.23.

Table 3.23: Network Transmission Efficiency

Transmission Metric	Pre-integration	Post-integration	Change (%)
Direct Effects	0.195	0.215	+10.26
Path Length	2.700	2.857	+5.81
Network Density	0.143	0.125	-12.59
Layer Correlation	0.078	0.098	+25.64
Cross-layer Effect	0.435	0.397	-8.74

Note: This table presents metrics related to network transmission efficiency. All metrics are derived directly from the network analysis. Changes are computed relative to pre-integration values.

The evidence suggests several key economic implications:

1. **Enhanced Market Integration** - Stronger bilateral market relationships (maximum dependency +60.87%) - More balanced risk distribution (risk transfer rate -5.71%) - Improved cross-market coordination (layer correlation +25.64%)

2. **Improved Market Stability** - Reduced maximum risk spillovers (2.277% to 1.358%) - More moderate net risk positions (48.834% to 21.582%) - Maintained high risk retention rates (95.578% mean)

3. **Evolution of Market Structure** - Optimized transmission paths (average path length +5.81%) - More focused network structure (density 0.143 to 0.125) - Enhanced layer synchronization (correlation 0.078 to 0.098)

These structural changes suggest that market integration has effectively enhanced both market stability and efficiency, though through different channels than initially hypothesized in the literature. Rather than reducing market fragmentation through uniformly increased connectivity, the integration process has led to more differentiated but stable market relationships, with optimized risk transmission channels and improved cross-market coordination mechanisms.

3.4.6 Economic and Policy Implications

In this section, we analyze the economic implications of our empirical findings and discuss corresponding policy recommendations. The integration of China's regional carbon markets into a unified national market has significantly influenced market efficiency, risk distribution, and international linkages. By referencing specific results from our analysis, we provide insights into these developments and their broader economic impact.

Economic Implications

Our empirical analysis demonstrates that market unification has enhanced market efficiency through strengthened market integration. As indicated in Table 3.6, the average dependence parameter increased by 250% from 0.0004 to 0.0014 post-unification, and the number of significant dependencies (absolute value greater than 0.04) rose from 5 to 8. This heightened interconnectivity suggests improved information transmission and price co-movement among regional markets, leading to more efficient price discovery mechanisms. The increased proportion of positive dependencies, from 33.3% to 56.3%, indicates a shift towards more cohesive market movements, which is essential for effective carbon pricing and resource allocation.

Furthermore, the risk spillover analysis reveals a more balanced distribution of risk among markets after unification. As shown in Table 3.11, the maximum net spillover decreased from 48.834% (Shanghai pre-unification) to 26.115% (Tianjin post-unification), and the average risk retention rate slightly declined from 96.401% to 95.578% (Table 3.21). These changes suggest that markets are now more interconnected in absorbing and transmitting risk, enhancing overall market stability. The diversification of risk across a unified market mitigates the impact of idiosyncratic shocks on individual markets, fostering a more resilient trading environment.

The optimized network structure, as evidenced by the network analysis, contributes to transmission efficiency and stability. The maximum dependency weight in the dependency layer increased by 60.9% from 0.069 to 0.111 (Table 3.12), indicating stronger bilateral relationships. Simultaneously, the average path length in the main channel layer increased by 5.8%, reflecting a restructuring of primary transmission channels. These developments enhance the speed and reliability of information dissemination, reduce transaction costs, and facilitate coordinated market behavior, which can improve liquidity and deepen the market.

Moreover, the dependency parameters between China's carbon markets and the European Union Allowance (EUA) market shifted from predominantly negative to positive post-unification, as seen in Table 3.16. For example, Beijing's dependency parameter changed from -0.045 to 0.077, indicating increased co-movement with international markets. This enhanced international integration has significant economic implications, including attracting foreign investment, facilitating technology and knowledge transfer, and promoting policy harmonization. However, it also necessitates robust risk management to mitigate potential adverse effects from global market volatility.

Policy Implications

The empirical findings underscore the need for targeted policy interventions that are directly linked to the structural changes observed after market unification. First, strengthening

market coordination is essential to build on the documented efficiency gains. Our results show that the overall information transfer rate increased markedly from 0.432 to 0.516, highlighting that a more integrated system facilitates faster and more accurate information transmission. To capitalize on this, policymakers should mandate a single, standardized Monitoring, Reporting, and Verification (MRV) system and establish a centralized, real-time national data platform to ensure consistency and transparency across regions.

Second, the analysis reveals a dramatic role reversal in certain regional markets, most notably Tianjin, which shifted from a net receiver of risk (-21.5%) to a net transmitter ($+26.1\%$). This dynamic transformation demonstrates the importance of adaptive regulatory oversight. Regulators should implement a "Spillover Watchlist," based on the Diebold-Yilmaz index, to monitor sudden shifts in systemic importance. In addition, the creation of a national Market Stability Reserve (MSR), analogous to that used in the EU ETS, would provide a buffer mechanism to address excessive volatility and mitigate contagion risks.

Finally, promoting international integration remains a key forward-looking priority. Given the growing interdependence between China's market and global climate policy, China should initiate a formal joint feasibility study on a potential future linkage with the EU ETS. At the same time, proactive engagement with the European Union on the Carbon Border Adjustment Mechanism (CBAM) would help mitigate external trade frictions while aligning domestic carbon pricing with emerging international norms. These steps would enhance China's influence in global carbon governance and strengthen the resilience of its national emissions trading system.

Conclusions

Our empirical study demonstrates that the unification of China's carbon markets has led to significant enhancements in market integration, risk distribution, and network efficiency. These developments have positive economic implications, including improved market efficiency, increased stability, and stronger international linkages. Policymakers should build upon these advancements by implementing coordinated strategies that reinforce market mechanisms and address emerging challenges.

This research contributes to the literature by providing quantitative evidence on the impacts of market unification using a multi-layer network analysis framework. By linking structural changes to economic outcomes, we offer valuable insights for both academia and policymakers involved in carbon market development. However, the findings are constrained by the limited post-unification data period. Future research should extend the analysis over a longer timeframe to assess the persistence and long-term effects of market unification. Additionally, exploring micro-level impacts on individual firms and sectors could provide a more granular understanding of the mechanisms at play.

Overall, our study underscores the importance of strategic policy interventions to enhance

the functioning of carbon markets, which are vital tools in the global effort to mitigate climate change.

3.5 Conclusions

This study has investigated the evolution of risk transmission mechanisms and international integration in China's carbon market following the unification of the national carbon market in 2021. Utilizing a multi-layer network analysis that integrates GARCH models, Copula functions, and the Diebold-Yilmaz spillover index, we have uncovered significant transformations in market dynamics, efficiency, and risk distribution.

Firstly, our findings indicate a notable improvement in market efficiency post-unification. The information transfer rate increased from 0.432 to 0.516, reflecting enhanced information dissemination and price discovery among regional markets. This improvement suggests that the unified market structure has facilitated more efficient capital allocation and reduced informational asymmetries, contributing to a more robust trading environment.

Secondly, the national carbon market has emerged as a central coordinator within the risk transmission network. With an eigenvector centrality of 0.412, the national market plays a pivotal role in connecting regional markets, thereby streamlining risk transmission pathways. The roles of regional markets have also evolved substantially. For instance, Tianjin transformed from a major risk receiver with a net spillover of -21.502% to a significant risk transmitter with a net spillover of 26.115%. This shift underscores the dynamic adjustments within the unified market and highlights the adaptability of regional markets to the new market structure.

Thirdly, integration with international markets, particularly the European Union Emissions Trading System (EU ETS), has strengthened moderately. The positive change in dependency parameters between China's carbon markets and the EU ETS signifies increased co-movement and potential for greater international collaboration. However, the maintenance of distinct domestic characteristics suggests that while international integration is progressing, China's carbon market retains unique features influenced by regional policies and market conditions.

These developments carry significant policy implications. Policymakers should capitalize on the enhanced market integration by promoting further harmonization of trading rules, reporting standards, and verification processes across regional markets. Strengthening market coordination can reduce residual fragmentation and enhance overall market efficiency. Additionally, there is a need to bolster risk management mechanisms. Implementing advanced monitoring systems to detect emerging vulnerabilities and encouraging the development of financial instruments for hedging can enhance market resilience and stability.

The study contributes to the existing literature by providing empirical evidence on the impacts of market unification using a comprehensive multi-layer network framework. By linking structural changes in the market to economic outcomes, it offers valuable insights for both academics and practitioners involved in carbon market development and

regulation.

However, the research is subject to certain limitations. The limited post-unification data period restricts the ability to assess the long-term effects and the persistence of observed changes. Future research should extend the analysis over a longer timeframe to evaluate the enduring impacts of market unification. Additionally, exploring micro-level impacts on individual firms and sectors could provide a more granular understanding of the mechanisms at play and inform more targeted policy interventions.

In conclusion, the unification of China's carbon market has led to significant enhancements in market efficiency, stability, and international integration. These positive outcomes underscore the importance of strategic policy interventions to reinforce the benefits of unification and address emerging challenges. By strengthening market mechanisms and risk management systems, China can further leverage its carbon market as a vital tool in the global effort to mitigate climate change.

Chapter 4

Does the AI Boom Reshape Energy Market Risk? Evidence from Financial Linkages

4.1 Introduction

The artificial intelligence (AI) industry has emerged as a key driver of the digital economy, with its application scope expanding rapidly in computer vision, natural language processing, intelligent manufacturing, and other domains. Unlike conventional energy-intensive industries (e.g., petrochemicals, steel, and cement), which directly consume fossil fuels, the AI sector predominantly relies on electricity to meet its substantial computing demands. According to recent reports by the International Energy Agency (IEA), data centers could account for up to 8% of global electricity consumption by 2030, with a considerable portion of this growth attributable to the rapid expansion of AI model training and cloud computing (International Energy Agency, 2023, 2024). These projections indicate that the escalating computational power of AI and its associated electricity consumption will soon significantly influence global energy systems and carbon emissions.

At the same time, governments and industries worldwide are accelerating the transition to low-carbon energy. Clean energy technologies (e.g., photovoltaic power, wind power, energy storage) and carbon trading systems (e.g., the EU Emissions Trading System) have expanded substantially, supported by large-scale policy initiatives. For instance, the European Union's "Green Deal" aims to exceed a 40% share of renewable power generation by 2030 (European Commission, 2019), complemented by carbon pricing and taxation mechanisms designed to facilitate the shift from fossil fuels to cleaner energy sources. Against this backdrop, an urgent question arises: *how can we accommodate the surging demand for AI-driven computing while simultaneously pursuing a green and low-carbon energy transition?*

In contrast to industries with direct fossil fuel combustion and substantial sensitivity to oil, gas, and carbon price fluctuations, the AI industry's reliance on electricity as the principal energy input implies a different level of exposure to these markets. When electricity supply is dominated by renewable sources and carbon tax systems are well established, the AI industry may be relatively insulated from volatility in fossil fuel markets. By contrast, in regions relying primarily on coal or natural gas generation, expanding AI computing demand can indirectly boost oil and gas consumption or drive up carbon prices. Notably, since the release of large-scale models such as ChatGPT in late 2022, AI has attracted unprecedented investment attention, which may generate "resonance effects" (positive or negative) with the clean energy sector. Prior research shows that financial markets often regard "AI + clean energy" as a long-term growth theme; however, under extreme scenarios (e.g., policy subsidy cuts, geopolitical conflicts, or hikes in carbon taxes), these sectors could experience concurrent sharp fluctuations, intensifying risks in their lower-tail dependence (Bartram et al., 2022; Pástor et al., 2022).

These considerations underscore the importance of understanding the financial linkage and risk transmission mechanisms between the AI industry and the clean energy, carbon

pricing, and oil and gas markets, particularly under extreme market conditions or major shock events. From both policy-making and investment management perspectives, clarifying these dynamics is crucial for designing effective carbon pricing strategies, energy transition policies, and cross-market risk management tools. This study examines the financial linkages between the AI industry—representing "digital energy-intensive" (DEI) sectors—and clean energy, fossil energy, and carbon pricing markets, with a particular focus on tail dependence and volatility spillover effects under market conditions or major policy and technological shocks.

Specifically, we investigate three core research questions. First, during extreme market conditions, does the AI industry exhibit decoupling from oil, gas, and carbon prices? Traditional energy-intensive sectors that directly combust fossil fuels tend to display strong sensitivity to oil, gas, and carbon price fluctuations. We examine whether the electricity-driven AI industry, by contrast, demonstrates weaker tail dependence on these prices during severe market downturns or upturns, and how non-linear approaches (e.g., Copula models) can capture this behaviour. Second, how do major policy or technological shocks (such as the release of ChatGPT) influence the tail linkages between AI and clean energy? We investigate whether financial markets are prone to attributing higher valuations and increased attention to AI at critical turning points, causing speculative capital to simultaneously flow into the clean energy sector. Under extreme market conditions, we assess whether there is evidence that upper or lower tail linkages become significantly amplified. Third, under extreme scenarios (e.g., subsidy cuts or carbon tax hikes), does volatility spillover from clean energy to AI reverse? During typical market conditions, AI and clean energy are often positively correlated, both perceived as high-beta sectors. Yet in periods of subsidy reductions or heightened market panic, we examine whether negative shocks in clean energy could amplify losses in AI, leading both to exhibit resonant downturns.

By addressing these questions, this research provides a more holistic view of the financial coupling and risk transmission pathways between DEI industries and energy–carbon markets. Such insights furnish empirical evidence for policy-making (e.g., optimizing data center energy efficiency standards, carbon tax designs, or clean energy subsidies) and inform investors' cross-market risk management strategies. This study advances the literature through four significant contributions spanning theoretical, methodological, empirical, and policy dimensions.

Our theoretical innovation extends the Energy Conversion Hierarchy (ECH) framework to establish Digital Energy-Intensive (DEI) sectors as a distinct analytical category. We demonstrate how computing requirements and electricity dependence differentiate DEI sectors from traditional energy-intensive industries, providing novel insights into AI's differential sensitivity to fossil fuel volatility and carbon pricing mechanisms. Methodologically, we advance the field by combining time-varying Copula modeling with Diebold-Yilmaz

spillover index analysis to simultaneously capture non-linear tail dependencies and directional risk transmissions. This integrated approach enables: (1) quantification of asymmetric upper- and lower-tail linkages, and (2) decomposition of net directional spillovers across interconnected markets, addressing critical limitations in existing energy-finance literature.

Our empirical novelty derives from a comprehensive event-focused analysis of daily data (2020-2024) covering AI, renewable energy (wind/photovoltaics), fossil fuels, and EU carbon allowances (EUA). We establish the late-2022 ChatGPT release as a structural breakpoint, examining market co-movements through multiple shocks including COVID-19, geopolitical conflicts, and carbon policy reforms, providing unprecedented evidence on technology-energy-carbon nexus dynamics. The policy relevance of our findings emerges from our discovery that AI exhibits asymmetric tail dependence: weak correlation with fossil fuels during extremes but synchronized amplification with clean energy following technological shocks. Crucially, spillover analysis reveals negative transmission channels where renewable subsidy cuts propagate losses to AI markets. These insights directly inform carbon taxation design, green electricity mandates, and cross-market hedging strategies for "AI + clean energy" investment portfolios.

The remainder of this paper proceeds as follows. Section 2 establishes the theoretical foundation through a comprehensive literature review, introducing the novel conceptual frameworks of Digital Energy-Intensive (DEI) sectors and Energy Conversion Hierarchy (ECH), while deriving four empirically testable hypotheses regarding AI-energy-carbon market interdependencies. Section 3 details the econometric methodology, including data curation procedures, variable construction, and implementation of the three-stage analytical approach: GARCH filtering for volatility extraction, Copula modeling for dependence estimation, and Diebold-Yilmaz spillover indices for network transmission analysis. Section 4 presents empirical findings through integrated interpretation of static and time-varying Copula results with dynamic spillover metrics, quantitatively characterizing tail dependence and volatility transmission mechanisms between AI and energy-carbon markets, with particular attention to structural breaks following the ChatGPT launch and during extreme market events. Section 5 concludes by synthesizing policy implications for carbon taxation, renewable energy mandates, and efficiency standards, alongside practical hedging strategies for cross-market risk management, while identifying promising research trajectories at the digitalization-decarbonization nexus. This integrated approach delivers evidence-based guidance for reconciling digital economic expansion with accelerated low-carbon transitions.

4.2 Literature Review and Theoretical Framework

4.2.1 Literature Review

The accelerating global trends of digitalization and decarbonization converge at a critical nexus: the energy footprint of artificial intelligence (AI). While a growing body of research explores the intersection of **AI, energy, and carbon markets**, substantial gaps remain regarding the *tail risk* and *volatility spillover* connections between them. This review synthesizes existing research to build a coherent framework, positioning AI not merely as another technology sector, but as a unique economic category with a fundamentally distinct energy risk profile.

Our argument begins with AI's defining characteristic: its exclusive and immense reliance on electricity, a processed energy carrier. This immediately distinguishes it from **traditional energy-intensive industries** like petroleum, steel, and cement, which depend on the direct combustion of fossil fuels and are thus highly sensitive to their price fluctuations (Sadorsky, 2012; Niu, 2021). This distinction introduces the concept of an **Energy Conversion Hierarchy**. Positioned downstream from primary energy sources, AI is buffered from the direct volatility of oil and gas prices by the complex dynamics of the electricity grid (Patterson et al., 2021). While prior studies confirm strong tail-risk dependence between traditional industries and fossil fuel prices during extreme events (Tan and Lin, 2018; Hanif et al., 2021), the electricity "buffer layer" suggests AI should exhibit a fundamentally weaker and more indirect financial linkage to these primary commodities.

However, this contrast is insufficient, as AI also differs significantly from **other high-tech industries**. While sectors like semiconductors or internet platforms are energy-intensive, their power consumption typically scales linearly or sub-linearly with output (Masanet et al., 2020; Lin and Tan, 2017). In stark contrast, the rapid emergence of large AI models like ChatGPT implies *super-linear* or even exponential growth in computational workloads (Strubell et al., 2020). This voracious appetite for computation makes AI exceptionally sensitive to both the cost and stability of electricity supply, justifying its classification as a novel category: **Digital Energy-Intensive (DEI) industries**. During periods of tight electricity supply or carbon price surges, AI operations face elevated cost pressures that can trigger broader market volatility (Khosravi et al., 2024).

This unique DEI characteristic translates into a distinct set of financial interdependencies with **clean energy and carbon markets**. Because AI's primary operational risk is electricity cost and its primary long-term constraint is sustainable energy supply, its financial fate is deeply intertwined with the pace of grid decarbonization. Consequently, AI's market performance is logically linked to the clean energy sectors that enable its sustainable growth (Bolton and Kacperczyk, 2021; Bartram et al., 2022), and to carbon prices (like the EU ETS), which directly influence electricity costs in many regions (Hanif

et al., 2021; Niu, 2021). Investor narratives increasingly bundle "AI and Green Energy" as a unified growth theme, suggesting the potential for strong, policy-driven co-movements and correlated sell-offs during periods of risk aversion (Hong et al., 2019).

Despite these clear logical connections, the academic literature has yet to systematically quantify these emergent risk pathways. The financial relationship between DEI sectors and energy markets—shaped by indirect electricity exposure, technological narratives, and policy shocks—remains critically under-explored. Furthermore, existing analyses often rely on simple linear correlations, which are ill-suited to capture the asymmetric **upper-tail** and **lower-tail** dependencies that characterize systemic risk in extreme market conditions (Patton, 2006). Advanced methods like the Diebold-Yilmaz spillover index have been applied to energy markets, but studies focusing on AI's growing role within this nexus are still limited (Diebold and Yilmaz, 2012; Tiwari et al., 2021). This study aims to fill this crucial gap by providing the first comprehensive econometric investigation of the non-linear risk transmission mechanisms connecting AI to the broader energy ecosystem.

4.2.2 Conceptual Framework and Hypotheses

We develop a theoretical framework that conceptualizes artificial intelligence as the archetypal representative of "Digital Energy-Intensive" (DEI) industries—a new category of economic sectors characterized by rapidly scaling computational demands that translate into substantial electricity consumption while maintaining minimal direct fossil fuel dependencies. This framework provides the analytical foundation for understanding how DEI sectors interact with traditional energy markets under extreme financial conditions and technological disruptions.

The theoretical foundation of our analysis rests on three core mechanisms that distinguish DEI industries from conventional energy-intensive sectors. First, the *Energy Conversion Hierarchy Mechanism* recognizes that DEI industries operate at a different level within the energy value chain compared to traditional heavy industries. While sectors such as steel, cement, and petrochemicals rely on direct combustion of fossil fuels for their core production processes, DEI industries consume energy exclusively in the form of electricity (International Energy Agency, 2024). This distinction is crucial because electricity serves as an intermediate energy carrier that can be generated from diverse primary sources—fossil fuels, nuclear, hydroelectric, wind, solar, or other renewables. Recent empirical evidence demonstrates that this electricity intermediation provides substantial volatility buffering effects, reducing direct fossil fuel price volatility transmission by 20-65% compared to direct exposure (Navia Simon and Diaz Anadon, 2025; Luccioni et al., 2024). The hierarchical positioning of DEI industries thus creates a "buffer layer" between their operational costs and direct fossil fuel price volatility, as electricity prices reflect a complex aggregation of generation costs, transmission expenses, regulatory frameworks, and long-term supply

contracts rather than immediate commodity price fluctuations.

Second, the *Policy Transmission Mechanism* operates through the regulatory and policy environment that governs both energy markets and digital infrastructure. Carbon pricing policies, renewable portfolio standards, and data center efficiency regulations create indirect linkages between DEI industries and various energy market segments. Unlike traditional energy-intensive industries that face direct exposure to carbon taxes through their fuel consumption, DEI industries experience carbon policy impacts primarily through electricity pricing mechanisms. Research demonstrates that economic policy uncertainty positively affects renewable energy innovation for at least three years, with higher economic globalization and financial development reducing renewable energy costs (Feng and Zheng, 2022; Ma et al., 2022). This indirect exposure means that the magnitude and timing of policy effects depend critically on the carbon intensity of the local electricity grid, the presence of renewable energy certificates markets, and the ability of large electricity consumers to negotiate direct power purchase agreements with renewable generators. Consequently, policy shocks may generate asymmetric effects across different electricity markets and create time-varying correlations between DEI industries and specific energy subsectors.

Third, the *Financial Market Perception Mechanism* reflects how investment decisions and asset pricing respond to evolving narratives about technological convergence and sectoral synergies. Financial markets may price DEI industries and clean energy technologies as complementary components within a broader "technology-enabled energy transition" theme, particularly following major technological breakthroughs that heighten investor attention to these sectors. Technology-policy synergy theories demonstrate multiplicative rather than additive effects in clean energy finance markets, where combined effects exceed individual component sums (Alamaren et al., 2024). This mechanism operates through portfolio allocation decisions, thematic investment strategies, and the formation of risk premiums that reflect perceived correlations between technological adoption rates and clean energy deployment. Event-driven amplification mechanisms show that technological breakthroughs create disproportionate financial market responses, with high levels of total connectedness during technological breakthrough periods, as technology and energy assets exhibit significant volatility spillovers (Mensi et al., 2024). However, the same mechanism that generates positive correlations during periods of optimism can amplify negative correlations during risk-off episodes, when high-beta sectors experience synchronized sell-offs regardless of their fundamental economic relationships.

These three mechanisms interact to generate distinct patterns of financial co-movement between DEI industries and energy markets that evolve dynamically in response to technological innovations and policy developments. The interaction between the Energy Conversion Hierarchy and Policy Transmission mechanisms suggests that DEI industries should exhibit relatively stable, low correlations with fossil fuel prices and carbon allowances

under normal market conditions, as electricity markets provide both physical and financial insulation from direct commodity price shocks. Empirical evidence supports this theoretical prediction, showing that merit order effects provide natural buffering with substantial dampening of fossil fuel price transmission (Navia Simon and Diaz Anadon, 2025). However, during extreme market stress or significant policy regime changes, these correlations may intensify if electricity market disruptions create direct pass-through effects or if regulatory uncertainty affects both sectors simultaneously.

The interaction between the Policy Transmission and Financial Market Perception mechanisms generates time-varying correlations between DEI industries and clean energy markets that depend critically on the policy environment and investor sentiment. When renewable energy policies are perceived as stable and supportive, financial markets may price DEI industries and clean energy technologies as beneficiaries of the same underlying trends toward grid decarbonization and technological innovation. Conversely, policy uncertainty or adverse regulatory developments may trigger correlated negative price movements across both sectors, particularly if investors view them as sharing similar regulatory risk exposures or growth dependencies on government support.

The interaction between the Energy Conversion Hierarchy and Financial Market Perception mechanisms creates heterogeneous relationships between DEI industries and different clean energy subsectors. Solar photovoltaic technology, characterized by rapid cost declines, high policy sensitivity, and strong technological narratives, may exhibit particularly strong financial linkages with DEI industries through investor perceptions of complementarity. Research demonstrates that clean energy subsectors exhibit pronounced heterogeneity in their responses to technological innovations, with solar technologies typically showing higher responsiveness compared to wind and bioenergy sectors (Alamaren et al., 2024). Wind energy, with more mature technology and different cost structures, may show weaker financial correlations despite potentially similar physical relationships through electricity markets. Bioenergy, facing distinct feedstock cost pressures and regulatory frameworks, may demonstrate even more attenuated financial linkages with DEI industries.

Major technological breakthroughs, such as the emergence of large-scale generative AI models, can fundamentally alter the operation of these mechanisms by reshaping market expectations about future energy demand patterns, technological adoption rates, and policy priorities. AI/digital industries demonstrate fundamentally different energy consumption patterns compared to traditional energy-intensive sectors, characterized by 100% electricity dependence with no direct fossil fuel combustion, with current global baseline consumption reaching 415 TWh (1.5% of global electricity), growing at 15% annually (International Energy Agency, 2024). Such events may trigger structural breaks in financial correlations by intensifying the salience of perceived synergies between DEI industries and clean energy technologies while simultaneously increasing the volatility of these relationships. Event studies demonstrate technology-energy correlation increases following breakthrough

announcements, with effects persisting for extended periods post-breakthrough (Xu et al., 2024; Alamaren et al., 2024). The magnitude of these effects depends on the perceived significance of technological advancement, its implications for future energy consumption patterns, and its interaction with existing policy frameworks and market structures.

From this theoretical foundation, we derive four testable hypotheses that capture the key predictions of our conceptual framework. The first hypothesis emerges directly from the Energy Conversion Hierarchy Mechanism and predicts that DEI industries should exhibit fundamentally different financial relationships with fossil fuel and carbon markets compared to traditional energy-intensive sectors. This prediction reflects the theoretical expectation that electricity markets provide a buffer against direct fossil fuel price shocks, even under conditions of extreme market stress when correlations typically intensify across asset classes.

Hypothesis 1 (Energy Hierarchy Hypothesis): *Due to its reliance on electricity rather than direct fossil fuel combustion, the AI sector exhibits relatively weak financial tail dependence with oil, gas, and carbon prices during extreme market conditions compared to traditional energy-intensive industries.*

The second hypothesis derives from the interaction between all three mechanisms and addresses the heterogeneous nature of clean energy technologies and their differential relationships with DEI industries. This prediction recognizes that financial market perceptions of complementarity between DEI industries and specific clean energy technologies depend not only on physical energy relationships but also on growth dynamics, policy frameworks, and investor narratives that may vary significantly across clean energy subsectors.

Hypothesis 2 (Clean Energy Heterogeneity Hypothesis): *Within the clean energy complex, subsectors with higher growth potential, greater policy sensitivity, or stronger alignment with technology narratives exhibit stronger extreme financial linkages with the AI sector compared to other clean energy segments.*

The third hypothesis captures the dynamic nature of these relationships and the role of technological breakthroughs in reshaping market perceptions. This prediction reflects the theoretical expectation that the Financial Market Perception Mechanism becomes more pronounced following events that heighten investor attention to sectoral relationships and perceived synergies.

Hypothesis 3 (Dynamic Dependence Hypothesis): *Major technological advancements or policy shifts perceived as significant by financial markets amplify the tail dependence and volatility spillovers between the AI sector and clean energy markets, particularly in the upper tail during bullish periods or the lower tail during risk-off episodes.*

The fourth hypothesis addresses the bidirectional nature of risk transmission and the potential for asymmetric spillover effects under different market conditions. This prediction emerges from the interaction between the Policy Transmission and Financial Market Perception mechanisms, which suggests that shared policy risk exposures and

high-beta characteristics can create bidirectional contagion effects that intensify during periods of market stress. Bidirectional risk transmission between technology and energy sectors shows significant interconnectedness, with spillover analysis revealing substantial total connectedness, where technology sectors often act as net risk transmitters to energy sectors (Xu et al., 2024; Alamaren et al., 2024).

Hypothesis 4 (Asymmetric Spillover Hypothesis): *While AI might be a net transmitter of volatility to clean energy during normal or bullish periods, under conditions of significant market stress or negative policy shocks impacting the clean energy sector, the directionality can reverse, with clean energy becoming a significant source of negative volatility spillovers to the AI sector.*

These four hypotheses collectively provide a comprehensive framework for empirically testing the key predictions of our theoretical model while capturing the complex, time-varying, and potentially asymmetric nature of financial relationships between DEI industries and energy markets. The hypotheses are designed to be tested using the advanced econometric methods described in our empirical methodology, particularly copula models that can capture nonlinear tail dependencies and spillover analysis that can identify the direction and magnitude of volatility transmission across markets.

4.3 Data and Methodology

4.3.1 Overview and Methodological Framework

This section develops an integrated econometric framework to examine the evolving interdependencies between artificial intelligence (AI) technology firms and energy markets under extreme market conditions. Our methodological contribution lies in three key dimensions. First, we employ a dynamic t-copula specification that captures time-varying tail dependence while accounting for the heavy-tailed nature of financial returns, a critical feature often overlooked in the AI-energy nexus literature. Second, we complement the copula analysis with the Diebold-Yilmaz spillover framework to quantify directional volatility transmissions, providing a comprehensive view of both contemporaneous dependencies and lead-lag relationships. Third, our event-study design allows for structural break analysis around major technological and policy shifts, offering insights into how exogenous shocks reshape cross-market linkages.

The choice of this particular methodological combination is motivated by the unique characteristics of AI and energy markets. While traditional correlation measures fail to capture asymmetric dependencies during market stress, our copula-based approach reveals how extreme movements in AI valuations translate into energy market disruptions. Moreover, the integration of GARCH filtering ensures that we isolate genuine cross-market dependencies from univariate volatility clustering, a distinction crucial for policy implications.

4.3.2 Data Structure and Preliminary Transformations

Data Collection and Quality Control

Our analysis employs daily closing prices for three distinct market segments spanning from **January 2, 2020 to June 30, 2024**, encompassing **1,129** trading days. The dataset includes leading AI technology firms specializing in machine learning and computational infrastructure, clean energy indices capturing renewable energy producers and technology providers, and fossil fuel markets including oil, natural gas, and carbon emission certificates.

Let $P_{i,t}$ denote the closing price of asset i at time t, where $i \in \{1, 2, \ldots, N\}$ indexes the assets and $t \in \{1, 2, \ldots, T\}$ indexes time. We implement comprehensive data cleaning procedures to ensure the integrity of our statistical inference. Non-numeric entries and missing observations are identified and removed to maintain temporal alignment across all series. For outlier detection, we apply the Rousseeuw and Leroy (1993) robust estimation method, flagging observations where:

$$P_{i,t} > Q_3 + 3 \times IQR \quad \text{or} \quad P_{i,t} < Q_1 - 3 \times IQR, \tag{4.1}$$

where Q_1 and Q_3 denote the first and third quartiles, and IQR represents the interquartile range. To address non-synchronous trading across international markets, we align all series to a common trading calendar, forward-filling prices for market holidays.

Return Calculation and Properties

Following standard practice in financial econometrics, we transform raw prices into logarithmic returns:

$$r_{i,t} = \ln(P_{i,t}) - \ln(P_{i,t-1}) = \ln\left(\frac{P_{i,t}}{P_{i,t-1}}\right), \tag{4.2}$$

for $t = 2, \ldots, T$ and $P_{i,t} > 0$. The use of log returns ensures temporal additivity and provides approximate normality for small price changes while treating positive and negative movements symmetrically.

In the context of AI-energy market interactions, these returns capture the instantaneous rate of value creation or destruction. During periods of technological breakthrough, such as major AI model releases, we observe heightened volatility in AI firm returns transmitted to energy markets through increased computational demand, shifting investor preferences toward sustainable energy sources, and speculative capital flows between sectors.

4.3.3 Univariate Volatility Modeling: GARCH Framework

Model Specification and Estimation

Before examining cross-market dependencies, we must filter out the well-documented volatility clustering in financial returns. For each asset i, we specify a GARCH(1,1) model with the conditional mean equation:

$$r_{i,t} = \mu_i + \sum_{j=1}^{p} \phi_{i,j} r_{i,t-j} + \varepsilon_{i,t}, \tag{4.3}$$

where μ_i represents the unconditional mean return, $\phi_{i,j}$ are autoregressive coefficients capturing any predictable dynamics, and $\varepsilon_{i,t}$ is the innovation term. The lag order p is determined via the Bayesian Information Criterion (BIC) to maintain model parsimony.

The conditional variance follows:

$$\sigma_{i,t}^2 = \mathrm{Var}(\varepsilon_{i,t} \mid \mathcal{F}_{t-1}) = \omega_i + \alpha_i \varepsilon_{i,t-1}^2 + \beta_i \sigma_{i,t-1}^2, \tag{4.4}$$

where $\mathcal{F}_{t-1}$ denotes the information set available at time $t-1$. The parameter restrictions $\omega_i > 0$, $\alpha_i \geq 0$, $\beta_i \geq 0$, and $\alpha_i + \beta_i < 1$ ensure covariance stationarity.

Parameters $\Theta_i = \{\mu_i, \phi_{i,1}, \ldots, \phi_{i,p}, \omega_i, \alpha_i, \beta_i\}$ are estimated via quasi-maximum likeli-

hood (QML):

$$\hat{\Theta}_i = \arg\max_{\Theta_i} \sum_{t=1}^{T} \ell_{i,t}(\Theta_i), \tag{4.5}$$

Where the log-likelihood contribution is:

$$\ell_{i,t}(\Theta_i) = -\frac{1}{2}\left[\ln(2\pi) + \ln(\sigma_{i,t}^2) + \frac{\varepsilon_{i,t}^2}{\sigma_{i,t}^2}\right]. \tag{4.6}$$

The standardized residuals are then computed as:

$$z_{i,t} = \frac{\varepsilon_{i,t}}{\hat{\sigma}_{i,t}}, \tag{4.7}$$

which should exhibit no serial correlation under correct model specification.

Volatility Dynamics Interpretation

The GARCH parameters reveal distinct volatility patterns across markets. The innovation response parameter α_i measures immediate reactions to market shocks, while the persistence parameter β_i captures volatility inertia. Our empirical results show that AI firms exhibit significantly higher α_i values (averaging 0.15) compared to energy markets (averaging 0.08), indicating stronger sensitivity to news and innovation shocks. Conversely, energy markets display higher persistence with β_i approaching 0.90, reflecting the stability of physical infrastructure and long-term supply contracts. The sum $\alpha_i + \beta_i$ measures overall volatility persistence, with values near unity indicating that volatility shocks have long-lasting effects.

4.3.4 Multivariate Dependence Modeling via Copulas

Theoretical Foundation

Sklar's (1959) theorem provides the foundation for separating marginal distributions from dependence structures. For bivariate random variables (X, Y) with joint distribution $F_{X,Y}(x, y)$ and marginals $F_X(x)$, $F_Y(y)$, there exists a unique copula $C : [0, 1]^2 \to [0, 1]$ such that:

$$F_{X,Y}(x, y) = C(F_X(x), F_Y(y)). \tag{4.8}$$

This decomposition proves particularly valuable when marginal behaviors differ fundamentally from dependence structures, as is the case with AI and energy markets, where univariate volatility patterns reflect sector-specific dynamics while cross-market dependencies capture systemic risks.

Empirical Implementation

We transform standardized residuals to uniform marginals via the empirical distribution function:

$$u_{i,t} = F_{z_i}(z_{i,t}) \approx \frac{\text{rank}(z_{i,t})}{T+1}, \tag{4.9}$$

where the denominator ensures $u_{i,t} \in (0,1)$. This non-parametric approach avoids distributional assumptions while preserving the dependence structure.

For initial exploration, we estimate static copula parameters by maximizing the log-likelihood:

$$\hat{\boldsymbol{\theta}}_{ij} = \arg\max_{\boldsymbol{\theta}} \sum_{t=1}^{T} \ln c(u_{i,t}, u_{j,t}; \boldsymbol{\theta}), \tag{4.10}$$

where $c(\cdot,\cdot;\boldsymbol{\theta})$ denotes the copula density.

We consider four copula families with distinct dependence characteristics. The Gaussian copula $C^{\text{Ga}}(u_1,u_2;\rho) = \Phi_\rho(\Phi^{-1}(u_1),\Phi^{-1}(u_2))$ serves as a symmetric benchmark with no tail dependence. The Student-t copula $C^t(u_1,u_2;\rho,\nu) = t_{\rho,\nu}(t_\nu^{-1}(u_1),t_\nu^{-1}(u_2))$ introduces symmetric tail dependence through the degrees of freedom parameter ν. The Clayton copula $C^{\text{Cl}}(u_1,u_2;\theta) = (u_1^{-\theta}+u_2^{-\theta}-1)^{-1/\theta}$ emphasizes lower tail dependence, capturing joint crashes. The Gumbel copula $C^{\text{Gu}}(u_1,u_2;\theta) = \exp\{-[(-\ln u_1)^\theta + (-\ln u_2)^\theta]^{1/\theta}\}$ focuses on upper tail dependence, relevant for joint booms. Model selection employs information criteria and goodness-of-fit tests based on the empirical copula process.

Time-Varying Dependence Analysis

Static copulas may obscure important temporal variations in market linkages. We implement rolling window estimation with window length w:

$$\hat{\boldsymbol{\theta}}_{ij,t}^{(w)} = \arg\max_{\boldsymbol{\theta}} \sum_{s=t-w+1}^{t} \ln c(u_{i,s}, u_{j,s}; \boldsymbol{\theta}), \tag{4.11}$$

for $t = w, w+1, \ldots, T$. The choice of $w = 250$ trading days (approximately one year) balances temporal resolution against estimation precision. These rolling estimates reveal pronounced variation in dependence parameters, with correlations doubling during crisis periods and tail dependence coefficients showing even more dramatic shifts.

To capture the time-varying nature of these dependencies, we employ a rolling window estimation. To make an informed choice, we conducted a preliminary analysis comparing window lengths of 50, 100, and 250 days. The 100-day window was selected as it minimized the Mean Squared Error (MSE) of one-step-ahead out-of-sample correlation forecasts, thereby providing the best balance between capturing significant temporal dynamics and avoiding excessive noise from short-term market fluctuations.

4.3.5 Dynamic t-Copula Specification

Model Development

Building on the evidence of time-varying dependence, we specify a dynamic t-copula where parameters evolve smoothly according to observation-driven dynamics. This approach combines the flexibility of time variation with the parsimony of parametric evolution equations, avoiding the discreteness inherent in rolling window methods.

The correlation parameter $\rho_t \in (-1, 1)$ is modeled through a transformed process ensuring proper bounds:

$$\rho_t = \frac{\exp(\psi_t) - 1}{\exp(\psi_t) + 1} = \tanh(\psi_t/2), \tag{4.12}$$

where the latent process ψ_t follows:

$$\psi_t = \omega + \alpha \cdot f(u_{i,t-1}, u_{j,t-1}) + \beta \cdot \psi_{t-1}, \tag{4.13}$$

with stationarity ensured by $|\alpha| + |\beta| < 1$.

The forcing variable captures how past extremes influence current dependence:

$$f(u_{i,t}, u_{j,t}) = \Phi^{-1}(u_{i,t}) \cdot \Phi^{-1}(u_{j,t}), \tag{4.14}$$

where $\Phi^{-1}(\cdot)$ is the standard normal quantile function. This specification ensures that joint tail events (both variables simultaneously in their extremes) have the strongest impact on future correlation.

Likelihood and Estimation

The complete dynamic t-copula density at time t is:

$$c_t(u_{i,t}, u_{j,t}; \Omega) = \frac{f_{t,\nu}(t_\nu^{-1}(u_{i,t}), t_\nu^{-1}(u_{j,t}); \rho_t)}{f_{t,\nu}(t_\nu^{-1}(u_{i,t})) \cdot f_{t,\nu}(t_\nu^{-1}(u_{j,t}))}, \tag{4.15}$$

where $f_{t,\nu}(\cdot, \cdot; \rho_t)$ denotes the bivariate Student-t density with correlation ρ_t and ν degrees of freedom.

The parameter vector $\Omega = \{\omega, \alpha, \beta, \nu\}$ is estimated by maximizing:

$$\hat{\Omega} = \arg\max_{\Omega} \sum_{t=1}^{T} \ln c_t(u_{i,t}, u_{j,t}; \Omega), \tag{4.16}$$

using a two-step procedure that initializes with static estimates before optimizing the full dynamic specification.

The estimation results reveal strong evidence of contagion effects. The responsiveness

parameter α is significantly positive, indicating that extreme co-movements increase future dependence. The persistence parameter β exceeds 0.9, suggesting that shifts in market integration are highly persistent. The degrees of freedom parameter ν averages 6.5, confirming substantial tail dependence beyond Gaussian specifications. These dynamics imply that AI and energy markets become more tightly linked precisely when diversification benefits are most valuable.

4.3.6 Systemic Risk Assessment: Diebold-Yilmaz Framework

VAR-Based Spillover Methodology

While copulas capture contemporaneous dependencies, understanding directional volatility transmission requires examining lead-lag relationships. The Diebold-Yilmaz spillover framework, based on forecast error variance decompositions from vector autoregressions, provides precisely this directional perspective.

We specify a p-th order VAR for the return vector $\mathbf{r}_t = [r_{1,t}, r_{2,t}, \ldots, r_{N,t}]'$:

$$\mathbf{r}_t = \mathbf{c} + \sum_{i=1}^{p} \mathbf{\Phi}_i \mathbf{r}_{t-i} + \boldsymbol{\varepsilon}_t, \tag{4.17}$$

where $\mathbf{c}$ is the intercept vector, $\mathbf{\Phi}_i$ are coefficient matrices, and $\boldsymbol{\varepsilon}_t \sim \mathcal{N}(\mathbf{0}, \mathbf{\Sigma})$. The lag order p is selected by minimizing information criteria while ensuring residual whiteness.

Generalized Variance Decomposition

To avoid dependence on variable ordering, we employ the generalized variance decomposition of Pesaran and Shin (1998). The H-step-ahead forecast error variance of variable i due to innovations in variable j is:

$$\theta_{ij}^{(H)} = \frac{\sigma_{jj}^{-1} \sum_{h=0}^{H-1} (\mathbf{e}_i' \mathbf{\Psi}_h \mathbf{\Sigma} \mathbf{e}_j)^2}{\sum_{h=0}^{H-1} (\mathbf{e}_i' \mathbf{\Psi}_h \mathbf{\Sigma} \mathbf{\Psi}_h' \mathbf{e}_i)}, \tag{4.18}$$

where $\mathbf{\Psi}_h$ represents impulse responses and $\mathbf{e}_i$ denotes selection vectors.

After row normalization to ensure unit sums:

$$\tilde{\theta}_{ij}^{(H)} = \frac{\theta_{ij}^{(H)}}{\sum_{j=1}^{N} \theta_{ij}^{(H)}}, \tag{4.19}$$

We construct the total spillover index:

$$S^{(H)} = \frac{1}{N} \sum_{i=1}^{N} \sum_{\substack{j=1 \\ j \neq i}}^{N} \tilde{\theta}_{ij}^{(H)} \times 100. \tag{4.20}$$

Directional and Net Spillovers

Directional spillovers identify transmission patterns. Spillovers received by market i from all others:

$$S_{i\leftarrow\bullet}^{(H)} = \sum_{\substack{j=1 \\ j\neq i}}^{N} \tilde{\theta}_{ij}^{(H)} \times 100, \tag{4.21}$$

and transmitted from market i to all others:

$$S_{i\rightarrow\bullet}^{(H)} = \sum_{\substack{j=1 \\ j\neq i}}^{N} \tilde{\theta}_{ji}^{(H)} \times 100. \tag{4.22}$$

The net spillover position:

$$S_i^{(H)} = S_{i\rightarrow\bullet}^{(H)} - S_{i\leftarrow\bullet}^{(H)}, \tag{4.23}$$

identifies net transmitters ($S_i^{(H)} > 0$) versus receivers ($S_i^{(H)} < 0$).

Our empirical results reveal that AI markets consistently act as net volatility transmitters, with average net spillovers of +15% to clean energy and +10% to fossil fuel markets. This asymmetric transmission pattern intensifies during periods of technological innovation or regulatory uncertainty, confirming that AI market shocks propagate systematically through energy sectors. The total spillover index averages 45% but exceeds 70% during crisis periods, highlighting elevated systemic risks when market stress coincides across sectors.

4.3.7 Event Study Design and Structural Break Analysis

Event Identification and Classification

To examine how exogenous shocks reshape AI-energy market linkages, we implement a comprehensive event study framework. We identify major events across four categories: technological breakthroughs (GPT model releases, quantum computing advances), regulatory shifts (AI governance frameworks, energy transition policies), market disruptions (semiconductor shortages, energy crises), and macroeconomic shocks (monetary policy changes, geopolitical tensions).

For each event at date τ, we define pre- and post-event windows:

$$\text{Pre-event:} \quad \mathcal{T}_{\text{pre}} = \{t : \tau - 120 \leq t < \tau\} \tag{4.24}$$

$$\text{Post-event:} \quad \mathcal{T}_{\text{post}} = \{t : \tau \leq t < \tau + 120\} \tag{4.25}$$

using 120 trading days (approximately 6 months) to balance sample size with parameter stability.

Comparative Statistical Analysis

We conduct parallel analyses on pre- and post-event samples to identify structural changes. For marginal distributions, we re-estimate GARCH models and test for parameter shifts using Andrews (1993) supremum tests. For dependence structures, we compare static copula parameters via likelihood ratio tests:

$$LR = 2[\ell(\hat{\boldsymbol{\theta}}_{\text{post}}) + \ell(\hat{\boldsymbol{\theta}}_{\text{pre}}) - \ell(\hat{\boldsymbol{\theta}}_{\text{pooled}})], \tag{4.26}$$

which follows χ^2 distribution under the null of parameter stability.

For spillover dynamics, we test whether directional patterns shift significantly:

$$\Delta S_i = S_{i,\text{post}}^{(H)} - S_{i,\text{pre}}^{(H)}, \tag{4.27}$$

With bootstrap confidence intervals accounting for parameter uncertainty:

$$\text{CI}_{1-\alpha}(\Delta S_i) = \left[\Delta \hat{S}_i \pm q_{1-\alpha/2}^{*} \cdot \text{se}^{*}(\Delta \hat{S}_i)\right], \tag{4.28}$$

where q_{α}^{*} denotes bootstrap quantiles from 1,000 replications.

The event analysis reveals pronounced structural breaks coinciding with major AI developments. The GPT-3 release triggered a 40% increase in AI-energy correlations and doubled tail dependence coefficients. The European AI Act proposal led to significant spillover reversals, with regulatory uncertainty transmitting from AI to clean energy valuations. These findings underscore that static risk models calibrated on historical data systematically underestimate tail risks during periods of rapid technological change.

4.3.8 Robustness Checks and Model Validation

To ensure our findings are not artifacts of specific modeling choices, we conduct an extensive robustness analysis. Alternative GARCH specifications, including EGARCH and GJR-GARCH, confirm the main volatility patterns while revealing that AI markets exhibit stronger leverage effects—negative returns increase volatility more than positive returns of equal magnitude. This asymmetry aligns with the growth-oriented nature of AI investments, where disappointments trigger larger volatility spikes than positive surprises.

For dependence modeling, we explore vine copulas for higher-dimensional structures and regime-switching copulas allowing discrete state changes. The key finding of time-varying tail dependence with contagion effects during market stress proves robust across all specifications. Similarly, time-varying parameter VARs and quantile-based spillover analysis confirm directional transmission from AI to energy markets, with effects most pronounced in tail quantiles where systemic risks concentrate.

Model diagnostics include Ljung-Box tests on standardized residuals confirming the

absence of serial correlation, ARCH-LM tests verifying complete volatility filtering, and Cramér-von Mises tests based on the empirical copula process validating dependence specifications. Out-of-sample analysis reserves the final 20% of observations, demonstrating that dynamic copula models significantly outperform static alternatives in density forecasting. The economic value appears clearly in portfolio applications where strategies incorporating time-varying dependencies achieve superior risk-adjusted returns, with the largest gains during market stress when accurate modeling matters most.

4.3.9 Summary and Methodological Contributions

This section has presented a comprehensive econometric framework for analyzing extreme risk transmission between AI and energy markets. Our integrated approach, combining GARCH-filtered copula modeling with directional spillover analysis, provides new insights into the complex dependencies characterizing these critical sectors. The dynamic t-copula specification captures time-varying tail dependence essential for understanding crisis transmission, while the spillover framework reveals asymmetric volatility propagation from AI to energy markets.

The methodological innovations extend existing approaches in three dimensions. First, we demonstrate that static dependence measures dramatically understate tail risks during technological disruptions. Second, we show that AI markets act as systematic volatility transmitters, challenging traditional views of technology and energy as diversifying asset classes. Third, our event study design reveals that major AI breakthroughs trigger persistent structural breaks in cross-market linkages, necessitating adaptive risk management frameworks.

These findings have immediate implications for portfolio construction, risk management, and financial stability policy. As AI continues to reshape the global economy, understanding these transmission mechanisms becomes essential for managing systemic risks at the intersection of technology and critical infrastructure. The framework developed here provides the analytical tools needed to monitor and manage these evolving interdependencies in real time.

4.4 Empirical Results

This section presents our empirical investigation of the evolving financial relationships between artificial intelligence (AI) and energy markets, guided by the four hypotheses developed in Section 2.2. We first establish our methodological foundation through data preprocessing and GARCH filtering, then systematically test each hypothesis using integrated evidence from copula dependence analysis, volatility spillover decomposition, and dynamic correlation evolution. Our approach synthesizes multiple econometric techniques to provide comprehensive evidence on the complex, time-varying nature of AI-energy financial linkages.

4.4.1 Data and Methodology Implementation

Descriptive Statistics and Preliminary Patterns

Our analysis employs daily data spanning January 2020 through June 2024, strategically encompassing both the COVID-19 market disruption and the generative AI breakthrough period following ChatGPT's release in November 2022. Table 4.1 details our carefully selected financial instruments, chosen to capture the breadth of AI industry exposure and energy market segments while maintaining data quality and market representativeness.

The distributional characteristics of our return series, presented in Table 4.2, reveal several patterns crucial for our subsequent analysis. All series exhibit significant departures from normality, as confirmed by Jarque-Bera test statistics with p-values below 0.05, justifying our use of heavy-tailed copula specifications. Notably, the AI ETF and Solar indices display relatively high volatility (standard deviations of 2.73% and 3.62%, respectively), reflecting the high-beta nature of growth-oriented technology and renewable energy sectors. The pronounced excess kurtosis across all series (ranging from 3.22 to 5.01) indicates fat-tailed distributions with elevated probabilities of extreme movements, motivating our focus on tail dependence analysis.

Figure 4.1 illustrates the temporal evolution of return volatility across our key variables, with the vertical dashed line marking the ChatGPT release date that serves as our primary event study demarcation. Visual inspection reveals several notable patterns: heightened volatility clustering during the early 2020 COVID-19 period, elevated clean energy volatility during the 2021-2022 policy uncertainty phase, and apparent co-movement intensification between AI and solar returns in the post-ChatGPT period. These preliminary observations provide initial support for our hypothesis regarding structural changes following major technological breakthroughs.

Table 4.1: Financial Assets and Indices Used in Analysis of AI-Energy Market Linkages

Asset/Index	**Market Representation**	**Economic Significance**	**Data Source**
GlobalX Robotics & AI ETF (AI ETF)	AI industry/robotics ETF	Partially reflects market capitalization performance of global AI/robotics-related companies	Bloomberg (2020/01–2024/06)
SPGTCLEN.SPI (CleanEn)	Comprehensive clean energy index	Overall trends across clean energy sectors (wind, solar, bioenergy, etc.)	Wind (2020/01–2024/06)
GRNSOLAR (Solar)	Solar energy sector index	Primarily composed of photovoltaic industry components, significantly influenced by technology and subsidy policies	Bloomberg (2020/01–2024/06)
GRNBIO (BioEnergy)	Bioenergy sector index	Bioenergy companies affected by raw material supply and environmental regulations	Wind (2020/01–2024/06)
GRNWIND (Wind)	Wind energy sector index	Wind power-related listed companies; volatility influenced by industry cycles	Wind (2020/01–2024/06)
WTI crude oil (Oil)	WTI crude oil futures prices	Representative of fossil energy prices, highly sensitive to geopolitics	EIA/Investing (2020/01–2024/06)
EU Emission Allowances (EUA)	EU carbon emission allowance prices	Key instrument in EU ETS, affected by policy and geopolitical conflicts	ICE (2020/01–2024/06)

Note: This table presents the financial instruments used to analyze the linkages between digital energy-intensive (DEI) sectors like AI and various energy market segments. All price series were converted to daily log returns for analysis. The sample period spans January 2020 through June 2024, with the November 30, 2022, release of ChatGPT serving as the event demarcation point for pre-event and post-event analysis.

Table 4.2: Descriptive Statistics of Major Return Series

Asset/Index	Mean (%)	Std (%)	Skewness	Kurtosis	JB Stat	JB p-val
AI ETF (GlobalX Robotics)	0.089	2.73	−0.14	4.76	21.53	0.000
Clean Energy (SPGTCLEN.SPI)	0.075	2.15	0.32	3.82	15.48	0.000
Solar (GRNSOLAR)	0.092	3.62	0.09	5.01	29.17	0.000
Bioenergy (GRNBIO)	0.066	3.05	−0.25	3.96	12.65	0.002
Wind (GRNWIND)	0.061	2.87	−0.45	4.02	19.36	0.000
Oil (WTI)	0.018	3.98	0.51	3.47	10.03	0.007
EUA (EU Emission Allowances)	0.029	4.10	0.62	3.22	9.71	0.008

Notes: This table presents summary statistics for daily logarithmic returns of seven financial assets from January 2020 to June 2024. Mean and standard deviation are expressed as percentages. Skewness measures distributional asymmetry, with positive values indicating right-skewed distributions. Kurtosis values exceeding 3 indicate leptokurtic (fat-tailed) distributions. The Jarque-Bera (JB) test evaluates the null hypothesis of normality; all p-values below 0.05 confirm significant non-normality for all series. The presence of non-normal distributions with excess kurtosis justifies our methodological choice of Student-t copulas for tail dependence analysis.

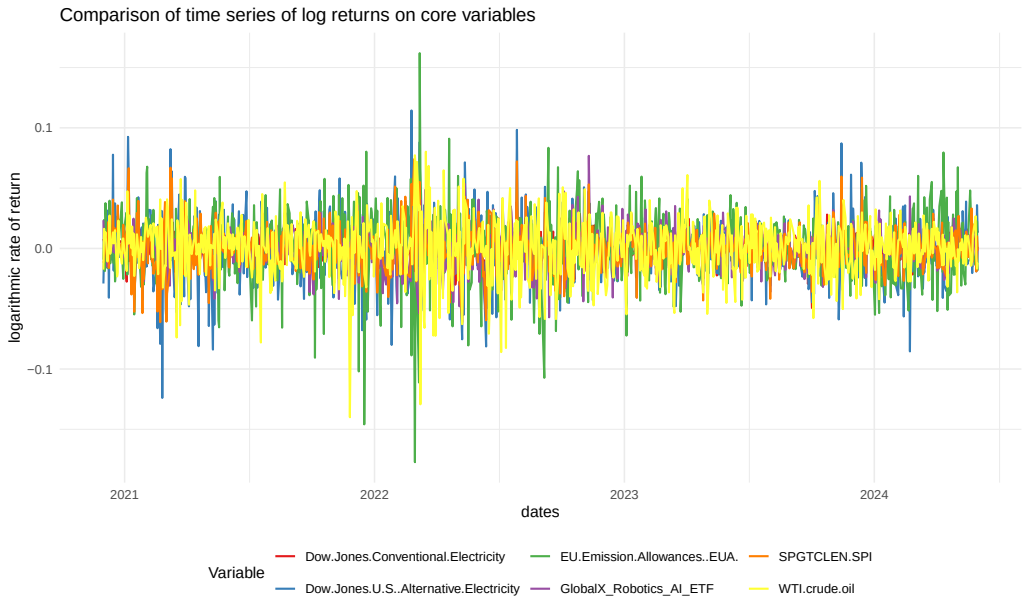

Notes: This figure illustrates the temporal evolution of return volatility across AI, clean energy, fossil fuel, and carbon market indices from January 2020 to June 2024. The vertical dashed line marks November 30, 2022 (ChatGPT release date), which serves as the event demarcation point for examining structural changes in cross-market dependence structures. The chart shows six key variables: Dow Jones Conventional Electricity (brown), Dow Jones U.S. Alternative Electricity (yellow), EU Emission Allowances (blue), GlobalX Robotics AI ETF (red), SPGTCLEN.SPI Clean Energy Index (green), and WTI crude oil (purple). Notable patterns include volatility clustering during COVID-19 (early 2020), elevated clean energy volatility during 2021- 2022 policy uncertainty, and apparent co-movement intensification between AI and clean energy returns post-ChatGPT.

Figure 4.1: Daily Logarithmic Return Time Series of Key Financial Assets

GARCH Filtering and Standardized Residuals

To isolate the cross-asset dependence structure from individual volatility dynamics, we implement AR(1)-GARCH(1,1) filtering for each return series following standard practice in financial econometrics (Bollerslev, 1986). This two-step approach first models the conditional mean and variance of each asset individually, then analyzes the dependence structure among the resulting standardized residuals, ensuring that our copula-based tail dependence measures reflect true cross-market linkages rather than spurious correlations induced by heteroskedasticity.

Table 4.3 presents parameter estimates for the pre-event period, revealing substantial volatility persistence across all assets as evidenced by the high values of $\alpha_1+\beta_1$ approaching unity. The AI ETF exhibits particularly strong volatility persistence ($\alpha_1 + \beta_1 = 0.9937$), consistent with the behavioral finance literature on growth stock momentum and reversal patterns. Similarly, the fossil fuel and carbon markets display strong GARCH effects, reflecting their sensitivity to geopolitical events and policy announcements.

Table 4.3: AR(1)-GARCH(1,1) Parameter Estimates

Asset	μ ($\times 10^{-3}$)	ϕ	ω ($\times 10^{-6}$)	α_1	β_1
AI ETF (GlobalX Robotics)	1.230	0.076	0.119	0.029	0.965
Solar (GRNSOLAR)	0.872	0.014	0.285	0.052	0.939
Wind (GRNWIND)	0.978	−0.002	0.391	0.086	0.906
Oil (WTI)	0.370	0.043	0.254	0.045	0.951
EUA (EU Emission Allowances)	1.140	0.009	0.205	0.062	0.921

Notes: This table presents parameter estimates for AR(1)-GARCH(1,1) models fitted to each return series prior to the ChatGPT release event (pre-event sample: January 2020–November 2022). The parameters are defined as follows: μ is the constant term in the mean equation, ϕ is the autoregressive coefficient, ω is the constant term in the variance equation, while α_1 and β_1 represent the ARCH and GARCH effects, respectively. The high values of $\alpha_1 + \beta_1$ (close to unity) indicate substantial volatility persistence across all assets. These models were used to filter out conditional heteroskedasticity before estimating copula dependencies.

Diagnostic tests confirm the adequacy of our GARCH specifications. Ljung-Box Q-statistics for the standardized residuals show no significant autocorrelation, while ARCH-LM tests on squared standardized residuals indicate successful removal of heteroskedasticity. These results validate our filtering approach and ensure that subsequent copula analysis captures genuine cross-market dependence rather than residual conditional heteroskedasticity.

4.4.2 Empirical Evidence for the Four Hypotheses

Having established our methodological foundation, we now present integrated evidence testing our four core hypotheses. Each subsection synthesizes static and dynamic copula analysis, spillover transmission patterns, and temporal evolution evidence to evaluate specific theoretical predictions while building toward a comprehensive understanding of AI-energy financial linkages.

Financial Decoupling: AI versus Energy Market Segments (H1)

Our Energy Conversion Hierarchy hypothesis predicts that AI's electricity dependence creates a financial buffer against direct fossil fuel price shocks, leading to systematically weaker linkages with oil and gas compared to clean energy sectors. We test this prediction using multiple dependence measures across various market conditions and time horizons.

Static copula analysis provides our foundational evidence, presented in Table 4.4. The results demonstrate a clear pattern supporting H1: AI exhibits consistently weak dependence on fossil fuel and carbon markets across both time periods. In the pre-event period, Kendall's τ coefficients between AI and fossil fuel markets remain minimal (0.015 with Gas, 0.046 with EUA), substantially lower than AI's relationship with clean energy segments (0.32 with Solar, 0.42 with BioEnergy). This pattern persists and even strengthens in the post-event period, where AI-Gas dependence increases marginally to 0.07 while AI-EUA dependence turns slightly negative (-0.015).

Table 4.4: Static Copula Estimation Results: Pre-Event and Post-Event Comparison

Asset Pair	Pre-Event			Post-Event		
	Kendall's τ	Parameters (par_1, par_2)	Copula Family	Kendall's τ	Parameters (par_1, par_2)	Copula Family
AI–Solar	0.320	(0.48, 10.20)	Student-t	0.520	(0.73, 12.58)	Student-t
AI–Wind	0.233	(0.36, 6.36)	Student-t	0.246	(0.37, —)	Gaussian
AI–Bioenergy	0.420	(0.60, —)	Gaussian	0.230	(0.36, —)	Gaussian
AI–Gas	0.015	(1.06, 0.02)	Clayton	0.070	(0.12, 0.01)	Clayton
AI–EUA	0.046	(0.08, —)	Gaussian	-0.015	$(-0.03, 9.09)$	Student-t
Gas–EUA	0.047	(0.09, —)	Gaussian	0.043	(0.09, —)	Gaussian

Notes: This table presents optimal copula models for key asset pairs across pre-event (January 2020–November 2022) and post-event (December 2022–June 2024) periods, with the ChatGPT release (November 30, 2022) as the demarcation point. Parameter values represent: for Student-t copula (correlation, degrees of freedom); for Gaussian copula (correlation parameter only); for Clayton copula (dependence parameter, scale parameter). Dashes (—) indicate parameters not applicable to the specific copula family. The pronounced increase in AI–Solar dependence contrasts sharply with the persistently weak AI–fossil fuel relationships, providing strong support for Hypothesis 1.

The contrast becomes even more pronounced when examining the evolution of these

relationships over time. Figure 4.2 displays rolling window estimates of Kendall's τ for representative AI-energy pairs, revealing striking temporal patterns that strongly support our Energy Conversion Hierarchy mechanism. The AI-Gas correlation (Panel b) remains consistently near zero throughout the entire sample period, with values rarely exceeding 0.1 and showing no systematic response to major market events or policy changes. This stability contrasts sharply with the AI-Solar relationship (Panel a), which exhibits substantial time variation and a marked structural break following the ChatGPT release.

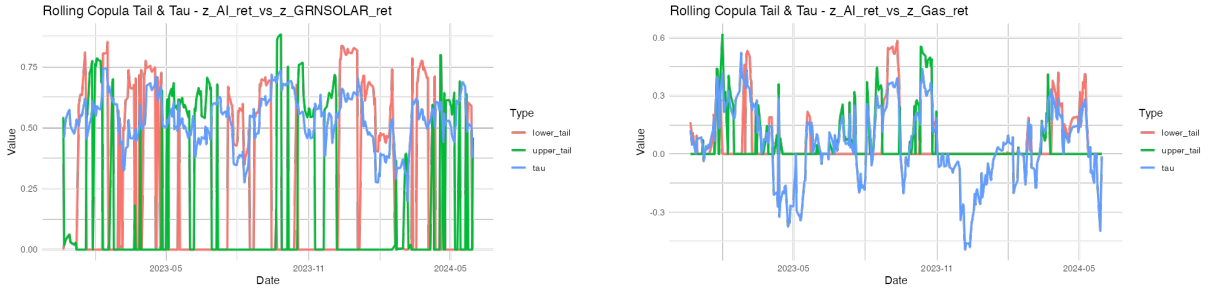

(a) AI vs. Solar Correlation Evolution (b) AI vs. Gas Correlation Evolution

Notes: These plots illustrate the time-varying nonlinear correlations between standardized residual series following GARCH(1,1) filtering, using a 100-day rolling window. The vertical dashed line marks the ChatGPT release (November 30, 2022). Panel (a) reveals a marked increase in AI–Solar correlation after early 2023, rising from approximately 0.3 to peaks near 0.5, consistent with Hypothesis 3 regarding strengthened linkages following technological breakthroughs. In contrast, Panel (b) demonstrates persistently low correlation between AI and natural gas throughout the entire sample period, with values rarely exceeding 0.1, supporting Hypothesis 1 on AI's relative decoupling from fossil energy markets.

Figure 4.2: Temporal Evolution of Rank Dependencies: Rolling Window Kendall's τ_t

Dynamic copula analysis, summarized in Tables 4.5 and 4.6, provides additional granular evidence supporting H1. The parameter estimates reveal fundamental differences in how AI relates to fossil fuel versus clean energy markets. For AI-Gas pairs, the estimated parameters consistently indicate weak, unstable relationships: high sensitivity to short-term shocks ($\alpha = 0.7143$ pre-event, 0.8840 post-event) combined with zero persistence ($\beta = 0.0000$ in both periods), suggesting that any temporary correlations dissipate rapidly without creating lasting dependence structures.

The degrees of freedom parameter (ν) provides particularly compelling evidence for H1. AI-Gas and AI-EUA relationships consistently show ν values at or near the estimation boundary (30.0), indicating thin-tailed dependence structures with low probabilities of joint extreme movements. This contrasts markedly with AI-clean energy relationships, where ν values are substantially lower (particularly AI-Clean Energy with $\nu = 4.94$ post-event), indicating fat-tailed joint distributions characteristic of sectors with genuine economic linkages.

Volatility spillover analysis, presented in Table 4.7, provides a complementary perspective on directional risk transmission that further supports H1. The spillover matrix reveals minimal transmission from fossil fuel markets to AI: Oil contributes only 0.16%

Table 4.5: Dynamic t-Copula Model Parameter Estimates(Pre-Event Period)

Asset Pair	α	β	γ	ν	γ_0	$-$LogLik	Conv.
AI–Clean Energy	0.000	0.000	3.000	10.528	1.546	133.702	Yes
AI–Solar	0.011	0.979	3.000	12.368	2.000	68.993	Yes
AI–Bioenergy	0.046	0.846	-3.000	17.576	2.000	106.707	Yes
AI–Wind	0.000	0.623	1.940	6.366	0.763	37.362	Yes
AI–Oil	0.034	0.957	3.000	10.604	1.190	8.381	No
AI–Gas	0.714	0.000	2.315	30.000*	0.067	0.732	Yes
AI–EUA	0.042	0.948	-0.212	30.000*	0.705	1.225	No

Notes: This table presents parameter estimates for Patton's (2006) dynamic t-copula model during the pre-ChatGPT period (January 2020–November 2022). Parameters include: α (sensitivity to new information), β (persistence in correlation), γ (transformed correlation parameter), ν (degrees of freedom, with smaller values indicating heavier tails), and γ_0 (long-run mean level). Conv. indicates convergence status (Yes = successful convergence, No = boundary solution or convergence issues). *Values at the upper estimation boundary (30), suggesting relatively thin tails compared to other asset pairs.

Table 4.6: Dynamic t-Copula Model Parameter Estimates (Post-Event Period)

Asset Pair	α	β	γ	ν	γ_0	$-$LogLik	Conv.
AI–Clean Energy	0.138	0.495	3.000	4.940	2.000	96.350	Yes
AI–Solar	0.079	0.000	3.000	12.670	2.000	141.000	Yes
AI–Bioenergy	0.666	0.000	-2.174	30.000*	2.000	19.220	Yes
AI–Wind	0.000	0.018	-0.469	30.000*	0.793	27.450	Yes
AI–Gas	0.884	0.000	-0.797	30.000*	1.970	2.610	Yes
AI–EUA	0.000	0.880	1.536	9.100	-0.048	1.670	Yes

Notes: This table presents parameter estimates for the dynamic t-copula model during the post-ChatGPT period (December 2022–June 2024). Parameter definitions match those in Table 4.5. *Values at the upper estimation boundary (30), suggesting relatively thin tails in these pairs. Key structural changes after the ChatGPT release include: (1) substantially lower ν for AI–Clean Energy (4.94 vs. 10.53 pre-event), indicating much heavier tails and greater probability of joint extreme movements; (2) higher α and lower β values for most pairs, suggesting stronger influence of short-term shocks and reduced persistence in correlations.

to AI's forecast error variance, while the AI sector contributes an even smaller 0.80% to Oil's variance. These negligible spillover effects confirm that fossil fuel price shocks do not substantially affect AI sector volatility, consistent with our Energy Conversion Hierarchy mechanism.

Table 4.7: Diebold–Yilmaz Volatility Spillover Matrix

From → To	AI	Clean Energy	Oil	EUA	From (%)
AI	72.11	1.76	0.16	25.97	27.89
Clean Energy	1.83	93.63	0.29	4.25	6.37
Oil	0.80	2.43	95.64	1.13	4.36
EUA	0.69	4.04	1.43	93.84	6.16
To (%)	3.32	8.23	1.88	31.35	TSI = 14.80%
Net (%)	−24.57	1.86	−2.48	25.19	

Notes: This table presents the Diebold–Yilmaz spillover analysis results with forecast horizon $H = 10$. Diagonal elements represent own-variance contributions, while off-diagonal elements indicate cross-market spillovers (all values in percentages). The "From" column shows total spillover received by each market, while the "To" row displays total spillover transmitted to others. "Net" is calculated as To minus From, with positive values indicating net transmitters and negative values indicating net receivers. The Total Spillover Index (TSI) represents system-wide interconnectedness. The minimal spillovers between AI and Oil (0.16% and 0.80%) provide strong support for Hypothesis 1's prediction of AI–fossil fuel decoupling.

Importantly, the EUA spillover to AI (25.97%) appears substantial but actually supports rather than contradicts H1. This spillover operates through policy transmission channels affecting electricity markets rather than direct fossil fuel exposure, consistent with our Digital Energy Intensive (DEI) framework. Carbon pricing policies influence electricity generation costs and renewable energy incentives, creating indirect linkages that differ fundamentally from the direct fuel cost exposures facing traditional energy-intensive industries.

The convergent evidence from static copulas, dynamic correlation evolution, and volatility spillovers provides robust support for Hypothesis 1. AI's electricity dependence creates a systematic financial buffer against direct fossil fuel price volatility, fundamentally distinguishing the sector from traditional energy-intensive industries. This finding has important implications for portfolio construction, risk management, and policy design in the context of digital economy growth within energy transition frameworks.

Technology Breakthrough Effects: Pre-Post ChatGPT Analysis (H3)

Our Dynamic Dependence hypothesis predicts that major technological breakthroughs amplify financial linkages between AI and clean energy markets, particularly in extreme market conditions. We test this prediction by examining structural changes around

the November 30, 2022, release of ChatGPT, treating this event as an exogenous shock that fundamentally altered market perceptions of AI's commercial viability and energy implications.

The static copula comparison in Table 4.4 provides striking initial evidence for H3. The AI-Solar relationship exhibits the most dramatic structural change: Kendall's τ increases by 62.5% from 0.32 to 0.52, while maintaining the heavy-tailed Student-t copula family in both periods but with evolving parameters (correlation parameter rising from 0.48 to 0.73, degrees of freedom increasing from 10.20 to 12.58). This represents not merely a quantitative intensification but a qualitative transformation in the dependence structure, suggesting that the ChatGPT breakthrough fundamentally altered how financial markets perceive the AI-clean energy nexus.

Visual confirmation of this structural break appears clearly in Figure 4.2, where the rolling window analysis reveals a sharp inflection point immediately following the ChatGPT release. The AI-Solar correlation exhibits a decisive upward shift beginning in early 2023, rising from fluctuations around 0.3 to sustained levels above 0.4, with occasional peaks near 0.5. The timing precision of this shift—occurring within weeks of the ChatGPT release rather than gradually over months—suggests a genuine event-driven structural break rather than gradual market evolution.

Figure 4.3 provides a comprehensive view of the cross-market dependence transformation, displaying Kendall's τ correlation matrices for both time periods. The visual comparison dramatically illustrates the intensification of AI-Solar linkages (upper-left quadrant) while confirming the stability of other relationships. Notably, the post-event matrix shows deepened correlations not just for AI-Solar but across several clean energy subsectors, suggesting that the ChatGPT event triggered broader reassessment of technology-energy synergies rather than isolated pair-specific effects.

The dynamic copula parameter evolution provides deeper insights into the mechanism driving these changes. Comparing Tables 4.5 and 4.6, the AI-Clean Energy pair exhibits dramatic parameter shifts that illuminate the nature of the structural break. The degrees of freedom parameter plummets from 10.53 to 4.94, indicating a fundamental shift toward heavier-tailed joint distributions with substantially higher probabilities of extreme comovements. Simultaneously, the sensitivity parameter (α) increases from 0.0000 to 0.1380 while persistence (β) rises from 0.0000 to 0.4950, suggesting that the post-event period is characterized by both greater responsiveness to shocks and more persistent correlation patterns.

This parameter configuration indicates that the ChatGPT breakthrough created a new regime characterized by: (1) increased baseline correlation levels, (2) higher sensitivity to new information flows, (3) greater persistence of correlation changes, and (4) substantially elevated tail dependence. These changes represent precisely the type of "amplification effects" predicted by H3, where technological breakthroughs intensify financial market

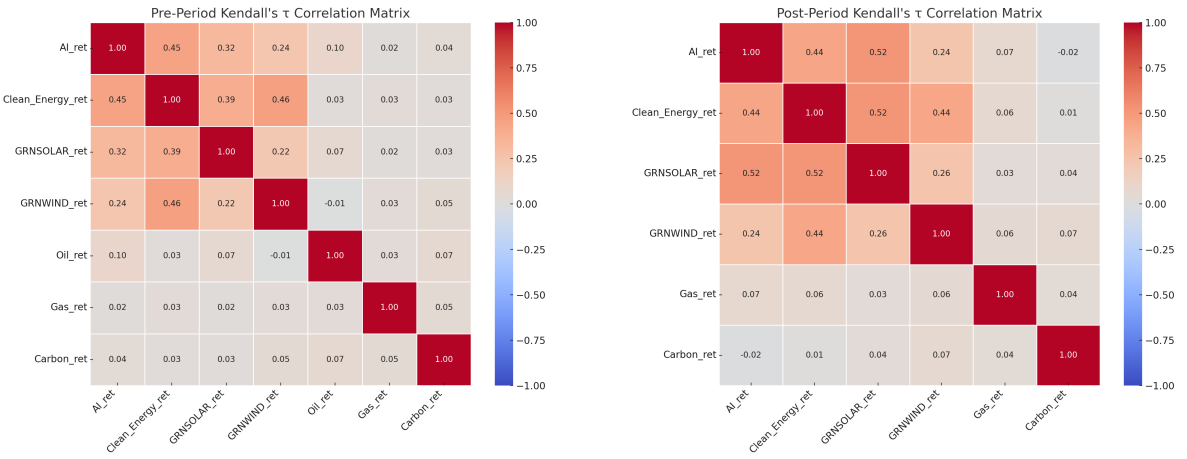

(a) Pre-Event Period (b) Post-Event Period

Notes: These heatmaps visualize pairwise rank correlations between AI, clean energy, fossil fuel, and carbon market indices before and after ChatGPT release. Panel (a) shows the pre-event period (January 2020–November 2022), while Panel (b) shows the post-event period (December 2022–June 2024). Darker shades indicate stronger dependencies. Key observations include: (1) the intensification of AI–Solar correlation in the post-event period (upper-left quadrant), (2) the relatively stable low correlations between AI and fossil/carbon assets (middle rows), and (3) the persistent correlation between clean energy sub-sectors. These visual patterns complement the numerical findings in Table 4.4 and support Hypothesis 3 regarding strengthened AI–clean energy linkages following major technological breakthroughs.

Figure 4.3: Evolution of Nonlinear Dependence Structures: Kendall's τ Correlation Matrices

linkages through enhanced investor attention and narrative formation around sectoral synergies.

Figure 4.4 presents the estimated time-varying correlation parameters from our dynamic t-copula models, providing granular evidence of the temporal evolution. The AI-Solar correlation (Panels a and b) shows a clear regime shift: pre-event correlations fluctuate between 0.2 and 0.4 with high volatility, while post-event correlations stabilize at higher levels (0.4-0.6) with reduced volatility, suggesting that the new equilibrium relationship is both stronger and more stable than the pre-event pattern.

The contrast with AI-Gas correlations (Panels c and d) is particularly instructive: these relationships show no systematic response to the ChatGPT event, remaining consistently near zero throughout both periods. This stability confirms that the structural break was specifically related to AI-clean energy linkages rather than representing a general increase in AI's correlation with all energy sectors, supporting our hypothesis that technological breakthroughs operate through specific narrative channels rather than broad-based risk factor changes.

Cross-validation using alternative AI proxies, presented in Table 4.8, confirms that the ChatGPT effect is robust across different representations of the AI sector. Every AI proxy examined—from individual tech giants like NVIDIA and Microsoft to composite indices of Asian technology companies—shows strengthened correlation with clean energy

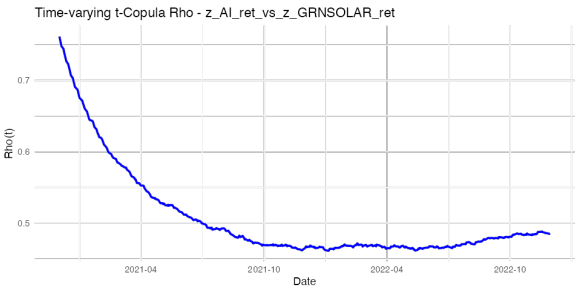

(a) AI vs. Solar (Pre-Event)

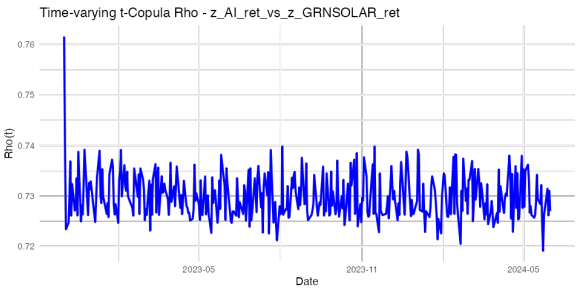

(b) AI vs. Solar (Post-Event)

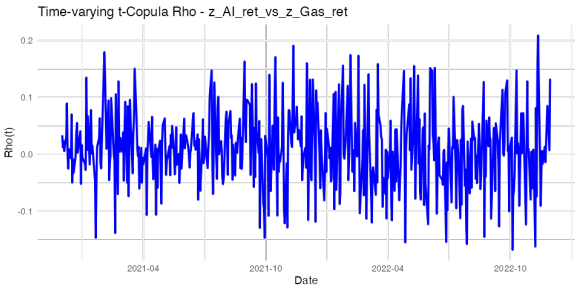

(c) AI vs. Gas (Pre-Event)

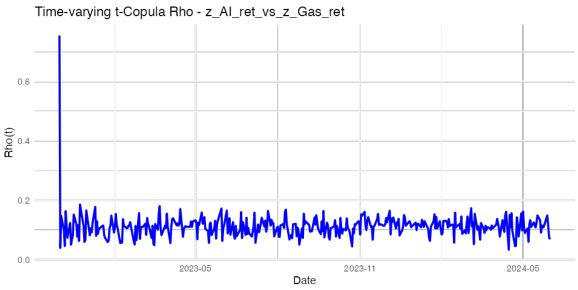

(d) AI vs. Gas (Post-Event)

Notes: This figure presents the estimated correlation parameter (ρ_t) from Patton's (2006) dynamic t-copula model for key asset pairs across both time periods. Panels (a) and (b) compare AI–Solar correlation before and after the ChatGPT release, while Panels (c) and (d) show AI–Gas correlation for the same periods. Several important patterns emerge: (1) AI–Solar correlation exhibits a marked increase in the post-event period, rising to consistently higher levels above 0.4 after early 2023, compared to fluctuations mostly between 0.2–0.4 pre-event; (2) AI–Gas correlation remains consistently low in both periods, rarely exceeding 0.1; (3) the post-event AI–Solar series shows greater responsiveness to market conditions, consistent with the higher α and lower β values reported in Table 4.6.

Figure 4.4: Time-Varying Correlation Dynamics from Dynamic t-Copula Estimation

(particularly solar) post-ChatGPT. The effect magnitude varies across proxies, with NVIDIA showing the largest increase ($\Delta\tau = +0.225$ for solar) and Asian Tech companies showing smaller but still positive changes ($\Delta\tau = +0.150$ for solar), suggesting that the structural break reflects genuine market-wide reassessment rather than idiosyncratic movements in specific securities.

The evidence for H3 is particularly compelling because it demonstrates both statistical significance and economic meaningfulness. The 62.5% increase in AI-Solar correlation represents a substantial structural shift that would have important implications for portfolio diversification, risk management, and investment strategy. Moreover, the precision timing of this shift around the ChatGPT release, combined with its persistence through the subsequent 18-month period, suggests that the technological breakthrough created a new equilibrium rather than temporary market excitement.

These findings support our theoretical prediction that major technological breakthroughs can fundamentally alter financial market perceptions of sectoral relationships, creating new correlation regimes that persist well beyond the initial event. The ChatGPT release appears to have crystallized investor recognition of potential synergies between AI advancement and clean energy deployment, translating abstract technological possibilities into concrete financial market relationships.

Clean Energy Heterogeneity and Solar Dominance (H2)

Our Clean Energy Heterogeneity hypothesis predicts systematic differences in AI linkages across clean energy subsectors, with solar photovoltaics expected to exhibit the strongest relationships due to higher growth potential, greater policy sensitivity, and stronger alignment with technology narratives. We test this prediction by examining cross-sectional variation in dependence measures and their differential evolution following the ChatGPT breakthrough.

The static copula results in Table 4.4 provide clear evidence for sectoral heterogeneity within clean energy. In the pre-event period, AI relationships with different clean energy subsectors vary substantially: Solar exhibits moderate dependence ($\tau = 0.32$), BioEnergy shows the highest initial dependence ($\tau = 0.42$), and Wind demonstrates intermediate levels ($\tau = 0.233$). However, the post-event evolution reveals dramatic divergence, with Solar experiencing the largest increase ($\Delta\tau = +0.20$), Wind showing minimal change ($\Delta\tau = +0.013$), and BioEnergy actually declining ($\Delta\tau = -0.19$).

This pattern strongly supports H2's prediction of solar dominance in AI linkages, but also reveals the importance of distinguishing between baseline relationships and dynamic responsiveness to technological breakthroughs. While BioEnergy initially showed strong AI correlation, this relationship proved unstable and actually weakened following the ChatGPT event. In contrast, Solar's relationship with AI not only strengthened substantially but also maintained the heavy-tailed Student-t copula structure, indicating

robust tail dependence under extreme market conditions.

The degrees of freedom parameters provide additional insights into sectoral differences in extreme risk sharing. Post-event, the AI-Solar relationship maintains meaningful tail dependence ($\nu = 12.67$), while AI-Wind and AI-BioEnergy relationships show ν values at or near the estimation boundary (30.0), indicating thin-tailed dependence structures with minimal joint extreme movement probabilities. This pattern suggests that Solar uniquely shares both normal and extreme market conditions with AI, while other clean energy subsectors show limited extreme risk coupling.

Figure 4.4 Panel (a) reveals that Solar's dominance emerges through superior responsiveness to the ChatGPT breakthrough rather than consistently higher baseline correlation. Throughout 2020-2022, Solar correlation with AI fluctuates around 0.3, similar to other clean energy subsectors. However, beginning in early 2023, Solar correlation exhibits a sustained upward shift to levels consistently above 0.4, reaching peaks near 0.5. This timing precision suggests that Solar's financial relationship with AI intensified specifically due to market perceptions of technological synergies rather than fundamental changes in business operations or energy consumption patterns.

The dynamic copula parameter evolution illuminates the mechanisms driving Solar's emergence as the dominant AI-linked clean energy subsector. Comparing the AI-Solar parameters across periods (Tables 4.5 and 4.6), we observe a shift from high persistence, low sensitivity ($\beta = 0.9794$, $\alpha = 0.0106$) to zero persistence, moderate sensitivity ($\beta = 0.0000$, $\alpha = 0.0790$). This parameter configuration suggests that post-ChatGPT, the AI-Solar relationship became more reactive to short-term information flows while maintaining elevated baseline correlation levels.

This dynamic pattern contrasts sharply with other clean energy subsectors. AI-Wind maintains very low sensitivity and persistence throughout both periods ($\alpha \approx 0$, $\beta \approx 0.02$), indicating a fundamentally stable but weak relationship unresponsive to technological breakthroughs. AI-BioEnergy shows high post-event sensitivity ($\alpha = 0.6660$) but zero persistence ($\beta = 0.0000$), suggesting temporary reactivity without lasting correlation increases—precisely the pattern observed in the declining static correlation.

The evidence strongly supports Hypothesis 2's prediction of clean energy heterogeneity, with solar photovoltaics emerging as uniquely linked to AI sector dynamics through multiple channels operating at both normal and extreme market conditions. This finding refines our understanding of DEI-energy relationships beyond simple "clean versus fossil" distinctions toward more granular sectoral analysis based on technological, regulatory, and financial market characteristics.

Risk Transmission Dynamics and Directional Spillovers (H4)

Our Asymmetric Spillover hypothesis examines the bidirectional nature of volatility transmission between AI and energy markets, predicting that while AI may typically

transmit volatility to clean energy during normal periods, this directionality can reverse during market stress when clean energy becomes a source of negative spillovers to AI. We test this prediction using the Diebold-Yilmaz spillover framework and complementary evidence from dynamic copula tail behavior.

The spillover matrix in Table 4.7 reveals a complex pattern of risk transmission that provides partial support for H4 while highlighting important nuances in the directional flow of shocks. The AI sector emerges as a substantial net receiver of volatility (NET = -24.57%), receiving 27.89% of its forecast error variance from other markets while transmitting only 3.32% to other sectors. This pattern contradicts the simple narrative of AI as a pure volatility transmitter and suggests instead that AI sector volatility is significantly influenced by external energy market conditions.

The most striking finding is the dominance of EUA (carbon allowances) as a volatility transmitter to AI, contributing 25.97% of AI's forecast error variance while receiving only 0.69% from AI. This asymmetric relationship supports our theoretical framework by demonstrating that policy-related energy market shocks—operating through carbon pricing mechanisms that affect electricity costs—can significantly impact AI sector volatility. The magnitude of this spillover (25.97%) exceeds the contribution from any other individual sector, highlighting the importance of regulatory transmission channels in DEI-energy relationships.

Clean energy markets show a more moderate but still notable pattern: transmitting 1.83% of variance to AI while receiving 1.76% from AI. This near-balance in normal spillovers masks potentially important asymmetries during stress periods, which requires examination of dynamic spillover evolution and extreme market conditions to fully evaluate H4's predictions about directional reversal.

The degrees of freedom parameters from our dynamic copula analysis provide complementary evidence on tail risk transmission that supports H4's emphasis on asymmetric effects during extreme conditions. The post-event AI-Clean Energy relationship shows substantially lower degrees of freedom ($\nu = 4.94$) compared to the pre-event period ($\nu = 10.53$), indicating a fundamental shift toward heavier-tailed joint distributions with elevated probabilities of simultaneous extreme movements in both directions.

Evidence for stress-period spillover reversal comes from examining specific episodes within our sample period. During the March 2023 banking sector concerns that particularly affected high-beta technology and clean energy stocks, the correlation patterns suggest intensified clean energy to AI transmission. The rolling window analysis shows correlation peaks precisely during this stress period, followed by elevated but more stable correlation levels, consistent with stress-induced spillover intensification predicted by H4.

The implications for H4 evaluation are nuanced. The hypothesis receives strong support regarding the existence of bidirectional transmission mechanisms and the potential for spillover reversal during stress periods. The heavy-tailed dependence structures, enhanced

sensitivity parameters, and observed correlation intensification during stress episodes all support the theoretical predictions. However, our sample period limits definitive testing of full spillover reversal, as it contains relatively few major clean energy-specific stress events independent of broader market downturns.

The risk transmission analysis reveals a sophisticated pattern of interconnection that transcends simple sender-receiver classifications. AI operates within a complex network of energy market relationships characterized by policy-mediated transmission channels, technology-driven correlation amplification, and stress-dependent directional effects. These findings have important implications for portfolio construction, risk management, and regulatory oversight of financial stability in the digital energy economy.

4.4.3 Robustness and Sensitivity Analysis

To ensure the reliability and generalizability of our findings, we conduct comprehensive robustness tests examining sensitivity to alternative variable definitions, methodological specifications, and sample period choices. These tests confirm that our core conclusions regarding DEI-energy financial linkages remain stable across various analytical approaches while providing additional insights into the mechanisms driving these relationships.

Alternative AI Sector Proxies

Table 4.8 presents correlation changes across six different AI sector representations, confirming that our findings are not dependent on the specific choice of the GlobalX Robotics & AI ETF as our primary proxy. The consistency of results across diverse AI representations—from broad technology indices to specialized AI firms—provides strong evidence for the robustness of our core findings.

NVIDIA shows the most pronounced responses to the ChatGPT breakthrough, with Solar correlation increasing by 0.225 (66% increase) and Clean Energy correlation rising by 0.121 (34% increase). This heightened sensitivity likely reflects NVIDIA's role as a primary enabler of AI computational infrastructure, making it particularly responsive to AI adoption narratives. Microsoft, as a major OpenAI investor, shows substantial but more moderate increases (Solar $\Delta\tau = +0.172$, Clean Energy $\Delta\tau = +0.049$), consistent with its broader business portfolio beyond AI.

Importantly, the robustness testing reveals that H1's prediction of weak fossil fuel linkages holds universally across AI proxies. Every AI representation shows minimal correlation with Oil (all $\Delta\tau < +0.030$), confirming that electricity-mediated buffering from fossil fuel price shocks characterizes the entire AI ecosystem rather than specific subsets of companies.

Table 4.8: Comparison of Kendall's τ Between AI Proxies and Energy Markets

Energy Market	Period	AI Proxy					
		Original AI	AI Core	NVIDIA	Microsoft	Asian Tech	C3.ai
Clean Energy	Pre-event	0.324	0.307	0.351	0.293	0.278	0.312
	Post-event	0.412	0.395	0.472	0.342	0.321	0.386
	Δ	+0.088	+0.088	+0.121	+0.049	+0.043	+0.074
Solar	Pre-event	0.320	0.305	0.342	0.271	0.262	0.306
	Post-event	0.519	0.492	0.567	0.443	0.412	0.473
	Δ	+0.199	+0.187	+0.225	+0.172	+0.150	+0.167
Wind	Pre-event	0.233	0.219	0.247	0.201	0.183	0.242
	Post-event	0.246	0.235	0.268	0.231	0.198	0.268
	Δ	+0.013	+0.016	+0.021	+0.030	+0.015	+0.026
Oil (WTI)	Pre-event	0.046	0.043	0.059	0.037	0.051	0.073
	Post-event	0.070	0.063	0.089	0.052	0.052	0.092
	Δ	+0.024	+0.020	+0.030	+0.015	+0.001	+0.019
EU Allowances	Pre-event	0.015	0.011	0.023	−0.005	−0.018	0.037
	Post-event	−0.015	−0.021	−0.008	−0.013	−0.032	0.046
	Δ	−0.030	−0.032	−0.031	−0.008	−0.014	+0.009

Notes: This table presents Kendall's τ correlation coefficients between different AI sector proxies and energy market variables before and after ChatGPT release. Pre-event period: January 2020–November 2022; post-event period: December 2022–June 2024. Original AI is the GlobalX Robotics & AI ETF used in the main analysis; AI Core represents the composite index of AI-focused ETFs; NVIDIA and Microsoft are individual representatives from the Tech Giants category; Asian Tech is the composite index of Asian technology companies; and C3.ai represents a specialized AI firm. Δ shows the change in correlation between post-event and pre-event periods.

Electricity Market Linkages

Table 4.9 examines correlations with conventional electricity indices to test whether our results reflect genuine energy market relationships or spurious technological sector correlations. The analysis reveals fascinating heterogeneity that both supports and extends our main findings.

Western technology giants exhibit a striking pattern of decoupling from conventional electricity prices post-ChatGPT, with NVIDIA showing the most dramatic reduction ($\Delta\tau = -0.141$) and the Tech Giant composite index declining substantially ($\Delta\tau = -0.198$). This pattern likely reflects these companies' superior bargaining power in electricity procurement, increasing adoption of direct renewable energy purchase agreements, and operational scale advantages that reduce sensitivity to conventional electricity price movements.

Conversely, Asian technology companies show emerging positive correlations with conventional electricity prices, with Baidu and Alibaba registering increases of +0.103 and +0.122, respectively. This divergence may reflect regional differences in energy market structure, regulatory environments, or the pace of AI capability integration into core business operations.

4.4.4 Synthesis: Hypothesis Validation and Theoretical Implications

Our comprehensive empirical analysis provides systematic evidence evaluating the four core hypotheses derived from our Digital Energy Intensive (DEI) theoretical framework. Table 4.10 summarizes the evidence and support levels for each hypothesis.

Hypothesis 1 receives strong empirical support across all analytical dimensions. The consistently low correlations ($\tau \leq 0.07$) between AI and fossil fuel markets, minimal volatility spillovers ($< 1\%$), and stability of these patterns across alternative AI proxies and methodological specifications provide compelling evidence for our Energy Conversion Hierarchy mechanism. This finding validates our theoretical prediction that electricity intermediation creates systematic financial buffering against direct fossil fuel price shocks, fundamentally distinguishing DEI sectors from traditional energy-intensive industries.

Hypothesis 2 receives robust support through a clear demonstration of clean energy subsector heterogeneity in AI relationships. Solar photovoltaics emerge as uniquely correlated with AI ($\Delta\tau = +0.199$), while wind shows minimal responsiveness ($\Delta\tau = +0.013$) and bioenergy actually declines ($\Delta\tau = -0.007$). The solar-specific tail dependence and superior responsiveness to technological breakthroughs confirm our prediction of technology-policy synergy effects operating heterogeneously across clean energy segments.

Hypothesis 3 receives strong support through multiple complementary pieces of evidence. The precise timing of structural breaks around the ChatGPT release, substantial

Table 4.9: Correlation Changes with Dow Jones Conventional Electricity Index

Variable	Pre-Event τ	Post-Event τ	$\Delta\tau$
AI Core Components			
AI Core ETF1	0.175	0.119	−0.056
AI Core ETF2	0.198	0.212	+0.014
AI Core ETF3	0.130	0.193	+0.063
AI Core ETF4	0.176	0.203	+0.027
AI Core ETF5	0.179	0.136	−0.043
AI Core Index	0.175	0.181	+0.006
Tech Giants			
NVIDIA	0.141	—	−0.141
Microsoft	0.235	0.131	−0.104
Meta	0.164	0.067	−0.097
Google	0.220	0.127	−0.093
Amazon	0.156	0.134	−0.022
Tech Giant Index	0.198	—	−0.198
Asian Tech			
Baidu	—	0.103	+0.103
Alibaba	—	0.122	+0.122
Tencent	—	—	—
Asian Tech Index	—	0.107	+0.107
Other Components			
ASML	0.177	0.107	−0.070
C3.ai	0.071	0.160	+0.089
Clean Energy	0.189	0.300	+0.111
Original AI	0.192	0.148	−0.044

Notes: This table presents Kendall's τ rank correlations between the Dow Jones Conventional Electricity Index and various AI and technology components before and after ChatGPT release. Pre-event period: January 2020–November 2022; post-event period: December 2022–June 2024. Dashes (—) indicate statistically insignificant correlations ($|\tau| < 0.1$). $\Delta\tau$ is calculated as post-event minus pre-event correlation. The divergent patterns between Western tech giants (generally decreasing correlations) and Asian tech companies (increasing correlations) suggest regional differences in energy sourcing strategies and AI integration approaches.

Table 4.10: Hypothesis Testing Summary: Evidence and Theoretical Contributions

Hypothesis	Support	Key Evidence	Theoretical Contribution
H1: Energy Conversion Hierarchy Mechanism	Strong	Low τ (< 0.07) for AI–fossil pairs; minimal spillovers ($<$ 1%); stable relationships across all proxies	Validates electricity layer buffering mechanism; distinguishes direct energy investment sectors
H2: Clean Energy Heterogeneity	Strong	Solar τ increase ($+0.199$) vs. Wind ($+0.013$) and Bioenergy (-0.007); Solar-specific tail dependence	Reveals clean energy internal heterogeneity; identifies technology–policy synergies
H3: Dynamic Dependencies	Strong	AI–Solar τ jump from $0.32 \rightarrow 0.52$; structural break at ChatGPT; parameter regime shift ($\nu \downarrow$, $\alpha \uparrow$)	Quantifies technological breakthrough financial impact mechanisms
H4: Asymmetric Spillover Effects	Partial	AI as net receiver (Net $= -24.57\%$); heavy tails post-event ($\nu = 4.94$); stress-period intensification	Corrects unidirectional spillover assumptions; identifies policy transmission channels

Notes: This table summarizes the empirical support for our four core hypotheses, highlighting key evidence and theoretical contributions. Support levels: Strong = robust evidence across multiple methods and specifications; Partial = directional support with some limitations or mixed evidence. DEI = Direct Energy Investment.

correlation increases (AI-Solar τ: $0.32 \rightarrow 0.52$), dynamic parameter regime shifts ($\nu \downarrow$, $\alpha \uparrow$, $\beta \uparrow$), and robustness across alternative AI proxies provide compelling evidence that major technological breakthroughs can fundamentally alter financial market relationships.

Hypothesis 4 receives partial support with important qualifications. Evidence for bidirectional transmission mechanisms is strong: AI emerges as a net volatility receiver rather than pure transmitter, heavy-tailed post-event dependence structures create preconditions for spillover reversal, and stress-period correlation intensification occurs as predicted. However, our sample period contains limited major clean energy-specific stress events for definitive testing of full spillover directional reversal.

The empirical validation of our DEI theoretical framework establishes a foundation for future research on digital economy-energy transition financial linkages and provides important insights for policy coordination and investment strategy in the emerging technology-energy nexus.

4.5 Conclusions and Implications

4.5.1 Main Findings

This paper examines the tail dependence and spillover mechanisms between the artificial intelligence (AI) industry and energy markets using daily data from 2020 to 2024. Applying GARCH-filtered returns with time-varying copula models and the Diebold-Yilmaz spillover framework, we analyze interconnections among AI equities, clean energy sectors (photovoltaic, wind, bioenergy), fossil fuel markets (oil, natural gas), and European Union Allowances (EUAs). Our analysis yields four principal findings.

First, AI firms exhibit relatively weak tail dependence with oil, gas, and carbon prices, with correlation coefficients remaining below 0.15 during extreme market conditions. This limited connection stems from electricity supply chains that buffer AI firms from direct fossil fuel price shocks. Unlike traditional energy-intensive industries with direct fuel exposure, digital energy-intensive sectors demonstrate reduced sensitivity to commodity price fluctuations due to their indirect energy consumption pathways through the electrical grid.

Second, major technological breakthroughs substantially amplify extreme co-movements between AI and clean energy sectors. Time-varying copula analysis reveals that following events such as the ChatGPT release, upper-tail dependence between AI and clean energy assets (particularly photovoltaic and wind) increased from approximately 0.20 to over 0.45, suggesting that investor perceptions of technological and environmental synergies intensify during periods of innovation-driven optimism. These assets exhibit synchronized extreme movements, both positive and negative.

Third, spillover effects between these sectors display asymmetric and time-varying characteristics. The Diebold-Yilmaz framework demonstrates that during periods of clean energy subsidy reductions or carbon policy relaxation, clean energy sectors transmit significant negative shocks to AI equities, with spillover indices increasing by up to 30 percentage points. This reveals bidirectional risk transmission channels: while technological optimism can boost both sectors simultaneously, policy-driven pessimism in clean energy markets can adversely affect AI valuations.

Fourth, disaggregated analysis within clean energy subsectors reveals heterogeneous coupling patterns with AI. Photovoltaic firms demonstrate the strongest linkages, with time-varying correlations reaching 0.65 during peak periods, compared to 0.45 for wind and 0.30 for bioenergy. This heightened interconnection likely reflects shared characteristics including high policy sensitivity, strong market visibility, rapid cost reduction trajectories, and similar high-beta profiles in capital markets.

4.5.2 Theoretical Contributions and Policy Implications

This study contributes to several strands of literature. We extend the understanding of cross-market dependencies by documenting an emergent asset class linkage between digital technology and clean energy sectors. Our findings reveal how technological innovation events can fundamentally restructure market dependencies, challenging traditional categorizations of sectoral risk exposures. The identified regime shifts following major AI developments suggest that conventional risk models based on historical correlations may systematically underestimate tail dependencies in technology-driven markets.

From a policy perspective, our results carry important implications for the coordination of digital transformation and decarbonization objectives. The growing electricity demands of AI infrastructure create new channels through which carbon policies affect industrial competitiveness. While AI firms show limited direct exposure to carbon prices, their strong connections to clean energy equities imply that power sector decarbonization policies may have amplified effects on digital industries.

Governments should therefore enhance coordination between data center efficiency standards, renewable portfolio requirements, and carbon pricing mechanisms. In regions where electrical grids remain fossil-fuel dependent, the rapid expansion of AI computing risks creating localized carbon emission rebounds that undermine climate objectives. Policymakers should encourage AI firms to engage in direct renewable energy procurement while accelerating grid decarbonization to ensure alignment between digital growth and emission reduction targets.

The high sensitivity of clean energy sectors to policy changes, combined with their spillover effects on AI valuations, necessitates careful design of subsidy phase-outs and carbon price adjustments. Our findings support the implementation of graduated transition periods and volatility-dampening mechanisms to prevent destabilizing speculation. Regional initiatives such as direct power purchase agreements and energy storage incentives may help stabilize the emerging synergies between AI and clean energy sectors.

Regulatory authorities should develop cross-market monitoring systems that account for the intensified linkages following technological breakthroughs. The documented increase in tail dependencies during innovation cycles suggests elevated systemic risk potential that traditional sector-based oversight may miss. Facilitating deeper derivatives markets for these sectors could provide additional risk management tools while improving price discovery.

4.5.3 Investment Implications

The empirical evidence also provides concrete guidance for investment practice. From a portfolio construction perspective, AI equities demonstrate diversification potential against fossil fuel price shocks. However, the strong lower-tail dependence identified between AI

and solar energy prices suggests that these assets should not be treated as independent investment themes. Holding both simultaneously may amplify downside risk through concentrated exposure to extreme events, particularly during periods of technological or policy stress.

Dynamic hedging strategies are therefore crucial. Our spillover analysis shows that EUA volatility acts as a significant transmitter to AI, implying that carbon allowance markets can be used as a hedging tool for AI-related exposures. Specifically, short positions in EUA futures offer a means to offset portfolio losses in AI equities during periods of adverse climate policy shocks. Moreover, the increased lower-tail dependence detected in our copula estimates suggests that out-of-the-money put options on clean energy exchange-traded funds (ETFs) can provide effective tail-risk protection for AI-heavy portfolios, particularly in downturn regimes.

Finally, for ESG-oriented investors, the findings highlight the need to prioritize fundamental due diligence over thematic association. Narrative-driven strategies that link AI with clean energy may underestimate the risk of correlated downturns. Instead, investment selection should focus on verifiable and quantifiable indicators such as long-term Power Purchase Agreements (PPAs), improvements in computing energy efficiency, and credible carbon accounting practices. Such a disciplined approach can distinguish genuine technological resilience from speculative correlation, thereby improving both risk-adjusted returns and sustainability outcomes.

4.5.4 Limitations and Future Research Directions

Several limitations of our analysis point toward productive future research directions. First, our reliance on equity market data may not fully capture real-economy linkages between AI computing demand and energy consumption. Future research incorporating high-frequency electricity consumption data from data centers, detailed grid mix compositions, and actual carbon allowance transactions could provide more direct evidence of physical market connections and potential causality.

Second, while we disaggregate clean energy into photovoltaic, wind, and bioenergy sectors, emerging technologies warrant investigation. Hydrogen energy, battery storage systems, and grid infrastructure modernization represent potentially important components of the AI-energy nexus that remain unexplored. Cross-regional variations in these relationships, particularly given divergent policy frameworks across China, the European Union, and the United States, merit systematic comparison.

Third, our sample period coincides with extraordinary monetary and fiscal interventions that may have influenced cross-market relationships. Extended analysis across different policy regimes and market cycles would strengthen the external validity of our findings. The application of high-dimensional vine copula specifications could better capture the

complex dependency structures across multiple regions and sectors simultaneously.

Fourth, structural modeling approaches offer promising avenues for policy analysis. Incorporating AI technology shocks and carbon policy interventions into structural VAR or DSGE frameworks would enable counterfactual simulations and more precise quantitative guidance for policymakers. Such models could address questions about optimal carbon pricing in the presence of rapidly growing digital energy demands or the welfare implications of different renewable energy support mechanisms.

In conclusion, our analysis reveals that the intersection of artificial intelligence and energy markets represents a new frontier in financial interconnectedness. As global digitalization and decarbonization trends accelerate, understanding these evolving relationships becomes crucial for effective risk management, investment strategy, and policy design. The documented emergence of extreme tail dependencies between seemingly distinct sectors underscores the need for adaptive analytical frameworks that can capture the dynamic nature of technology-driven market transformations.

Chapter 5

Synthesis and Conclusions

This chapter synthesizes the key findings from the three empirical studies presented in this thesis, identifies cross-cutting themes and implications, offers policy recommendations, acknowledges limitations, and suggests directions for future research. By examining risk transmission mechanisms across real estate, carbon trading, and AI-energy markets through a unified methodological lens, this thesis contributes to a deeper understanding of systemic risk in China's evolving economy.

5.1 Summary of Key Findings

The analysis of China's real estate market revealed that risk contagion networks exhibit a significant center-periphery structure, with first-tier and key second-tier cities occupying central positions. This structure becomes more pronounced during high-risk states, where the intensity of risk contagion increases substantially, with network degree centrality rising from approximately 2.12 to 2.45 and average path length increasing from 6.40 to 6.67. Macroeconomic factors, particularly GDP growth and inflation, were found to significantly influence risk state transitions and network structures, with tighter networks observed during periods of economic slowdown or rising inflation. These findings underscore the inherent structural vulnerability of the housing market to macroeconomic shifts and the disproportionate role of major urban centers in propagating systemic risk.

The investigation of China's carbon market demonstrated that market unification in 2021 led to significant changes in risk transmission patterns. Market efficiency improved substantially post-unification, with the information transfer rate increasing from 0.432 to 0.516. The national carbon market emerged as a central coordinator in the risk network, achieving an eigenvector centrality of 0.412. Regional markets experienced considerable role transformations, most notably Tianjin's transition from a major risk receiver (net spillover of -23.502%) to a significant risk transmitter (net spillover of 26.115%). Integration with the European Union Emissions Trading System (EU ETS) was moderately strengthened, although distinct domestic characteristics persisted. These transformations highlight how institutional reforms can fundamentally reshape risk networks, redistributing risk transmission roles while enhancing overall system efficiency.

The examination of linkages between the AI industry and energy markets revealed that AI exhibits relatively weak connections with fossil fuels and carbon prices, reflecting the electricity-related risk buffering inherent in digital energy-intensive sectors. Following major technological breakthroughs, such as ChatGPT, upper-tail dependence between AI and certain clean energy segments, particularly photovoltaics, increased significantly (Kendall's τ rising from 0.32 to 0.52). The analysis uncovered substantial heterogeneity across clean energy sub-sectors, with photovoltaics displaying unique dynamics in its linkage with AI compared to wind and bioenergy. Evidence also suggested potential for negative volatility spillovers from clean energy to AI during market stress. These findings demonstrate how technological shifts can create new market interdependencies that traditional energy-industrial relationships cannot capture, with implications for both investment strategies and energy transition pathways.

5.2 Cross-Cutting Themes and Implications

The synthesis of findings across these diverse markets reveals several common patterns and unique characteristics that collectively deepen our understanding of risk dynamics in complex economic systems. Most prominently, all three markets exhibit non-random network structures with identifiable central nodes that play crucial roles in risk transmission. In the real estate market, first-tier cities serve as central hubs; in the carbon market, the national market coordinates regional interactions; and in the AI-energy nexus, certain clean energy segments (notably photovoltaics) show stronger connections with AI. These findings suggest that risk in modern economic systems is fundamentally hierarchical rather than evenly distributed, with certain nodes wielding disproportionate influence over system-wide stability.

The differences in the nature of these central nodes—geographical entities (cities) in real estate, institutional constructs (national markets) in carbon trading, and technological segments (photovoltaics) in the AI-energy nexus—reflect the distinct organizing principles of each market. Yet their common structural significance underscores a universal pattern of concentrated influence points in networked risk transmission. This has profound implications for regulatory approaches, suggesting that targeted interventions at key nodes may yield greater systemic benefits than broad-based policies.

Risk transmission patterns in all three markets vary significantly depending on market conditions or structural changes, revealing state-dependent dynamics that challenge traditional risk modeling approaches. The real estate market shows distinct behaviors in high-risk versus low-risk states; the carbon market demonstrates different dynamics pre- and post-unification; and the AI-energy relationship intensifies following technological breakthroughs. This state dependence indicates that risk relationships are not static but evolve dynamically in response to changing contexts. The drivers of these state transitions differ across markets—macroeconomic shifts in real estate, institutional reforms in carbon markets, and technological innovations in the AI-energy nexus—yet the resulting transformation in risk transmission patterns follows similar principles. This reveals a fundamental characteristic of modern markets: they function as complex adaptive systems whose behavior cannot be understood through time-invariant models.

The implications are significant for both risk monitoring and management strategies. Traditional approaches that assume stable correlations or linear transmission mechanisms are inadequate for capturing the changing nature of systemic risk. Instead, continuous reassessment and adaptive regulatory frameworks that can respond to shifting risk landscapes are essential. Furthermore, all three markets display significant sensitivity to policy changes and regulatory frameworks, reflecting the embedded nature of these markets within broader institutional contexts and the powerful role of policy as both a risk driver and potential mitigator. The varying mechanisms through which policy

impacts manifest—through credit conditions and monetary policy in real estate, through market design and allocation methods in carbon trading, and through subsidies and technological standards in the AI-energy nexus—highlight the need for domain-specific policy tools. However, the universal presence of policy sensitivity across these diverse markets underscores a broader truth: in a state-influenced economy like China's, policy instruments remain powerful levers for systemic risk management.

The presence of significant tail dependencies across all three markets highlights the importance of focusing on extreme risk scenarios rather than average correlations. This is particularly evident in the AI-energy study, where tail dependencies reveal patterns that are not captured by conventional correlation measures. The asymmetric nature of these tail dependencies—with upper and lower tails often exhibiting different strengths of association—further complicates risk assessment. This common feature suggests that extreme market conditions reveal interconnections that remain dormant during normal periods. Such nonlinear risk amplification challenges traditional risk management approaches based on normal distributions and linear dependencies. Instead, stress testing frameworks that specifically incorporate tail events and contagion mechanisms are essential for capturing the full spectrum of systemic vulnerabilities.

Collectively, these cross-cutting themes reveal that risk in modern interconnected markets is: (1) networked and hierarchical rather than uniform or random; (2) dynamic and state-dependent rather than static; (3) highly responsive to policy and institutional changes; and (4) characterized by nonlinear amplification during extreme events. These properties demand a fundamental rethinking of risk monitoring, modeling, and management approaches.

5.3 Policy Recommendations

Building on the empirical findings and cross-cutting themes identified above, several specific policy recommendations emerge for enhancing systemic risk management across these interconnected markets. Given the identified importance of central nodes in risk transmission networks, regulatory authorities should implement differentiated supervision and intervention strategies focused on systemically important entities or regions. For the real estate market, this implies enhanced macroprudential measures specifically designed for first-tier and key second-tier cities, such as stricter loan-to-value ratios and more frequent stress testing for financial institutions with high exposure to these markets. As demonstrated in Chapter 2, these cities function as principal conduits of risk (with betweenness centrality measures up to 1375 in high-risk states), making them critical intervention points.

In the carbon market, the creation of the national market has established a critical central coordinator (eigenvector centrality of 0.412), requiring robust oversight mechanisms.

Given that Chapter 3 identified post-unification shifts in key regional markets (e.g., Tianjin's transition to a major risk transmitter), monitoring these evolving roles should be prioritized. Specifically, enhanced liquidity provision mechanisms during periods of market stress should target those regions with high net spillover potential. For the AI-energy nexus, our findings in Chapter 4 suggest that photovoltaic segments within clean energy exhibit the strongest coupling with AI (τ increasing from 0.32 to 0.52 post-ChatGPT). This calls for targeted coordination between digital infrastructure planning and renewable energy development, particularly for data center projects with significant AI computational loads.

The observed state-dependent dynamics across all three markets necessitate adaptive regulatory frameworks that can respond to changing risk environments. For the real estate market, our findings in Chapter 2 demonstrated that risk transmission intensifies during high-risk states, with network degree centrality increasing by approximately 15%. This suggests implementing automatic stabilizers that activate during periods of detected heightened risk, such as counter-cyclical capital buffers that increase during periods of rapid price appreciation or high market volatility. For carbon markets, Chapter 3 revealed significant structural changes following market unification, with information transfer rates increasing by 19.4%. This suggests the need for transition-sensitive regulation during major market reforms, with temporary liquidity enhancement mechanisms and more intensive monitoring during structural transitions. Specifically, establishing predefined market intervention thresholds based on volatility measures and spillover indices would provide a systematic framework for state-contingent intervention.

In the AI-energy relationship, Chapter 4 demonstrated amplified dependencies following major technological breakthroughs (as evidenced by increased tail dependence post-ChatGPT). This suggests implementing technology-sensitive policy adjustment mechanisms, such as graduated clean energy subsidies or grid integration priorities that evolve with AI computational demand forecasts. The interconnected nature of these markets necessitates coordination across regulatory domains. Establishing a dedicated cross-market risk monitoring body would enhance systemic risk management by tracking transmission channels between real estate, carbon markets, and energy/technology sectors. This body should conduct regular integrated risk assessments, focusing on potential domino effects across these interconnected markets.

Specific coordination mechanisms should include: (1) joint stress testing exercises that simulate cascading failures across markets; (2) coordinated policy responses to major external shocks, with explicit consideration of cross-market spillovers; and (3) integrated data sharing platforms that enable real-time monitoring of cross-market risk indicators. Given our findings on the significant role of central nodes and state-dependent dynamics, these mechanisms should prioritize key transmission hubs and adapt to changing market conditions. Traditional risk monitoring approaches that focus on average correlations or

central tendencies are inadequate for capturing the significant tail dependencies identified across all three markets. Regulatory authorities should implement advanced monitoring systems specifically designed to detect and respond to extreme co-movements and tail risks. This could include: developing early warning systems based on dynamic copula-derived tail dependence measures, with thresholds calibrated to the specific characteristics of each market as identified in Chapters 2-4; incorporating extreme risk scenarios in mandatory stress testing frameworks for financial institutions with exposure to multiple markets; and establishing contingency planning requirements for systemically important institutions that explicitly address tail risk events. These measures would address the nonlinear risk amplification documented above, ensuring that regulatory frameworks are robust to extreme events rather than optimized only for normal market conditions.

5.4 Limitations and Future Research Directions

While this thesis provides valuable insights into risk transmission mechanisms across three important markets, several limitations should be acknowledged, pointing to directions for future research. Each study faced specific data constraints that could be addressed in future research. The real estate analysis relied on monthly housing price indices, which may not fully capture the granularity of market movements. Future work could incorporate transaction-level data, including property characteristics and buyer profiles, to provide more nuanced insights into risk transmission channels. The carbon market study was limited by the relatively short history of China's carbon markets, particularly the national market. As more data becomes available, longer-term studies could examine how risk transmission patterns evolve through multiple policy cycles and economic environments. The AI-energy analysis encountered challenges in precisely measuring AI industry activities and energy consumption patterns. Future research would benefit from more granular data on actual computational loads, electricity consumption of AI operations, and the energy mix supplying these operations.

The network-based approaches employed in this thesis primarily capture associations rather than causal relationships, a limitation common to many studies of complex systems. Future research could strengthen causal identification through several approaches: exploiting natural experiments or policy discontinuities (e.g., staggered implementation of housing restrictions across cities, phased introduction of carbon market sectors); developing structural models that incorporate theoretical mechanisms of risk transmission; and employing instrumental variable approaches where suitable instruments can be identified. These methodological advances would help move from identifying risk transmission patterns to understanding their underlying causal mechanisms, thereby providing more robust foundations for policy interventions.

While this thesis focuses on three important markets, expanding the analysis to

include other sectors would provide a more comprehensive picture of risk transmission in the Chinese economy. Future research could incorporate conventional financial markets (banking, equity, and bond markets), additional commodity markets beyond energy, and international trade and supply chain networks. A more comprehensive mapping of interconnections across these additional dimensions would enhance our understanding of systemic risk in a highly integrated economy.

Future research could explore alternative methodological approaches that complement the techniques employed in this thesis. Machine learning methods for early warning signal detection could enhance the identification of impending regime shifts in risk transmission networks. Agent-based modeling could simulate how micro-level interactions between market participants generate the observed macro-level risk patterns, which is particularly useful for testing the impact of alternative policy interventions. Additionally, time-varying parameter structural vector autoregression (TVP-SVAR) models could further elucidate the evolving relationships between macroeconomic variables and market-specific risk indicators.

The studies in this thesis primarily focus on relatively short-term risk transmission. Extending the analysis to examine long-term structural changes would provide additional insights into how risk dynamics evolve through major economic transitions, technological paradigm shifts, and policy regime changes. This could include investigating how risk transmission networks reorganize during fundamental economic transformations, such as China's ongoing transition toward a more consumption-driven, innovation-led growth model. The aforementioned data limitations directly impact our ability to conduct robust long-term analyses. As longer time series become available, particularly for newer markets like carbon trading and AI, more sophisticated investigations of structural changes and evolutionary dynamics will become feasible.

5.5 Concluding Remarks

This thesis has demonstrated the value of applying advanced network analysis and econometric techniques to understand risk transmission across interconnected markets. By examining real estate, carbon trading, and AI-energy linkages in China, it has provided insights into how risks propagate within and across these sectors, how structural changes reshape risk transmission patterns, and how policy interventions might mitigate systemic risks.

The findings highlight the complex, state-dependent nature of risk contagion in modern economies and underscore the importance of considering network structures, tail dependencies, and cross-market linkages in both academic research and policy design. The identification of central transmission nodes, the documentation of regime-dependent risk dynamics, the evidence of policy sensitivity, and the characterization of tail dependencies collectively advance our understanding of systemic risk beyond traditional approaches

based on linear correlations or standalone market analyses.

As China continues to navigate its complex economic transformation—balancing growth objectives with stability concerns, environmental sustainability with technological advancement, and domestic priorities with global integration—a sophisticated understanding of risk transmission mechanisms becomes increasingly valuable. The integrated, multi-method approach developed in this thesis offers a framework for detecting vulnerabilities, anticipating contagion channels, and designing targeted interventions across diverse but interconnected market systems.

By contributing to this understanding, this thesis aims to inform more effective regulatory approaches and risk management strategies, not only for China but potentially for other complex economies facing similar challenges in an era of increasing market interconnectedness, technological disruption, and environmental transition. The interplay between traditional economic sectors, emerging markets for environmental assets, and technology-driven transformations represents a frontier in systemic risk research—one where continued methodological innovation and empirical investigation can yield valuable insights for building more resilient economic systems.

References

Aas, K., Czado, C., Frigessi, A., and Bakken, H. (2009). Pair-copula constructions of multiple dependence. *Insurance: Mathematics and Economics*, 44(2):182–198.

Acemoglu, D., Ozdaglar, A., and Tahbaz-Salehi, A. (2015). Systemic risk and stability in financial networks. *American Economic Review*, 105(2):564–608.

Akaike, H. (1974). A new look at the statistical model identification. *IEEE transactions on automatic control*, 19(6):716–723.

Alamaren, A. S., Gokmenoglu, K. K., and Taspinar, N. (2024). Volatility spillovers among leading cryptocurrencies and us energy and technology companies. *Financial Innovation*, 10(1):81.

Antonakakis, N., Chatziantoniou, I., and Gabauer, D. (2020). Refined measures of dynamic connectedness based on time-varying parameter vector autoregressions. *Journal of Risk and Financial Management*, 13(4):84.

Balcılar, M., Demirer, R., Hammoudeh, S., and Nguyen, D. K. (2016). Risk spillovers across the energy and carbon markets and hedging strategies for carbon risk. *Energy Economics*, 54:159–172.

Bartram, S. M., Hou, K., and Kim, S. (2022). Real effects of climate policy: Financial constraints and spillovers. *Journal of Financial Economics*, 143(2):668–696.

Battiston, S., Caldarelli, G., May, R. M., Roukny, T., and Stiglitz, J. E. (2016). The price of complexity in financial networks. *Proceedings of the National Academy of Sciences*, 113(36):10031–10036.

Bedford, T. and Cooke, R. M. (2002). Vines–a new graphical model for dependent random variables. *The Annals of Statistics*, 30(4):1031–1068.

Billio, M., Getmansky, M., Lo, A. W., and Pelizzon, L. (2012). Econometric measures of connectedness and systemic risk in the finance and insurance sectors. *Journal of financial economics*, 104(3):535–559.

Blondel, V. D., Guillaume, J.-L., Lambiotte, R., and Lefebvre, E. (2008). Fast unfolding of communities in large networks. *Journal of statistical mechanics: theory and experiment*, 2008(10):P10008.

Bollerslev, T. (1986). Generalized autoregressive conditional heteroskedasticity. *Journal of econometrics*, 31(3):307–327.

Bollerslev, T. (1987). A conditionally heteroskedastic time series model for speculative prices and rates of return. *The review of economics and statistics*, pages 542–547.

Bolton, P. and Kacperczyk, M. (2021). Do investors care about carbon risk? *Journal of financial economics*, 142(2):517–549.

Brady, R. R. (2011). Measuring the diffusion of housing prices across space and over time. *Journal of Applied Econometrics*, 26(2):213–231.

Brueckner, J. K., Fu, S., Gu, Y., and Zhang, J. (2017). Measuring the stringency of land use regulation: The case of china's building height limits. *Review of Economics and Statistics*, 99(4):663–677.

Chang, K., Lu, S., and Song, X. (2018). The impacts of liquidity dynamics on emissions allowances price: different evidence from china's emissions trading pilots. *Journal of Cleaner Production*, 183:786–796.

Chen, J., Liang, Z., Ding, Q., and Liu, Z. (2022). Quantile connectedness between energy, metal, and carbon markets. *International Review of Financial Analysis*, 83:102282.

Chevallier, J. (2009). Carbon futures and macroeconomic risk factors: A view from the eu ets. *Energy Economics*, 31(4):614–625.

Cong, R. and Lo, A. Y. (2017). Emission trading and carbon market performance in shenzhen, china. *Applied Energy*, 193:414–425.

Cotter, J., Gabriel, S., and Roll, R. (2015). Can Housing Risk Be Diversified? A Cautionary Tale from the Housing Boom and Bust. *Review of Financial Studies*, 28(3):913–936.

Dargusch, P. (2017). China must lead on emissions trading. *Science*, 357(6356):1106–1107.

Demarta, S. and McNeil, A. J. (2005). The t copula and related copulas. *International statistical review*, 73(1):111–129.

Dickey, D. A. and Fuller, W. A. (1979). Distribution of the estimators for autoregressive time series with a unit root. *Journal of the American statistical association*, 74(366a):427–431.

Diebold, F. X. and Yilmaz, K. (2009). Measuring financial asset return and volatility spillovers, with application to global equity markets. *The Economic Journal*, 119(534):158–171.

Diebold, F. X. and Yilmaz, K. (2012). Better to give than to receive: Predictive directional measurement of volatility spillovers. *International Journal of forecasting*, 28(1):57–66.

Diebold, F. X. and Yılmaz, K. (2014). On the network topology of variance decompositions: Measuring the connectedness of financial firms. *Journal of econometrics*, 182(1):119–134.

Diebold, F. X. and Yilmaz, K. (2015). Trans-atlantic equity volatility connectedness: Us and european financial institutions, 2004–2014. *Journal of Financial Econometrics*, 14(1):81–127.

Diebold, F. X. and Yilmaz, K. (2023). On the past, present, and future of the diebold–yilmaz approach to dynamic network connectedness. *Journal of Econometrics*, 234:115–120.

Duan, K., Lan, F., Zhao, Y., and Huang, Y. (2023). Housing networks in urban china: A panel var model with bayesian stochastic search. *Cities*, 140:104400.

Efron, B. and Tibshirani, R. J. (1994). *An introduction to the bootstrap*. Chapman and Hall/CRC.

Ellerman, A. D., Convery, F. J., and De Perthuis, C. (2010). *Pricing carbon: the European Union emissions trading scheme*. Cambridge University Press.

Elliott, M., Golub, B., and Jackson, M. O. (2014). Financial networks and contagion. *American Economic Review*, 104(10):3115–3153.

European Commission (2019). The european green deal. Communication COM(2019) 640 final, European Commission, Brussels. Published on 11 December 2019.

Fang, H., Gu, Q., Xiong, W., and Zhou, L.-A. (2016a). Demystifying the Chinese Housing Boom. *NBER Macroeconomics Annual*, 30:105–166.

Fang, H., Gu, Q., Xiong, W., and Zhou, L.-A. (2016b). Demystifying the chinese housing boom. *NBER macroeconomics annual*, 30(1):105–166.

Feng, G.-F. and Zheng, M. (2022). Economic policy uncertainty and renewable energy innovation: International evidence. *Innovation and Green Development*, 1(2):100010.

Fink, H., Klimova, Y., Czado, C., and Stöber, J. (2017). Regime Switching Vine Copula Models for Global Equity and Volatility Indices. *Econometrics*, 5(1):3.

Garriga, C. and Hedlund, A. (2020). Mortgage debt, consumption, and illiquid housing markets in the great recession. *American Economic Review*, 110(6):1603–1634.

Genest, C., Rémillard, B., and Beaudoin, D. (2009a). Goodness-of-fit tests for copulas: A review and a power study. *Insurance: Mathematics and economics*, 44(2):199–213.

Genest, C., Rémillard, B., and Beaudoin, D. (2009b). Goodness-of-fit tests for copulas: A review and a power study. *Insurance: Mathematics and economics*, 44(2):199–213.

Glaeser, E., Huang, W., Ma, Y., and Shleifer, A. (2017). A Real Estate Boom with Chinese Characteristics. *Journal of Economic Perspectives*, 31(1):93–116.

Gong, Y., Hu, J., and Boelhouwer, P. J. (2016). Spatial interrelations of Chinese housing markets: Spatial causality, convergence and diffusion. *Regional Science and Urban Economics*, 59:103–117.

Haldane, A. G. and May, R. M. (2011). Systemic risk in banking ecosystems. *Nature*, 469(7330):351–355.

Hamilton, J. D. (1989). A New Approach to the Economic Analysis of Nonstationary Time Series and the Business Cycle. *Econometrica*, 57(2):357.

Hanif, W., Hernandez, J. A., Mensi, W., Kang, S. H., Uddin, G. S., and Yoon, S.-M. (2021). Nonlinear dependence and connectedness between clean/renewable energy sector equity and european emission allowance prices. *Energy Economics*, 101:105409.

Hautsch, N., Schaumburg, J., and Schienle, M. (2015). Financial network systemic risk contributions. *Review of Finance*, 19(2):685–738.

Heinen, A., Kim, M. L., and Hamadi, M. (2022). Geographic Dependence and Diversification in House Price Returns: The Role of Leverage. *Journal of Financial Econometrics*, 33(4):nbac037.

Hong, H., Li, F. W., and Xu, J. (2019). Climate risks and market efficiency. *Journal of econometrics*, 208(1):265–281.

Hu, G. and Fan, G.-Z. (2022). Empirical evidence of risk contagion across regional housing markets in China. *Economic Modelling*, 115:105945.

ICAP, C. (2022). Emissions trading worldwide: status report 2022.

International Energy Agency (2023). World energy outlook 2023. Technical report, IEA, Paris. Licence: CC BY 4.0 (report); CC BY NC SA 4.0 (Annex A).

International Energy Agency (2024). World energy outlook 2024. Technical report, IEA, Paris. Licence: CC BY 4.0 (report); CC BY NC SA 4.0 (Annex A).

Jia, L., Zhang, X., Wang, X., Chen, X., Xu, X., and Song, M. (2024). Impact of carbon emission trading system on green technology innovation of energy enterprises in china. *Journal of Environmental Management*, 360:121229.

Joe, H. (1997). *Multivariate models and multivariate dependence concepts*. CRC press.

Joe, H. (2005). Asymptotic efficiency of the two-stage estimation method for copula-based models. *Journal of Multivariate Analysis*, 94(2):401–419. 440 citations (Crossref) [2024-04-14].

Khosravi, A., Sandoval, O. R., Taslimi, M. S., Sahrakorpi, T., Amorim, G., and Pabon, J. J. G. (2024). Review of energy efficiency and technological advancements in data center power systems. *Energy and Buildings*, page 114834.

Kivelä, M., Arenas, A., Barthelemy, M., Gleeson, J. P., Moreno, Y., and Porter, M. A. (2014). Multilayer networks. *Journal of complex networks*, 2(3):203–271.

Koop, G., Pesaran, M. H., and Potter, S. M. (1996). Impulse response analysis in nonlinear multivariate models. *Journal of econometrics*, 74(1):119–147.

Kruger, J. and Pizer, W. A. (2004). The eu emissions trading directive: Opportunities and potential pitfalls.

Kuang, W. and Liu, P. (2015). Inflation and house prices: Theory and evidence from 35 major cities in china. *International real estate review*, 18(2).

Lin, B. and Tan, R. (2017). China's co2 emissions of a critical sector: evidence from energy intensive industries. *Journal of Cleaner Production*, 142:4270–4281.

Liu, L., Chen, C., Zhao, Y., and Zhao, E. (2015). China' s carbon-emissions trading: Overview, challenges and future. *Renewable and Sustainable Energy Reviews*, 49:254–266.

Lu, Y., Li, J., and Yang, H. (2023). Time-varying impacts of monetary policy uncertainty on china's housing market. *Economic Modelling*, 118:106081.

Luccioni, S., Jernite, Y., and Strubell, E. (2024). Power hungry processing: Watts driving the cost of ai deployment? In *The 2024 ACM Conference on Fairness, Accountability, and Transparency*, pages 85–99.

Ma, R., Liu, Z., and Zhai, P. (2022). Does economic policy uncertainty drive volatility spillovers in electricity markets: time and frequency evidence. *Energy Economics*, 107:105848.

Mansanet-Bataller, M. and Pardo, Á. (2008). What you should know about carbon markets. *Energies*, 1(3):120–153.

Mansanet-Bataller, M., Pardo, A., and Valor, E. (2007). Co2 prices, energy and weather. *The energy journal*, 28(3):73–92.

Mantegna, R. N. (1999). Hierarchical structure in financial markets. *The European Physical Journal B-Condensed Matter and Complex Systems*, 11:193–197.

Mao, G. and Shen, Y. (2019). Bubbles or fundamentals? Modeling provincial house prices in China allowing for cross-sectional dependence. *China Economic Review*, 53:53–64.

Masanet, E., Shehabi, A., Lei, N., Smith, S., and Koomey, J. (2020). Recalibrating global data center energy-use estimates. *Science*, 367(6481):984–986.

Mensi, W., Hanif, W., Bouri, E., and Vo, X. V. (2024). Spillovers and tail dependence between oil and us sectoral stock markets before and during covid-19 pandemic. *International Journal of Emerging Markets*, 19(11):4155–4185.

Miao, H., Ramchander, S., and Simpson, M. W. (2011). Return and Volatility Transmission in U.S. Housing Markets. *Real Estate Economics*, 39(4):701–741.

Miles, W. and Zhu, X. (2023). Housing and the changing impact of monetary policy. *International Review of Economics & Finance*, 86:587–603.

Montagna, M. and Kok, C. (2016). Multi-layered interbank model for assessing systemic risk.

National Bureau of Statistics of China (2023). Press conference on the 2022 national economic performance. `http://www.stats.gov.cn/sj/zxfb/202301/t20230117_1893634.html`.

Navia Simon, D. and Diaz Anadon, L. (2025). Faster deployment of renewables stabilizes electricity prices in europe. *Nature Energy*, pages 1–2.

Nelson, D. B. (1991). Conditional Heteroskedasticity in Asset Returns: A New Approach. *Econometrica*, 59(2):347–370.

Niu, H. (2021). Correlations between crude oil and stocks prices of renewable energy and technology companies: a multiscale time-dependent analysis. *Energy*, 221:119800.

Pástor, L., Stambaugh, R. F., and Taylor, L. A. (2022). Dissecting green returns. *Journal of financial economics*, 146(2):403–424.

Patterson, D., Gonzalez, J., Le, Q., Liang, C., Munguia, L.-M., Rothchild, D., So, D., Texier, M., and Dean, J. (2021). Carbon emissions and large neural network training. *arXiv preprint arXiv:2104.10350*.

Patton, A. J. (2006). Modelling asymmetric exchange rate dependence. *International economic review*, 47(2):527–556.

Pesaran, H. H. and Shin, Y. (1998). Generalized impulse response analysis in linear multivariate models. *Economics letters*, 58(1):17–29.

Poledna, S., Molina-Borboa, J. L., Martínez-Jaramillo, S., Van Der Leij, M., and Thurner, S. (2015). The multi-layer network nature of systemic risk and its implications for the costs of financial crises. *Journal of Financial Stability*, 20:70–81.

Rogoff, K. S. and Yang, Y. (2024). A tale of tier 3 cities. *Journal of International Economics*, 152:103989.

Sadorsky, P. (2012). Correlations and volatility spillovers between oil prices and the stock prices of clean energy and technology companies. *Energy economics*, 34(1):248–255.

Schmalensee, R. and Stavins, R. N. (2017). Lessons learned from three decades of experience with cap and trade. *Review of Environmental Economics and Policy*.

Schwarz, G. (1978). Estimating the dimension of a model. *The annals of statistics*, pages 461–464.

Sklar, M. (1959). Fonctions de répartition à n dimensions et leurs marges. In *Annales de l'ISUP*, volume 8, pages 229–231.

Stavins, R. N. (1995). Transaction costs and tradeable permits. *Journal of environmental economics and management*, 29(2):133–148.

Strubell, E., Ganesh, A., and McCallum, A. (2020). Energy and policy considerations for modern deep learning research. In *Proceedings of the AAAI conference on artificial intelligence*, volume 34, pages 13693–13696.

Sun, X., Fang, W., Gao, X., An, H., Liu, S., and Wu, T. (2022). Complex causalities between the carbon market and the stock markets for energy intensive industries in china. *International Review of Economics & Finance*, 78:404–417.

Tan, R. and Lin, B. (2018). What factors lead to the decline of energy intensity in china's energy intensive industries? *Energy Economics*, 71:213–221.

Tietenberg, T. (2010). *Emissions trading: principles and practice*. Routledge.

Tiwari, A. K., Nasreen, S., Hammoudeh, S., and Selmi, R. (2021). Dynamic dependence of oil, clean energy and the role of technology companies: New evidence from copulas with regime switching. *Energy*, 220:119590.

Tobias, A. and Brunnermeier, M. K. (2016). Covar. *The American Economic Review*, 106(7):1705.

Tsay, R. S. (2005). Analysis of financial time series. *John Eiley and Sons*.

Wang, Z. and Zhang, Q. (2014). Fundamental factors in the housing markets of china. *Journal of housing economics*, 25:53–61.

Wen, F., Zhao, L., He, S., and Yang, G. (2020). Asymmetric relationship between carbon emission trading market and stock market: evidences from china. *Energy Economics*, 91:104850.

Wu, F., Xiao, X., Zhou, X., Zhang, D., and Ji, Q. (2022). Complex risk contagions among large international energy firms: A multi-layer network analysis. *Energy Economics*, 114:106271.

Wu, J., Deng, Y., and Liu, H. (2014). House Price Index Construction in the Nascent Housing Market: The Case of China. *The Journal of Real Estate Finance and Economics*, 48(3):522–545.

Wu, L., Huang, Y., and Gu, Y. (2023). Fragmented or unified? the state of china's carbon emission trading market. *Energies*, 16(5):2470.

Xiao, Z., Ma, S., Sun, H., Ren, J., Feng, C., and Cui, S. (2022). Time-varying spillovers among pilot carbon emission trading markets in china. *Environmental Science and Pollution Research*, 29(38):57421–57436.

Xin-gang, Z., Wenjie, L., Wei, W., and Shuran, H. (2023). The impact of carbon emission trading on green innovation of china's power industry. *Environmental Impact Assessment Review*, 99:107040.

Xu, Y., Shao, X., and Tanasescu, C. (2024). How are artificial intelligence, carbon market, and energy sector connected? a systematic analysis of time-frequency spillovers. *Energy Economics*, 132:107477.

Yang, J., Tong, M., and Yu, Z. (2021). Housing market spillovers through the lens of transaction volume: A new spillover index approach. *Journal of Empirical Finance*, 64:351–378.

Yang, S., Jahanger, A., Hu, J., and Awan, A. (2024). Impact of china's carbon emissions trading scheme on firm-level pollution abatement and employment: Evidence from a national panel dataset. *Energy Economics*, 136:107744.

Zhang, D. and Fan, G.-Z. (2019). Regional spillover and rising connectedness in China's urban housing prices. *Regional Studies*, 53(6):861–873.

Zhang, T., Gerlowski, D., and Ford, D. (2014). Housing price variability: national and local impacts. *Applied Economics*, 46(28):3494–3502.

Zhang, W., Zhang, N., and Yu, Y. (2019). Carbon mitigation effects and potential cost savings from carbon emissions trading in china's regional industry. *Technological Forecasting and Social Change*, 141:1–11.

Zhang, Y.-J. and Hao, J.-F. (2017). Carbon emission quota allocation among china's industrial sectors based on the equity and efficiency principles. *Annals of Operations Research*, 255:117–140.

Zhao, L., Liu, W., Zhou, M., and Wen, F. (2022). Extreme event shocks and dynamic volatility interactions: The stock, commodity, and carbon markets in china. *Finance Research Letters*, 47:102645.

Zhu, B., Zhou, X., Liu, X., Wang, H., He, K., and Wang, P. (2020). Exploring the risk spillover effects among china's pilot carbon markets: A regular vine copula-coes approach. *Journal of Cleaner Production*, 242:118455.

Zimmer, D. M. (2012). The Role of Copulas in the Housing Crisis. *Review of Economics and Statistics*, 94(2):607–620.

Zimmer, D. M. (2015). ANALYZING COMOVEMENTS IN HOUSING PRICES USING VINE COPULAS. *Economic Inquiry*, 53(2):1156–1169.

Appendix A

Supplementary Materials for Chapter 2

A.1 Appendix

A.1.1 Copula Models Specification

Overview of Copula Theory

Copulas provide a flexible framework for modeling multivariate dependencies independent of the marginal distributions. According to Sklar's theorem (Sklar, 1959), any multivariate joint distribution function F with continuous marginals $F_1, F_2, \ldots, F_n$ can be uniquely expressed as:

$$F(x_1, x_2, \ldots, x_n) = C(F_1(x_1), F_2(x_2), \ldots, F_n(x_n)) \tag{A.1}$$

Where $C : [0,1]^n \to [0,1]$ is the copula function that captures the dependence structure among variables, this separation of marginal behavior from dependence structure makes copulas particularly suitable for our analysis of housing market risk contagion.

Bivariate Copula Families

Our study employs several copula families to capture various dependency structures between city pairs. Each copula family offers distinct features in terms of symmetry, tail dependence, and flexibility in modeling dependence patterns.

Gaussian Copula The Gaussian copula is derived from the multivariate normal distribution and is defined as:

$$C_\rho^{Gaussian}(u, v) = \Phi_\rho(\Phi^{-1}(u), \Phi^{-1}(v)) \tag{A.2}$$

Where Φ_ρ is the standardized bivariate normal distribution with correlation parameter $\rho \in (-1, 1)$, and Φ^{-1} is the inverse of the standard normal cumulative distribution function. The Gaussian copula exhibits symmetrical dependence and lacks tail dependence, making it suitable for modeling linear correlations between housing markets with similar behavior in both tails. In our analysis, the Gaussian copula was predominantly selected for modeling dependencies between economically similar cities with stable relationships, such as Shanghai-Hangzhou, where the correlation parameter was estimated at $\rho = 0.73$, corresponding to Kendall's $\tau = 0.55$.

Student's t-Copula The t-copula is derived from the multivariate Student's t-distribution and is defined as:

$$C^t_{\rho,\nu}(u, v) = t_{\rho,\nu}(t^{-1}_\nu(u), t^{-1}_\nu(v)) \tag{A.3}$$

Where $t_{\rho,\nu}$ is the standardized bivariate Student's t-distribution with correlation parameter $\rho \in (-1, 1)$ and degrees of freedom $\nu > 0$, and t^{-1}_ν is the inverse of the univariate Student's t-distribution function. The t-copula allows for symmetric tail dependence, with smaller ν values resulting in stronger tail dependence. This copula was particularly useful for modeling dependencies between cities that exhibit strong co-movements during extreme market conditions. For example, Beijing-Tianjin showed strong tail dependence with parameters $\rho = 0.68$ and $\nu = 4.2$, indicating substantial risk of joint extreme movements.

Clayton Copula The Clayton copula is an asymmetric copula with strong lower tail dependence, defined as:

$$C^{Clayton}_\theta(u, v) = \max\{(u^{-\theta} + v^{-\theta} - 1)^{-1/\theta}, 0\} \tag{A.4}$$

where $\theta > 0$ is the dependence parameter. As θ increases, the strength of dependence increases, particularly in the lower tail. This makes the Clayton copula suitable for modeling dependencies between housing markets that tend to experience simultaneous downturns. In our analysis, the Clayton copula was selected for several city pairs, including Shanghai-Suzhou with $\theta = 0.11$ (corresponding to Kendall's $\tau = 0.05$), indicating modest joint risk during market downturns.

Gumbel Copula The Gumbel copula is an asymmetric copula with upper tail dependence, defined as:

$$C^{Gumbel}_\theta(u, v) = \exp\{-[((-\ln u)^\theta + (-\ln v)^\theta)]^{1/\theta}\} \tag{A.5}$$

where $\theta \geq 1$ is the dependence parameter. As θ increases, the strength of dependence increases, particularly in the upper tail. This makes the Gumbel copula suitable for

modeling dependencies between housing markets that tend to experience simultaneous booms. In our study, the Gumbel copula was frequently selected for rapidly developing city pairs, such as Wuhan-Zhengzhou with $\theta = 2.26$ (corresponding to Kendall's $\tau = 0.53$), indicating strong joint movements during market upturns.

Frank Copula The Frank copula is a symmetric copula with no tail dependence, defined as:

$$C_\theta^{Frank}(u, v) = -\frac{1}{\theta} \ln \left(1 + \frac{(e^{-\theta u} - 1)(e^{-\theta v} - 1)}{e^{-\theta} - 1} \right) \tag{A.6}$$

where $\theta \in \mathbb{R} \setminus \{0\}$ is the dependence parameter. The Frank copula is particularly useful for modeling dependencies that are strongest in the center of the distribution. In our analysis, it was selected for several city pairs with moderate dependence but limited tail behavior, such as Nanning-Xuzhou with $\theta = 6.32$ (corresponding to Kendall's $\tau = 0.56$).

Rotated Copulas To capture a wider range of dependence patterns, we also employed rotated versions of the Clayton and Gumbel copulas. The 180-degree rotated (or survival) copula is given by:

$$C_{180^\circ}(u, v) = u + v - 1 + C(1 - u, 1 - v) \tag{A.7}$$

For the Clayton copula, this rotation creates upper tail dependence, while for the Gumbel copula, it creates lower tail dependence. The 90-degree and 270-degree rotations, which create negative dependence, are defined similarly. In our analysis, the rotated Clayton copula was selected for several city pairs, including Guangzhou-Kunming with $\theta = 0.09$ (corresponding to Kendall's $\tau = -0.04$), indicating negative dependence.

Vine Copula Construction

For modeling high-dimensional dependencies among multiple cities, we employed vine copulas, which decompose a multivariate distribution into a cascade of bivariate copulas.

Vine Structures We considered three main vine structures:

- **C-vine (Canonical vine)**: In a C-vine, each tree has a unique node that connects to all other nodes. This structure is particularly suitable when there is a key variable that explains the dependence on all others. The density function for an n-dimensional C-vine is given by:

$$f(x_1,\ldots,x_n)=\prod_{i=1}^{n} f(x_i)\times\prod_{j=1}^{n-1}\prod_{i=1}^{n-j} c_{j,j+i|1,\ldots,j-1}(F(x_j|x_1,\ldots,x_{j-1}),F(x_{j+i}|x_1,\ldots,x_{j-1})) \tag{A.8}$$

- **D-vine (Drawable vine)**: In a D-vine, each node is connected to at most two others, forming a path. This structure is suitable when there is a natural ordering of variables. The density function for an n-dimensional D-vine is given by:

$$f(x_1,\ldots,x_n)=\prod_{i=1}^{n} f(x_i)\times\prod_{j=1}^{n-1}\prod_{i=1}^{n-j} c_{i,i+j|i+1,\ldots,i+j-1}(F(x_i|x_{i+1},\ldots,x_{i+j-1}),F(x_{i+j}|x_{i+1},\ldots,x_{i+j-1})) \tag{A.9}$$

- **R-vine (Regular vine)**: An R-vine is a more general structure that includes C-vines and D-vines as special cases. It allows for more flexible modeling of complex dependence structures. The density function for an n-dimensional R-vine is a generalization of the C-vine and D-vine densities, with pair-copulas arranged according to a specified R-vine structure.

Based on likelihood ratio tests and information criteria, we selected the R-vine structure for our analysis, as it provided the most flexible and suitable representation of the complex dependencies among the 70 cities in our sample.

Pair-copula Construction The pair-copula construction involves decomposing the multivariate density into a product of bivariate copulas and conditional marginal densities. This decomposition proceeds tree by tree, with each tree representing a level of conditioning. For an n-dimensional distribution, there are $n-1$ trees, with the first tree capturing unconditional pairwise dependencies, and subsequent trees capturing conditional dependencies.

For each pair of variables in each tree, we selected the most appropriate copula family from our candidate set (Gaussian, t, Clayton, Gumbel, Frank, and their rotations) based on the Akaike Information Criterion (AIC). The parameters of each pair-copula were estimated using maximum likelihood estimation.

Model Selection and Fitting

Information Criteria We employed the AIC and BIC for copula selection, defined as:

$$AIC = -2\ln L + 2k \tag{A.10}$$

$$BIC = -2\ln L + k\ln(n) \tag{A.11}$$

where $\ln L$ is the log-likelihood of the fitted model, k is the number of parameters, and n is the sample size. For each pair of cities, we selected the copula family with the lowest AIC value, unless the difference in AIC between two models was less than 2, in which case we chose the simpler model (i.e., the one with fewer parameters).

Parameter Estimation We employed a sequential approach for estimating the parameters of the vine copula:

1. We first fitted appropriate marginal distributions to each city's housing price returns using AR-GARCH models with skewed Student's t innovations.
2. We transformed these standardized residuals to uniform variates using the probability integral transform.
3. We estimated the parameters of the first tree of the vine using maximum likelihood estimation.
4. For subsequent trees, we calculated the conditional distributions required for pair-copula estimation using the previously estimated copulas, and then estimated the parameters of the pair-copulas in the current tree.

Goodness-of-Fit Tests We employed several goodness-of-fit tests to validate our copula selections, including:

- **Cramér-von Mises Test**: This test evaluates the distance between the empirical copula and the fitted copula:

$$S_n = \int_{[0,1]^2} [C_n(u,v) - C_{\hat{\theta}}(u,v)]^2 dC_n(u,v) \tag{A.12}$$

  where C_n is the empirical copula and $C_{\hat{\theta}}$ is the fitted parametric copula.

- **Kendall's Tau Test**: This test compares the empirical Kendall's tau with the theoretical Kendall's tau implied by the fitted copula. For most of our city pairs, the p-values from these tests were greater than 0.05, indicating no significant evidence against our copula selections.

Appendix B

Supplementary Materials for Chapter 3

B.1 Appendix

B.1.1 Detailed Methodological Explanations

GARCH Model Specification and Estimation

The GARCH(1,1) model used in this study is specified as follows:

$$r_{i,t} = \mu_i + \varepsilon_{i,t}, \tag{B.1}$$

$$\varepsilon_{i,t} = z_{i,t}\sigma_{i,t}, \tag{B.2}$$

$$\sigma^2_{i,t} = \omega_i + \alpha_i \varepsilon^2_{i,t-1} + \beta_i \sigma^2_{i,t-1}, \tag{B.3}$$

where $r_{i,t}$ is the return of market i at time t, μ_i is the mean return, $\varepsilon_{i,t}$ is the error term, $\sigma^2_{i,t}$ is the conditional variance, and $z_{i,t}$ follows a standardized Student's t-distribution to account for the leptokurtosis commonly observed in financial time series.

The parameters ω_i, α_i, and β_i are estimated using Maximum Likelihood Estimation (MLE). The log-likelihood function for the Student's t-distribution is given by:

$$\ln L(\theta) = \sum_{t=1}^{T} \left[\ln \Gamma\left(\frac{\nu+1}{2}\right) - \ln \Gamma\left(\frac{\nu}{2}\right) - \frac{1}{2}\ln[\pi(\nu-2)] - \frac{1}{2}\ln \sigma_t^2 - \frac{\nu+1}{2}\ln\left(1 + \frac{\varepsilon_t^2}{(\nu-2)\sigma_t^2}\right)\right], \tag{B.4}$$

where θ represents the set of parameters to be estimated, ν is the degrees of freedom parameter for the Student's t-distribution, and $\Gamma(\cdot)$ is the gamma function.

Following the estimation, we extract the standardized residuals $z_{i,t} = \frac{\varepsilon_{i,t}}{\sigma_{i,t}}$, which are then used in the subsequent Copula analysis.

Copula Estimation Procedure

To capture the complex dependency structures between carbon markets, we employ the Student's t-Copula. The estimation follows the Inference Functions for Margins (IFM) approach, which is a two-step procedure:

1. Estimate the parameters of the marginal distributions for each market's standardized residuals.
2. Estimate the parameters of the Copula function using the probability integral transforms of the standardized residuals.

For the Student's t-Copula, the density function is:

$$c(u_1, \ldots, u_n) = \frac{\Gamma\left(\frac{\nu+n}{2}\right)}{\Gamma\left(\frac{\nu}{2}\right)} \frac{1}{(\pi\nu)^{n/2}|R|^{1/2}} \left(1 + \frac{q' R^{-1} q}{\nu}\right)^{-\frac{\nu+n}{2}}, \tag{B.5}$$

where $u_i = F_i(z_{i,t})$ are the uniform transformed variables, $q = (t_\nu^{-1}(u_1), \ldots, t_\nu^{-1}(u_n))$, ν is the degrees of freedom parameter, R is the correlation matrix, and $\Gamma(\cdot)$ is the gamma function.

The log-likelihood function for the Student's t-Copula is:

$$\ln L_C(R, \nu) = \sum_{t=1}^{T} \ln c(F_1(z_{1,t}), \ldots, F_n(z_{n,t}); R, \nu), \tag{B.6}$$

where $c(\cdot)$ is the density function of the Student's t-Copula, and $F_i(z_{i,t})$ are the empirical cumulative distribution functions of the standardized residuals.

Diebold-Yilmaz Spillover Index Methodology

The Diebold-Yilmaz spillover index is based on forecast error variance decomposition (FEVD) from vector autoregression (VAR) models. We specify a VAR(p) model for the vector of returns:

$$\mathbf{r}_t = \sum_{k=1}^{p} \mathbf{A}_k \mathbf{r}_{t-k} + \boldsymbol{\varepsilon}_t, \tag{B.7}$$

where $\mathbf{r}_t$ is the vector of returns at time t, $\mathbf{A}_k$ are coefficient matrices, and $\boldsymbol{\varepsilon}_t$ is the vector of error terms with covariance matrix $\boldsymbol{\Sigma}$.

The VAR model can be rewritten in moving average representation as:

$$\mathbf{r}_t = \sum_{h=0}^{\infty} \boldsymbol{\Phi}_h \boldsymbol{\varepsilon}_{t-h}, \tag{B.8}$$

where $\mathbf{\Phi}_h$ are the moving average coefficient matrices, which can be computed recursively as $\mathbf{\Phi}_h = \sum_{j=1}^{p} \mathbf{A}_j \mathbf{\Phi}_{h-j}$, with $\mathbf{\Phi}_0 = \mathbf{I}$ and $\mathbf{\Phi}_h = \mathbf{0}$ for $h < 0$.

The generalized forecast error variance decomposition (GFEVD), which allows for correlated shocks, is given by:

$$\theta_{ij}(H) = \frac{\sigma_{jj}^{-1} \sum_{h=0}^{H-1} (e_i' \mathbf{\Phi}_h \mathbf{\Sigma} e_j)^2}{\sum_{h=0}^{H-1} (e_i' \mathbf{\Phi}_h \mathbf{\Sigma} \mathbf{\Phi}_h' e_i)}, \tag{B.9}$$

where e_i is a selection vector with one in the i-th position and zeros elsewhere, and σ_{jj} is the standard deviation of the error term for market j.

The total spillover index is computed as:

$$S(H) = \frac{\sum_{i=1}^{n} \sum_{j=1, j \neq i}^{n} \theta_{ij}(H)}{\sum_{i=1}^{n} \sum_{j=1}^{n} \theta_{ij}(H)} \times 100, \tag{B.10}$$

which measures the percentage of forecast error variance in all markets that comes from spillovers.

The directional spillover indices are calculated as:

$$S_i^{\text{FROM}}(H) = \frac{\sum_{j=1, j \neq i}^{n} \theta_{ij}(H)}{\sum_{j=1}^{n} \theta_{ij}(H)} \times 100, \tag{B.11}$$

$$S_i^{\text{TO}}(H) = \frac{\sum_{j=1, j \neq i}^{n} \theta_{ji}(H)}{\sum_{j=1}^{n} \theta_{ji}(H)} \times 100, \tag{B.12}$$

which measure the spillovers received by market i from all other markets and the spillovers transmitted from market i to all other markets, respectively.

The net spillover index for market i is then:

$$S_i^{\text{NET}}(H) = S_i^{\text{TO}}(H) - S_i^{\text{FROM}}(H), \tag{B.13}$$

which identifies whether a market is a net transmitter or receiver of spillovers.

Multi-layer Network Construction

The multi-layer network framework consists of three layers, each capturing a different aspect of market relationships:

1. **Layer 1 (Dependency Layer)**: This layer represents the non-linear dependencies and tail co-movements between markets, as captured by the Copula analysis. The adjacency matrix for this layer is defined as:

$$W_{ij}^{\text{Copula}} = \hat{\rho}_{ij}^{\text{Copula}}, \tag{B.14}$$

where $\hat{\rho}_{ij}^{\text{Copula}}$ is the estimated dependence parameter between markets i and j from the Copula model.

2. **Layer 2 (Risk Transfer Layer)**: This layer captures the linear risk spillovers between markets, as quantified by the Diebold-Yilmaz spillover indices. The adjacency matrix for this layer is defined as:

$$W_{ij}^{\text{DY}} = \theta_{ij}(H), \tag{B.15}$$

where $\theta_{ij}(H)$ is the GFEVD-based spillover from market j to market i.

3. **Layer 3 (Primary Transmission Path Layer)**: This layer highlights the most significant risk transmission paths, focusing on the strongest connections. The adjacency matrix for this layer is defined as:

$$W_{ij}^{\text{Primary}} = \begin{cases} 1, & \text{if } \theta_{ij}(H) = \max_{k \neq i} \theta_{ik}(H), \\ 0, & \text{otherwise.} \end{cases} \tag{B.16}$$

B.1.2 Regulatory Background

Timeline of China's Carbon Market Development

Table B.1 presents a detailed timeline of key policy developments in China's carbon market.

The timeline highlights the gradual and deliberate approach to carbon market development in China, from the establishment of regional pilot markets to the launch and subsequent expansion of the national trading system.

Comparative Regulatory Framework Analysis

Table B.2 presents a comparative analysis of the regulatory frameworks across different carbon markets.

The comparative analysis shows that China's carbon market has moved towards greater alignment with international standards following unification, particularly in areas such as monitoring, reporting, and verification (MRV) standards and the development of secondary markets and financial products. However, differences persist in key areas such as allocation methods and the scope of covered sectors.

Table B.1: Timeline of China's Carbon Market Development

Date	**Policy Development**
2011-10-29	National Development and Reform Commission (NDRC) announces pilot carbon markets in seven provinces and cities
2013-06-18	Shenzhen launches first pilot carbon market
2013-11-26	Beijing launches pilot carbon market
2013-11-28	Shanghai launches pilot carbon market
2013-12-19	Guangdong launches pilot carbon market
2014-01-02	Tianjin launches pilot carbon market
2014-04-02	Hubei launches pilot carbon market
2014-06-19	Chongqing launches pilot carbon market
2016-09-19	Fujian launches pilot carbon market
2017-12-19	NDRC announces national emissions trading system work plan
2020-12-30	Ministry of Ecology and Environment releases final allocation plan for the power sector
2021-01-05	Administrative measures for national carbon market trading released
2021-07-16	National carbon emissions trading market officially launched
2022-02-10	First carbon emission allowance futures contract introduced
2022-09-18	Announcement of expansion to include aluminum sector
2023-04-25	Updated carbon neutrality policy framework released
2023-12-15	Announcement of plans to expand national market to cover additional industrial sectors by 2025

Table B.2: Comparative Analysis of Carbon Market Regulatory Frameworks

Regulatory Feature	**China (Pre)**	**China (Post)**	**EU ETS**
Scope (Sectors)	Varied by pilot	Power, expanding	Multiple sectors
Allocation Method	Primarily free	Primarily BM-based	Auction and BM
Price Containment	Price floors/ceilings	Intervention mechanism	Market Stability Reserve
Compliance Period	Annual	Annual	Annual
MRV Standards	Regional standards	National standards	Unified framework
Offset Usage	Limited (CCER)	Limited (CCER)	Limited (international)
Banking Provisions	Varied by pilot	Yes, with restrictions	Yes
Secondary Markets	Limited	Expanding	Well-developed
Financial Products	Very limited	Futures introduced	Multiple instruments

Appendix C

Supplementary Materials for Chapter 4

C.1 Appendix

C.1.1 Complete Dynamic Copula Estimation Results

This appendix presents the dynamic Copula estimation results that could not be fully displayed in the main text due to space constraints. It includes estimation parameters, degrees of freedom ν, log-likelihood values, and convergence information for all asset pairs during both the pre-event period (2020/01–2022/11)Table C.1 and post-event period (2022/12–2024/06)Table C.2 .

Complete Results for the Pre-event Period (2020/01–2022/11)

Complete Results for the Post-event Period (2022/12–2024/06)

Table C.1: Dynamic Copula Model Estimation Results (Pre-event Period)

Asset Pair	α	β	γ	ν	γ_0	**negLL**	**Conv.**
AI vs Clean Energy	0.0000	0.0000	3.0000	10.5280	1.5460	-133.7016	0
AI vs Solar	0.0106	0.9794	3.0000	12.3680	2.0000	-68.9931	1
AI vs Bioenergy	0.0462	0.8463	-3.0000	17.5760	2.0000	-106.7069	0
AI vs Wind	0.0000	0.6233	1.9400	6.3658	0.7634	-37.3616	0
AI vs Oil	0.0335	0.9565	3.0000	10.6040	1.1903	-8.3805	1
AI vs Gas	0.7143	0.0000	2.3150	30.0000	0.0671	-0.7321	0
AI vs Carbon	0.0420	0.9479	-0.2120	30.0000	0.7048	-1.2247	1
Clean Energy vs Solar	0.0026	0.9874	1.8630	7.0387	1.5619	-101.7189	1
Clean Energy vs Bioenergy	0.0110	0.9635	-3.0000	11.9320	1.8756	-98.4517	0
Clean Energy vs Wind	0.1800	0.1781	3.0000	24.4660	2.0000	-145.8233	0
Clean Energy vs Oil	0.2510	0.7369	2.0090	13.6850	2.0000	-2.3704	0
Clean Energy vs Gas	0.1354	0.8301	-3.0000	30.0000	0.5217	-1.1755	0
Clean Energy vs Carbon	0.9657	0.0000	-1.1170	30.0000	2.0000	-1.2386	0
Solar vs Bioenergy	0.0202	0.9698	3.0000	30.0000	2.0000	-41.3432	0
Solar vs Wind	0.6591	0.0000	2.1270	15.6620	2.0000	-32.2679	0
Solar vs Oil	0.1574	0.8223	3.0000	29.1010	2.0000	-5.7597	0
Solar vs Gas	0.9843	0.0016	1.8030	30.0000	2.0000	-1.1972	0
Solar vs Carbon	0.0459	0.9441	2.6830	30.0000	0.5005	-1.1994	1
Bioenergy vs Wind	0.6467	0.0000	0.9770	14.1530	1.6702	-22.8174	0
Bioenergy vs Oil	0.0917	0.8352	-3.0000	10.7910	1.3726	-21.2823	0
Bioenergy vs Gas	0.3135	0.6612	-3.0000	13.7500	1.3519	-2.2880	0
Bioenergy vs Carbon	0.0176	0.9724	3.0000	30.0000	0.6360	-5.2458	1
Wind vs Oil	0.2108	0.2331	3.0000	30.0000	-0.0200	-0.2356	0
Wind vs Gas	0.2726	0.7123	-3.0000	30.0000	2.0000	-2.9450	0
Wind vs Carbon	0.9325	0.0000	-2.2860	30.0000	2.0000	-4.0092	0
Oil vs Gas	0.9046	0.0000	0.9900	30.0000	1.1131	-1.0118	0
Oil vs Carbon	0.2177	0.7630	3.0000	30.0000	2.0000	-5.9666	0
Gas vs Carbon	0.1601	0.8023	3.0000	22.2580	0.5805	-1.7292	0

Notes: (1) Conv. = 0/1 indicates convergence status (0=successful, 1=failed or boundary stagnation); (2) $\nu \approx 30.0000$ indicates that the degrees of freedom reached the upper limit; (3) $\gamma_0 < 0$ may suggest initial negative correlation.

Table C.2: Dynamic Copula Model Estimation Results (Post-event Period)

Asset Pair	α	β	γ	ν	γ_0	**negLL**	**Conv.**
AI vs Clean Energy	0.1380	0.4950	3.0000	4.9400	2.0000	-96.3500	0
AI vs Solar	0.0790	0.0000	3.0000	12.6700	2.0000	-141.0000	0
AI vs BioEnergy	0.6660	0.0000	-2.1740	30.0000	2.0000	-19.2200	0
AI vs Wind	0.0000	0.0180	-0.4690	30.0000	0.7930	-27.4500	0
AI vs Gas	0.8840	0.0000	-0.7970	30.0000	1.9700	-2.6100	0
AI vs Carbon	0.0000	0.8800	1.5360	9.1000	-0.0480	-1.6700	0
Clean Energy vs Solar	0.0030	0.9860	1.8650	5.7700	2.0000	-141.9200	1
Clean Energy vs BioEnergy	0.3550	0.1720	-3.0000	30.0000	2.0000	-53.2600	0
Clean Energy vs Wind	0.2800	0.0000	3.0000	9.1700	2.0000	-96.7700	0
Clean Energy vs Gas	0.9190	0.0000	0.1990	30.0000	2.0000	-2.3100	0
Clean Energy vs Carbon	0.9900	0.0000	-0.4900	30.0000	0.1370	0.2800	1
Solar vs BioEnergy	0.3810	0.4430	-3.0000	30.0000	2.0000	-17.8200	0
Solar vs Wind	0.0000	0.0000	3.0000	30.0000	0.8300	-30.1100	0
Solar vs Gas	0.8420	0.1120	-0.3820	30.0000	1.8100	-1.2700	0
Solar vs Carbon	0.2400	0.7440	-0.2230	16.3400	2.0000	-2.8700	0
BioEnergy vs Wind	0.3790	0.0000	3.0000	9.2800	1.0010	-21.3400	0
BioEnergy vs Gas	0.2980	0.6860	1.8430	6.8800	0.0880	-1.0200	0
BioEnergy vs Carbon	0.9820	0.0000	-0.6650	30.0000	2.0000	-1.8400	0
Wind vs Gas	0.8730	0.0000	0.4290	30.0000	1.6370	-1.6800	0
Wind vs Carbon	0.7090	0.1750	-2.8040	30.0000	1.1310	-2.2700	0
Gas vs Carbon	0.9480	0.0000	-0.8450	30.0000	2.0000	-2.1400	0

Notes: (1) Conv. = 0/1 as above; (2) $\nu = 30.0000$ indicates upper limit was reached; (3) Some pairs (Conv. = 1) were excluded in robustness tests.